University of Glasgow

DEPARTMENT OF

AEROSPACE ENGINEERING



# A FEASIBILITY STUDY INTO THE GENERATION OF TRANSVERSE AND LONGITUDINAL VORTICES IN LOW SPEED WIND TUNNELS

(FINAL report for DRA agreement No. ASF/2163/U)

by

F.N. Coton, R.A.McD. Galbraith and C.M. Copland

# A FEASIBILITY STUDY INTO THE GENERATION OF TRANSVERSE AND LONGITUDINAL VORTICES IN LOW SPEED WIND TUNNELS

(FINAL report for DRA agreement No. ASF/2163/U)

by

F.N. Coton, R.A.McD. Galbraith and C.M. Copland

Glasgow University
Department of Aerospace Engineering

**Internal Report Number 9828**

# A Feasibility Study into the Generation of Transverse and Longitudinal Vortices in Low Speed Wind Tunnels

**Final Report for DRA Agreement No. ASF/2163/U**

by

**Dr. F.N. Coton**
**Prof. R. Galbraith**
**Dr. C.M. Copland**

Department of Aerospace Engineering
University of Glasgow
Glasgow
G12 8QQ

## SUMMARY

This report details the work carried out during a fundamental study into the generation of transverse and longitudinal vortices in the working sections of wind tunnels. In the initial phases of the project, effort was focused on the generation and measurement of longitudinal vortex pairs to mimic the vortex system produced by the Westland Helicopter's Vane tip. The results from this part of study have already been used in an EPSRC funded study of main rotor blade-vortex interaction (BVI). Attention was then directed towards the development and testing of a transverse vortex generator for studies of tail rotor BVI. The successful demonstration of this generator has resulted in a follow-on EPSRC funded study of helicopter tail rotor BVI in a larger wind tunnel facility.

## BACKGROUND

The aerodynamic flowfield around the helicopter is not only complex but laced with strong vortices that interact with aircraft components resulting in a variety of unwanted phenomena. Of particular concern is the radiated noise and the additional effect of the main rotor vortex system on the tail rotor's performance. The prime events are normally termed blade vortex interactions and, although they have been extensively modelled numerically, the experimental facilities available are both varied and limited.

The crucial factor in all experiments to date has been the manner in which the interacting vortices have been generated and their subsequent trajectory through the wind tunnel's working section. These two features are of critical importance in interpreting the resultant data collected and in the application of such interpretations to the real aircraft. When data pertaining to blade vortex interactions are acquired from experiments in which the generation of the interacting vortex differs, there are clear differences in the flow development. How important these differences are is not clear, and it may be that they simply affect the peripheral response and not the fundamental interaction. Nonetheless, whatever system is used, it is essential that the detailed structure of the interacting vortex in known. It is also important to have a good knowledge of the vortex trajectory, its stability and tendency to "wander" from its mean path. This applies irrespective of the method of generation.

This feasibility study was concerned with the generation of two types of vortex systems. The first of these is representative of that trailed from a new helicopter blade tip design which

may have beneficial noise reduction characteristics. In this case, it is necessary to produce a vortex pair which may wrap around each other as the system progresses downstream.

The other system under consideration was that of a vortex orthogonal to the plane of the aerofoil. This interaction models the main rotor tip vortex interaction with the tail rotor and requires a transverse vortex travelling in a stable fashion through the tunnel's working section. The conventional generation method for such a vortex is to place an aerofoil at the entrance of the working section and subject it to a rapid change in incidence. Although this procedure is fraught with difficulty, it does produce a vortex, but one in which the structure may not comprehensively mimic the trailing vortex from the tip of the rotor. In the present study, the generation of the tip vortex was via a rotor placed in the settling chamber of a wind tunnel such that the blade tip entered the contraction.

## DESCRIPTION OF WORK CARRIED OUT

### Twin longitudinal vortices

In the initial stages of this work, a survey of existing methods for vortex generation was carried out. Subsequently, a twin vortex generator was designed, manufactured and installed in the Department of Aerospace Engineering 1.15m x 0.85m low speed wind tunnel. Hot-wire tests were then conducted to measure the sensitivity of the vortex structure to the configuration of the generator. The results obtained are detailed in Ref. 1 and described in summary in Appendix 1 where they are compared with a simple numerical model .

### Transverse vortex

Initial work in this area concentrated on the development of a suitable numerical model to assist in the design of the proposed facility. The developed model is fully three-dimensional and is comprised of a free vortex rotor model and a source panel method to represent the tunnel walls. The model was used extensively in a parametric study to determine the optimum operating conditions for the test rig as described in Appendix 2. Two possible operating modes were considered for the generator. In the first of these, the rotor motion is constrained within one and a half cycles to limit disturbances to the main flow. Unfortunately, the accelerations in the optimum motion profile would be extreme and would have required powerful actuation systems and complex control strategies. The resulting cost of such a facility would have been around £60,000 which was considered to be prohibitively expensive.

The second option considered was that of a rotor rotating at constant Rpm. This option was financially more attractive as the actuation of the rotor could be achieved by a simple DC motor. In addition, the vortex structure produced was not significantly different to that of the limited azimuth case. Consequently, this configuration was adopted for the experimental part of the study.

The design, construction and initial testing of the transverse vortex generator are outlined in Appendix 3. The results show that a clean periodic signal indicative of a vortex is obtained. This is the case over a wide range of operating conditions. Further detailed analysis of the measurements has indicated that the vortex geometry predicted by the numerical model is, in fact, realised despite the simplifications inherent in the model. This has provided the confidence to utilise the same approach in the forthcoming EPSRC funded study of tail rotor BVI.

## Analysis of BVI Results

An additional element of the study involved preliminary analysis of results from an EPSRC funded study of main rotor interaction. The main findings of this preliminary analysis are presented in Appendix 4.

## VARIATIONS FROM THE PROPOSED WORK PROGRAMME

Two particular events introduced variations into the work programme. The first of these was the repeated failure of the TSI IFA 300 hot wire system. On each occasion, this required the system to be sent to the U.S. for repair. In the final year of the project the system failed for the third time and was replaced free of charge, with a new system, by the manufacturers. Nevertheless, the system downtime was greater than one full year because of these problems.

The second problem was the mechanical failure of the rotor blade during testing. This meant that a second blade had to be manufactured and resulted in a delay to the programme.

As a consequence of the above problems and a delay in an associated EPSRC project, the tests involving surface pressure measurements on a blade interacting with the transverse vortex have not yet been conducted. The blade is, however, ready and will be tested in the very near future as part of the follow-on EPSRC study. The results of these tests will be conveyed to DERA as they become available.

## CONCLUSIONS

A method has been developed to generate twin longitudinal vortices in a wind tunnel. The sensitivity of the generated vortices to generator configuration has been extensively studied using hot-wire anemometry and modelled using a simple quasi-three-dimensional algorithm.

A transverse vortex generator has been developed with the aid of a numerical model. The generator has been manufactured and installed in a low-speed wind tunnel. The vortex system produced by this generator has been studied using a hot-wire system and found to exhibit the strong signature of a tip vortex. Having established the suitability of the generator for BVI studies, funding has been obtained from the EPSRC to carry out a follow-on tail rotor BVI study in a large scale wind tunnel.

## REFERENCES

1. Copland, C.M., 'On the Generation of Transverse and Longitudinal Vortices in Low Speed Wind Tunnels', Ph.D. Thesis, University of Glasgow 1998

# Appendix 1

## AN EXPERIMENTAL STUDY OF THE IDEALISED VORTEX SYSTEM OF A NOVEL ROTOR BLADE TIP

by

C.M. Copland
F.N. Coton
R.A.McD. Galbraith

Presented at the 23rd European Rotorcraft Forum, Dresden, 1997 also to be Published in the Aeronautical Journal, August/September 1998 issue.

# AN EXPERIMENTAL STUDY ON THE IDEALISED VORTEX SYSTEM OF A NOVEL ROTOR BLADE TIP

by

C.M. Copland, F.N. Coton, R.A.McD. Galbraith

Department of Aerospace Engineering,
The University of Glasgow,
Glasgow, G12 8QQ
Scotland

## Abstract

Experiments have been conducted to investigate the flow field associated with two co-rotating vortices which represent the idealised vortex system associated with a novel rotor blade tip planform. These vortices were generated by two rectangular NACA 0015 half wings positioned upstream of the working section of a low speed wind tunnel. Hot-wire measurements were conducted downstream of the generators using X-wire probes to document the strength, position and size of the vortices. A numerical model was utilised to provide an accurate means of determining vortex strength, position and size. Finally, the model was successfully extended to consider the rotation of the vortex system.

## Nomenclature

| | |
|---|---|
| $a$ | General constant |
| $c$ | Vortex generator chord. |
| $n$ | General constant |
| $r$ | Radial distance, $m$. |
| $r_c$ | Vortex core radius, $m$. |
| $\bar{r}$ | Non-dimensional radius $\left( r/r_c \right)$. |
| $u_\theta$ | Tangential velocity, $ms^{-1}$. |
| $\bar{u}_\theta$ | Non-dimensional tangential velocity, $2\pi r_c u_\theta / \Gamma$ |
| $u, v$ | Vertical and Horizontal velocity components respectively, $ms^{-1}$. |
| $x, y$ | Measurement grid co-ordinate system. |
| $\Gamma$ | Vortex circulation, $m^2 s^{-1}$ . |

## Introduction

The association of vortex systems with the production of aerodynamic forces is, for most aeronautical applications, well understood. In some cases, however, such as rotary wing aircraft, the vortex systems are particularly complex and highly unsteady and their interaction with the rotating lifting surfaces creates additional undesirable effects such as noise emission and structural vibration. On a helicopter, this phenomenon is termed Blade-Vortex Interaction (BVI) and occurs when the tip vortices trailed from the rotor pass close to, or impact directly with, any of the blades in the main rotor or tail rotor systems. In some flight conditions BVI can be particularly severe and is manifest as high-frequency impulsive loads on the rotor blades.

The importance of BVI has been recognised for many years and has been the focus of several experimental[1-4] and numerical[5,6] studies. Of these, most have concentrated on main rotor BVI although some, notably the in-flight study of Ellin[7], have considered the interaction of the main rotor wake with the tail rotor.

Experimental studies have been predominantly wind-tunnel based and have utilised a variety of test geometries to create the BVI phenomenon. Early studies attempted to isolate single interactions in the hope that a clear description of the process would be forthcoming. Unfortunately, these tests were often hampered by problems associated with vortex generation or poor measurement resolution. In recent years, improvements in instrumentation technology have allowed more detailed studies of BVI, both as an isolated phenomenon and also in the full rotor domain to be conducted. Of particular relevance to the present study is the surface pressure measurement and flow visualisation work of Kokkalis et al.[1] and, subsequently, Horner et al.[2,3,4]. In these tests, a vortex generator was located upstream of a single-bladed rotor in the working section of a low-speed wind tunnel. During the interaction of the vortex with the rotor blade, unsteady surface pressures were measured and Particle Image Velocimetry was used to obtain quantitative flow field information.

In most of the work described above, the emphasis has been on developing an understanding of BVI events associated with a conventional helicopter blade tip. Recently, however, several novel blade tip designs such as the BERP tip, have been developed and have entered service on operational aircraft. It has been documented by Scott et. al.[8] that this tip may generate two trailed vortices at moderate-to-high incidence (Fig. 1) the outboard vortex being relatively stronger than the inboard which is of opposite sense. Lowson [9] also stated that this tip reduces the noise in low speed descent, where BVI is predominant.

It has also been possible to consider the design of tip platforms specifically to modify the tip vortex structure in a manner which potentially reduces the severity of the associated BVI events. One such design is the so-called 'Vane-Tip' (Fig. 2) proposed by Brockelhurst and Pike[10] and which distributes the vorticity at the blade tip as a pair of co-rotating vortices. Theoretically, this has the potential to considerably reduce the severity of individual BVI events thus producing a corresponding reduction in noise [11]. Unfortunately, little is known about the temporal and spatial development of two such closely spaced trailed vortices and so it is difficult to assess the actual effect which such a tip design would have.

In an attempt to alleviate this problem, the present study examines the generation and subsequent behaviour of a vortex pair in a wind tunnel environment. It is shown that the vortices can be modelled accurately using a simple two-dimensional core model and that their rotation can be predicted in a straightforward manner.

## Methods

The experiments were conducted in the 1.15m x 0.85m low speed wind tunnel of the Department of Aerospace Engineering, Glasgow University. This is a closed return facility capable of speeds up to

33 m/s. The test section length is 1.8m. The tunnel is equipped with an automated two component traverse which can be wall mounted vertically or on a support structure horizontally. The traverse is actuated via stepper motors controlled through a data acquisition board by software written under Labview. When a probe is mounted on the traverse, the positional error due to the traverse in both the $x$ and $y$ directions is of the order of 0.5% of the distance between the origin of the measurement grid and the actual position of the probe.

The vortex generators, in this investigation, consisted of two rectangular cantilever wings of chord 0.1m, one mounted from the floor of the wind tunnel and the other from the roof (Fig. 3). The length of each wing, 0.4m, was almost half of the tunnel height at the generator location such that, when the wings were exactly aligned, they formed a near continuous vertical blade. In a manner similar to Refs. 1-4, a single vortex could be generated at the junction of the two wings by setting the wings at opposite incidence to each other. Similarly, twin trailed vortices could easily be produced by introducing lateral spacing of the two wings.

The wings were manufactured from wood and the base plates from aluminium. Each blade was secured to its base plate by a locking mechanism which passed through the quarter chord position of its NACA 0015 aerofoil section. The base plates were then surface mounted to the floor and roof of the tunnel. Looking upstream, the vortex generator mounted on the floor of the tunnel was positioned left of the centre-line and the top generator on the right. The base plates allowed each blade to be varied laterally form the centre line of the tunnel by approximately 1.5 chord lengths. A blade incidence variation of $\pm 12^{o}$ could be achieved in $2^{o}$ increments.

Measurements of the magnitude and associated direction of the time-dependant velocity vector were obtained using a cross-wire probe connected to a TSI IFA-300 three-channel constant temperature anemometer system. For a single cross-wire, the maximum sampling rate for this system is 400 kHz. The cross-wire probes used in this study were DANTEC 55P61 probes. The sensor wires on these probes are $5\mu m$ diameter platinum plated tungsten wires with a length/diameter ratio of 250, which form a measuring volume of approximately 0.8mm in diameter and 0.5mm in height. The wires are orientated perpendicular to each other corresponding to 45 degrees from the freestream direction which gives the best angular resolution. An additional temperature probe was used to correct the anemometer output voltages for any variation in ambient flow temperature.

For calibration, an open jet vertical wind tunnel with a maximum operating velocity of 43 m/s was used. A support allowed the sensors of X-wire probe to be rotated by $\pm 30^{o}$ in the plane of the sensors. Variation of the flow velocity and yaw angle then enabled the coefficients of the effective velocity method to be determined.

In order to fully determine the lateral and vertical components of velocity, the probe had to be rotated around its axis by 90 degrees to adjust the wire plane (horizontal and vertical) against the main flow direction. Thus, two traverse sweeps were necessary to obtain the vertical ($u$) and lateral ($v$) components respectively. The streamwise component of velocity was thus acquired twice but this component was strongly effected by the unmeasured velocity component which is perpendicular to the wire plane. This transverse contamination, as noted in Ref. 12, does not adversely effect the other in-plane measured velocity component which is of primary interest.

## Description of Tests

Flow field measurements were conducted in a plane perpendicular to the freestream direction for a constant freestream velocity of 30 m/s. This gives a Reynolds number of approximately $Re=2.1x10^{5}$ based on the chord of the vortex generator. On the basis of previous studies, this Reynolds number is above the threshold below which low Reynolds number effects become significant on the NACA 0015 section.

The sampling frequency for each channel was set at 2 kHz. The anemometer signals were then automatically low pass filtered at 1 kHz before digitising to counter aliasing. The sampling time for each point was 2 seconds which enabled a single grid traverse to be acquired in 2 hours.

The measurement grid size varied depending on the orientation of the traverse and was dependent on the position of the traverse with respect to the walls of the working section. A grid size of 100mm horizontal and 200mm vertical was attainable with the traverse in a vertical orientation. Horizontally, the maximum grid size was 160mm horizontally and 160mm vertically. Measurements were conducted every 10mm and so 231 points and 289 points were acquired for the vertical and horizontal traverse orientations respectively.

Table 1 documents the tests conducted. Initial tests were carried out to investigate the general flow field associated with two co-rotating and counter rotating vortices as well as the single vortex. These tests were conducted at two downstream positions corresponding to 2.5c and 6c behind the trailing edge of the vortex generators. The vortex generators were also varied to generate different sense vortex rotation in the single and twin vortex cases.

Further tests were then implemented at the optimum settings which generated a 0.5c separation of vortex cores - as produced by the Vane Tip. The first test was an investigation of the effect of the vortex generator blade incidence on the cross-flow geometry at a measurement station 4.3 chord lengths downstream of the generator. Detailed flow field measurements were then conducted at 10 degrees incidence from 0.1c to 10c downstream. Finally an investigation into the effects of generator blade separation was carried out. Blade separation was varied from 0c to 1c with measurements at 4c and 8c downstream of the generator.

## Model Formulation

As with all measurements in vortex flows, a consistent method must be used to determine the relative parameters of the flow field. Previous investigations have utilised an analytical vortex model to curve fit the two dimensional tangential velocity component. These models are usually derived from fixed wing studies. This is perfectly satisfactory for single vortex configurations but when dealing with two vortices, which are closely spaced, the tangential component of velocity varies significantly between the cores. The two primary factors for determining the vortex strength, core size and maximum (tangential) velocity, are difficult to predict when dealing with a discretised grid. Measurements may not provide values for the maximum velocity and so underestimate the vortex strength and overestimate core size.

For a single vortex the rule that the tangential velocity is proportional to $1/r$ must break down for small values of $r$ to avoid unphysical singularities on the axis itself. The fluid velocity can never be infinite in the real world, and in so far as it reverses direction between two points which lie close to the axis but on opposite sides, the change cannot be a discontinuous one. Thus every free vortex line must have a core of some sort.

The immense complexities associated with concentrated vortices have prevented the derivation of a theoretically rigorous vortex model which describes the phenomena in every respect. For this reason several empirical formulae[13-17] for the tangential velocity have been used by many to study different aspects of concentrated vortices. The best known among these are the Rankine, Lamb-Oseen and Scully models. Vatistas[14] et. al. proposed an equation which represents a series of general velocity profiles for rectilinear vortices and which provides a link between Rankine's model and the Scully model. The tangential velocity in the core is expressed by Vatistas in non-dimensional terms as

$$\bar{u}_\theta = \frac{\bar{r}}{\left(1+\bar{r}^{an}\right)^{1/n}} \qquad (1)$$

The Scully model corresponds to $n=1$ and the Rankine model to $n \rightarrow \infty$ where $n$ and $a$ are integer constants. Since the above equation must have a maximum at $\bar{r} = 1$, $a$ has to be equal to 2

A numerical model of this type can be used in conjunction with experimental data to provide a means to determine two dimensional parameters which could represent the two measured in-plane velocity components. For the present study, the Scully model was chosen due to its common use in curve fitting experimental single vortex data[16,17].

Each of the Scully vortices induces a velocity component on each of the discrete grid points. This velocity component is derived from the Biot-Savart law applied in two dimensions. At these points the tangential velocity from each vortex is decoupled into the appropriate grid horizontal and vertical velocity components which are then superposed. The numerical model grid and experimental grid are of the same dimensions which enabled a direct point for point comparison to be conducted.

As a prerequisite for the numerical model, initial values for the position ($x$ and $y$ co-ordinates), core size ($r_c$) and vortex strength ($\Gamma$) must be specified for the two vortices. These parameters are then altered via a manual iteration process to obtain a best fit to the majority of the horizontal and vertical mean velocity components acquired experimentally. Two sets of experimental data (one for each in plane velocity component) are fitted to one set of numerical data. There were slight differences between the two separately acquired components in some configurations (as can be seen from Fig. 5). This was primarily due to vortex meander and probe interference. In some cases, however, this proved insignificant compared with the discrepancies attributable to the highly three-dimensional nature of the flow field. Outside the cores, the two wake structures from the vortex generators were dominant flow features. These errors were localised to specific regions of the grid for the vertical velocity component when measurements were conducted close to (<5c) the generator blades. An adequate curve fit to both sets of data ($u,v$) could, however, be determined from the horizontal component of velocity.

Once the fitting parameters had been obtained for all the experimental data in the cross-flow plane, a quasi three-dimensional adaptation was used to predict the rotation of the vortex system as it travelled downstream. In this model, a two-dimensional Biot-Savart calculation was conducted to obtain the two induced velocity components in the cross-flow plane at each vortex core position. An Adams-Bashforth multi-step integration routine was then used to advance the core positions in time from an initial condition close to the vortex generator. The orientation of the vortex system at any location downstream could then be estimated by assuming that the vortex system travelled downstream at a given velocity. Measurements of the streamwise velocity components at each measurement plane indicated that variations from the freestream velocity were small and so the freestream velocity was used in the model. This simple model proved successful with errors primarily arising from the interference effect of the traverse and the time dependant change in vortex size and strength.

## Results and Discussion

Comparisons of the experimental data with the numerical model are provided in Figs. 4 and 5 for the same case. Figure 4 depicts the flow field associated with the optimum configuration to produce a similar flow to that generated by the Vane Tip. For this case, each vortex generator was set at an incidence of 10 degrees with a 0.5c separation between the quarter chord locations of the aerofoils. In this configuration, the trailing edges of the vortex generators were pointing towards the tunnel walls (as opposed to pointing towards the centre line). The vector plots are shown looking upstream and clearly illustrate the level of correlation between the experiment and numerical model. The vortex parameters were obtained from the numerical model (line in Figs. 5a & b). These correspond to, for position 1 in Fig. 4 (where the vortex originates from the lower vortex generator), a strength of 0.95 $m^2s^{-1}$, vertical position x=0.03m and horizontal position y=-0.01m and, for position 2, a strength of $1.0m^2s^{-1}$ at x=-0.017m, y=0.012m. Both vortices have a core radius of 0.01m.

With a single finite wing, it is expected that the vortex will roll-up inboard of the tip. However, in the twin vortex configuration documented here, the second vortex induces a velocity

which acts against this inboard motion. When the trailing edges of the blades are oriented towards the centre line (reversing the sense of rotation) the induced velocities are in the same direction as the inboard roll-up.

When consideration is given to the movement of the wake from the vortex generators, a configuration with the trailing edges oriented towards the tunnel walls results in the wake being convected away from the centre of the tunnel. Correspondingly, the wake is convected toward the centre of the tunnel and the other vortex when the blades are oriented towards the centre-line. For BVI investigations it is inadvisable to have the wake structure convecting across the interacting plane as this may have a significant effect on the BVI event.

In Figs. 5a and 5b the individual comparisons of the $u$ (vertical) and $v$ (horizontal) components are presented for Y=-20 to 30 mm (horizontal positions). Each individual plot corresponds to a vertical slice of the grid and the plots depicted in Figs 5a and 5b correspond to the regions of highest velocity gradients associated with the core region. As can be seen from the figures, there is a discrepancy in the $u$ velocity magnitudes (Fig. 5a) at positive x-coordinate values and especially for Y=0-30mm. This discrepancy is evident for two localised regions in the complete grid (Y=-80 to 80mm) and is due to the momentum deficit in the wake behind each generator. The region does grow due to the reduction in velocity when moving away from the core. All the regions are of positive x and positive y-coordinates corresponding to a location on the right and above the centre line. This is the region of the upper vortex generator. A corresponding effect is noted in the measurement plane for the lower generator.

The $v$-component is not as adversely affected by the generator wake and so the strengths of the vortices, in this case, were determined from the $v$-components. The general distribution of velocity through the vortex cores, and in the irrotational region outside the cores, is very good. The interference problem with the wake reduces with increasing distance from the generator.

It should be noted that when fitting the numerical model to the two experimental velocity components, initially the vortex strength is varied to obtain the correct irrotational velocity magnitudes and then the core size is varied to alter the velocity gradients for each core. The curve fit is highly sensitive to the vortex position (x,y co-ordinate specification) but not to vortex strength.

The output from the fitting process provides estimates of the vortex strength, core size and position which, when calculated for a series of cases, can be used to interpret the behaviour of the vortex system. The information presented in Figs. 6 to 12 has been calculated in this way.

In Fig. 6 the vortex strengths produced by each blade of the generator are plotted against blade incidence setting. The measurement position was 4.3 chord lengths downstream of the trailing edge and each vortex generator was set at an incidence of 10 degrees with a 0.5c separation between the quarter chord locations of the aerofoils (same parameters for Figs. 7 & 8). As may be expected from the Kutta-Joukowsky theorem, the strength was found to vary linearly with incidence at moderate incidence settings. There was, however, a consistent difference between the strength of the vortices trailed from each blade of the generator. This was apparently due to flow angularity in the test section of the wind tunnel.

Figure 7 depicts the variation in vortex core separation with respect to blade incidence. The graph shows an almost linear relationship with the vortices moving closer together as the incidence is increased. This relationship initially appears surprising since the increase in blade incidence also corresponds to an increase in trailing edge separation. For example, a blade incidence of 2 degrees corresponds to a trailing edge separation of 0.552c and a blade incidence of 10 degs corresponds to a trailing edge separation of 0.76c. Obviously, the initial development of the twin vortex system cannot be considered purely on the basis of the generator geometry. Consideration must also be given to the fluid dynamic behaviour at the two wing tips.

As the blade incidence is increased, there is a corresponding increase in mass flow over the blade tips. On a single finite wing, this has the effect of moving the vortex roll-up location in-board and slightly raising the height of the core above the trailing edge. In the present case, the situation is

complicated by the inevitable confluence of the two wing-tip flows. It has been established that one consequence of this is a reduction in the inboard movement of the tip vortices due to the induced effect of one tip vortex on the other. Given this behaviour, momentum considerations would suggest that this should be accompanied by an increase in the distance between the vortex and the suction side of the trailing edge in the direction normal to the chord line. Further, it would be expected that this distance would progressively increase with blade incidence in a manner which is consistent with the results of Fig.7. Also, there is an initial inward convection of the vortices between 0.1 and 2 chord lengths downstream of the trailing edge which is illustrated in Figure 13. This was detailed for one incidence case only, where the blades were at 10 degrees incidence with a separation of 0.5c. It is possible that this inward convection is related to vortex strength and hence incidence. If the incidence is reduced there should be a reduction in the inward convection and so an increase in vortex separation as shown in Fig.7.

In Fig. 8 the variation in core size with incidence is presented. It may be observed that, over the incidence range considered in this study, the core size was found to be insensitive to the blade incidence setting. This result is interesting, when taken together with Fig. 9 which documents the growth of the core radius with downstream position. Clearly the rate of growth is approximately linear with a core radius of 0.004m (0.04c) at 0.1 chords behind the trailing edge growing to 0.017m (0.17c) at 10 chord lengths downstream. It is interesting to note that these two results suggest that regardless of blade setting, the growth of the vortex cores will be linear and the size of the core will be consistent with Fig. 9. It is inevitable that the test Reynolds number will influence the core size and its rate of growth. Nevertheless, the result presented above has implications for wind tunnel based BVI tests which aim to reproduce core sizes of equivalent non-dimensional scale to those anticipated at full scale. Clearly, the distance between the point of generation and the interaction location must be chosen carefully.

In Fig. 10 the variation in vortex separation distance with downstream measurement position is shown. Here, the blade were held at a constant incidence of 10 degrees with a blade separation of 0.5c between quarter chord locations (same parameters for figs 9 & 11). There is an initial reduction of the core spacing from just over 0.06m to approximately 0.05m within 2 chord lengths. Further downstream the core separation varies slightly and this can be attributed to the interference effect of the horizontally mounted traverse. This interference effect causes the vortex, which is convected downwards (towards the traverse), to be forced toward the other vortex and so reduce the spacing. This occurs when the vortices are vertically oriented to one another between 5c and 6c downstream. Subsequently, as the vortices convect horizontally away from each other the spacing increases before returning to the general downward trend of the curve. Nevertheless, this apparent reduction in the separation distance is very slow and the vortices maintain their approximate half chord spacing throughout the graph.

Figure 11 illustrates the growth in vortex strength with downstream position. Here, there is an initial growth in vortex strength up to approximately 4c. This corresponds to the growth in core size downstream illustrated in Figure 9. This behaviour is due to the vorticity from the wake rolling up into the vortex. After 4c, however, the cores are fully rolled up and the core strength remains constant whilst the core radius continues to increase. This is associated with a redistribution of vorticity within the core, through diffusion, resulting in an enlargement of the core radius.

As may be observed in Fig. 12, the variation of vortex separation with generator blade spacing is approximately linear when measured at 4 chord lengths downstream. However, at 8 chord lengths, there is a dramatic change in vortex separation distance for 0.25c blade separation case. The behaviour illustrated for the 0.25c blade separation case is indicative of vortex merging. Rossow[18,19] documented that vortex merging is dependent primarily on vortex core diameter and vortex separation distance. When the ratio of separation distance to vortex core diameter is approximately 1.9 the two cores will merge downstream to form one vortex.

Based on the core radius documented in Fig. 9 for 4c, the ratio of core separation (0.025m) to core diameter (0.018m) is approximately 1.4 and the vortices, at this location, should be in the process of merging as this value is below the threshold for vortex merging to begin. At 8 chord

lengths downstream the vortices are virtually completely merged and so the rapid formation of the single vortex agrees with the Rossow condition.

There is a slight discrepancy between the vortex separation depicted in Figs. 10 and 12 for 8 chord lengths downstream, 0.5c blade separation. This gives an indication of the sensitivity of the results to the accuracy with which the blade incidence and spacing could be set. In Fig. 10, the blades were set at the required incidence and spacing and not altered when the downstream investigation was conducted. However, in the blade separation investigation (Fig.12) the blades were altered significantly between individual measurements. A small discrepancy between the blade spacings in the two cases would be enough to produce the slight discrepancy between the two figures. This was one of the main reasons for adopting a consistent systematic approach to the investigation of each parametric effect rather than attempting to extract trends from a general test matrix.

In Figure 13 the measured spatial evolution of each vortex with respect to the centre line of the tunnel (looking upstream) is compared with that predicted using the simple quasi three dimensional model. The data presented in this figure correspond to the measurement locations indicated in Figs. 10 and 11. For modelling purposes, the inputs to the model were the vortex strength, position and size determined from experiment at one chord length downstream of the vortex generator. At this location, which is identified in the figure for both vortices, the modelled and experimental results are coincident and so only the symbol representing the numerical model is visible. Each subsequent point represents a downstream progression of one chord length. It should be noted that at the one chord length position, the vortex has not completely rolled up and so the vortex strength is slightly underestimated. This was investigated by using input parameters at the 2c,3c and 4c positions. No appreciable difference from the present prediction was noted in these cases.

The figure illustrates a significant initial inward convection of the two vortices with a slight clockwise rotation before the vortex system assumes the typical full rotational behaviour expected. The early inboard convection is consistent with the reduction in core separation with increasing blade incidence discussed in relation to Fig. 7. In the case of the upper vortex (vortex 1), however, no movement was detected between 0.1c and 0.5c downstream and so these points are coincident.

As can be seen from the figure, the upper vortex follows the theoretical trajectory very well and the predicted locations up to 7 chord lengths are satisfactory. However, the cross-flow velocities recorded at nine and ten chord lengths downstream were low and the vortex cores were particularly diffuse. This made accurate determination of the x-axis (horizontal) core locations very difficult. This may account for the deterioration in agreement between the model and experiment at these points.

The trajectory of the lower vortex (vortex 2) is, unfortunately, significantly different from that predicted by the numerical model. In these experiments the traverse was oriented horizontally and rested below the centre line of the wind tunnel. It is believed that this vortex was influenced by a vertical velocity component created by the blockage of the traverse which, on the right of Fig. 13, acted against the induced velocity from vortex 1 and correspondingly acted with the induced velocity on the left. Despite this the lateral movement of the vortex is well predicted.

## Conclusions

A study of the flow field created by a twin vortex generator has been conducted. It has been demonstrated that the cross-flow created by the resulting vortex system can be adequately represented by a simple vortex core model. On the basis of this model, the strength, growth, lateral spacing and rotation of the vortex system were studied. It was found that the core size of the twin vortices grew almost linearly with downstream distance while the strength remained constant. The spacing between the two cores remained almost constant with only a slight decrease as the downstream distance increased

Finally the rotation of the vortex system was modelled by a straight forward consideration of the induced velocity field. Generally, good agreement with experiment was obtained despite the influence of interference effects on the experimental data

## Acknowledgements

The authors would like to acknowledge the support of the British Ministry of Defence through the Defence Evaluation Research Agency (DERA). The work was funded by the DERA under extra-mural agreement ASF/2163U.

## References

1. Kokkalis A., "An Experimental Investigation of Parallel Blade-Vortex Interaction for a NACA00015 Airfoil", *PhD Dissertation, University of Glasgow, Dept. of Aerospace Eng., 1988.*

2. Horner M.B., Saliveros E., Galbraith R.A.McD., "An Experimental Investigation of the Oblique Blade-Vortex Interaction", *17th European Rotorcraft Forum, Berlin, Germany, Sept. 1991.*

3. Horner M.B., Stewart J.N., Galbraith R.A.McD., Grant I., Coton F., Smith G.H., "Preliminary Results from a Particle Image Velocimetry Study of Blade-Vortex Interaction", *19th European Rotorcraft Forum, Cernobbio, Italy, Sept. 1993.*

4. Horner M.B., Stewart J.N., Galbraith R.A.McD., Grant I., Coton F., "An Examination of Vortex Deformation during Blade-Vortex Interaction Utilising Particle Image Velocimetry", *19th Congress of the International Council of the Aero. Sciences, Anaheim, California, Sept 1994.*

5. Coton F.N., De la Iglesia F., Galbraith R.A.McD., Horner M.B., "A Three-Dimensional Model of Low Speed Blade-Vortex Interaction", *20th European Rotorcraft Forum, Amsterdam, The Netherlands, Oct 1994.*

6. Padakannaya R., "The Vortex Lattice Method for the Rotor-Vortex Interaction Problem", *NASA CR-2421, July 1974.*

7. Ellin A.D.S., "An In-Flight Investigation of Lynx AH Mk5 Main Rotor/Tail Rotor Interactions", *19th European Rotorcraft Forum, Cernobbio, Italy, Sept. 1993.*

8. Scott M.T., Sigl D., Strawn R.C., "Computational and Experimental Evaluation of Helicopter Rotor Tips for High -Speed Flight", *J.Aircraft 28, 403-409, June 1991.*

9. Lowson M.V., "Progress Towards Quieter Civil Helicopters", *Aero. J. , 209-23, June/July 1992.*

10. Brocklehurst A., Pike A.C., "Reduction of B.V.I. Noise Using a Vane Tip", *A.H.S. Aeromechanics Specialists Conf., San Francisco, Jan. 1994.*

11. Tyler D.J., Vincent A.H., "Future Rotorcraft Technology Developments", *Aero. J., 451-60, Dec.1996.*

12. Clausen P.D., Piddington D.M., Wood D.H., "An Experimental Investigation of Blade Element Theory for Wind Turbines - Part 1. Mean Flow Results", *J. Wind Eng. Ind. Aero. 25, 189-206, 1987.*

13. Lamb H., "Hydrodynamics" , 6th Edition, Cambridge University Press, 1932.

14. Vatistas G.H., Kozel V., Mih W.C., "A Simpler Model for Concentrated Vortices", *Exp. Fluids 11, 73-6, 1991.*

15. Scully M.P., "Computation of Helicopter Rotor Wake Geometry and its Influence on Rotor Harmonic Airloads", *ASRL TR-178, M.I.T., March 1975.*

16. Leishman J.G., Baker A., Coyne A., "Measurements of Rotor Tip Vortices Using Three-Component Laser Doppler Velocimetry", *J. American Helicopter Soc. 41, 342-353, Oct. 1996*

17. Han Y.O., Leishman J.G., Coyne A.J., "Measurements of the Velocity and Turbulence Structure of a Rotor Tip Vortex", *AIAA J. 35, 477-85, Feb.1997.*

18. Rossow V.J., "Convective Merging of Vortex Cores in Lift-Generated Wakes", *J. Aircraft 14, 283-290, 1977.*

19. Rossow V.J., "Prospects for Destructive Self-Induced Interactions in a Vortex Pair", *J. Aircraft 24, 433-40, 1987.*

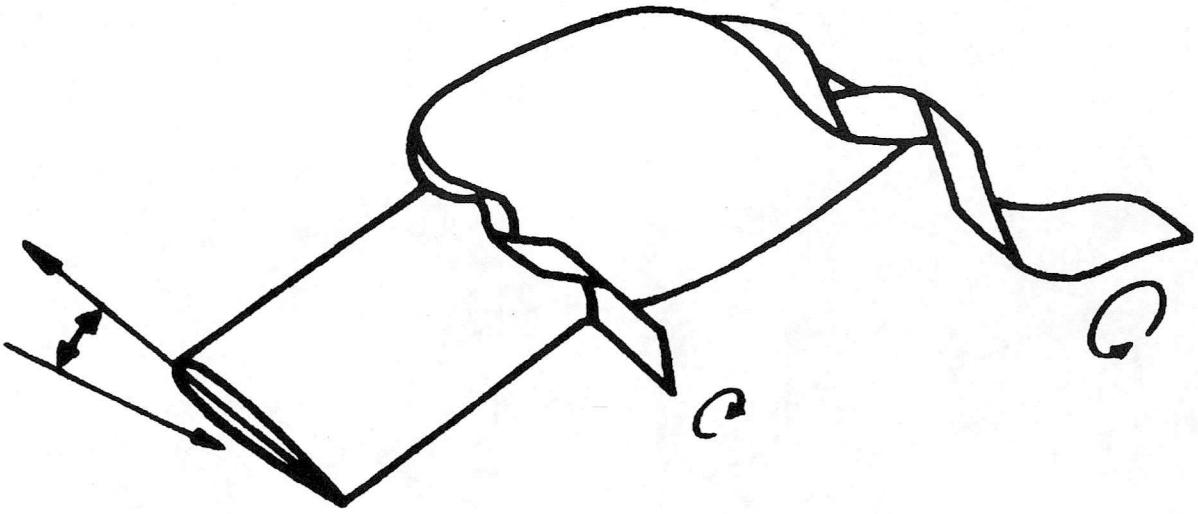

Fig. 1. Illustration of the vortical flow field associated with the BERP tip at high incidence (Ref.8)

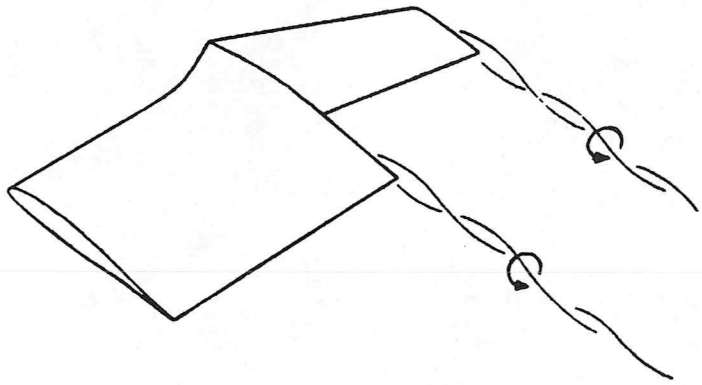

Fig. 2. Illustration of the vortical flow field associated with the Vane Tip (Ref. 10)

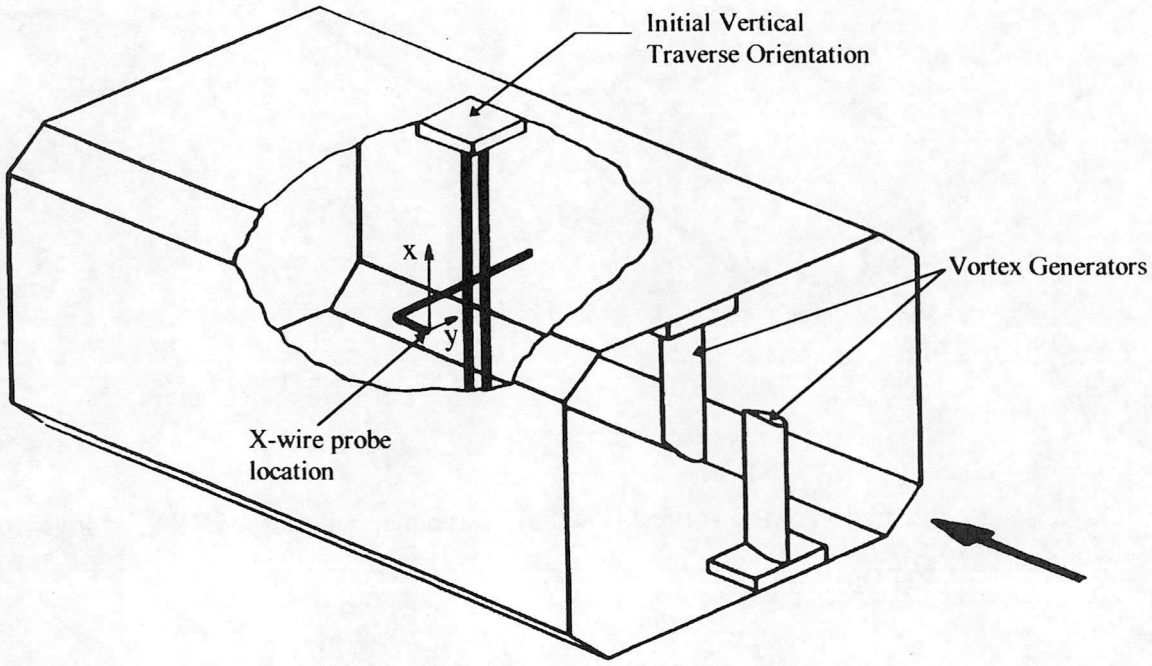


Fig. 3. Illustration of experimental set-up

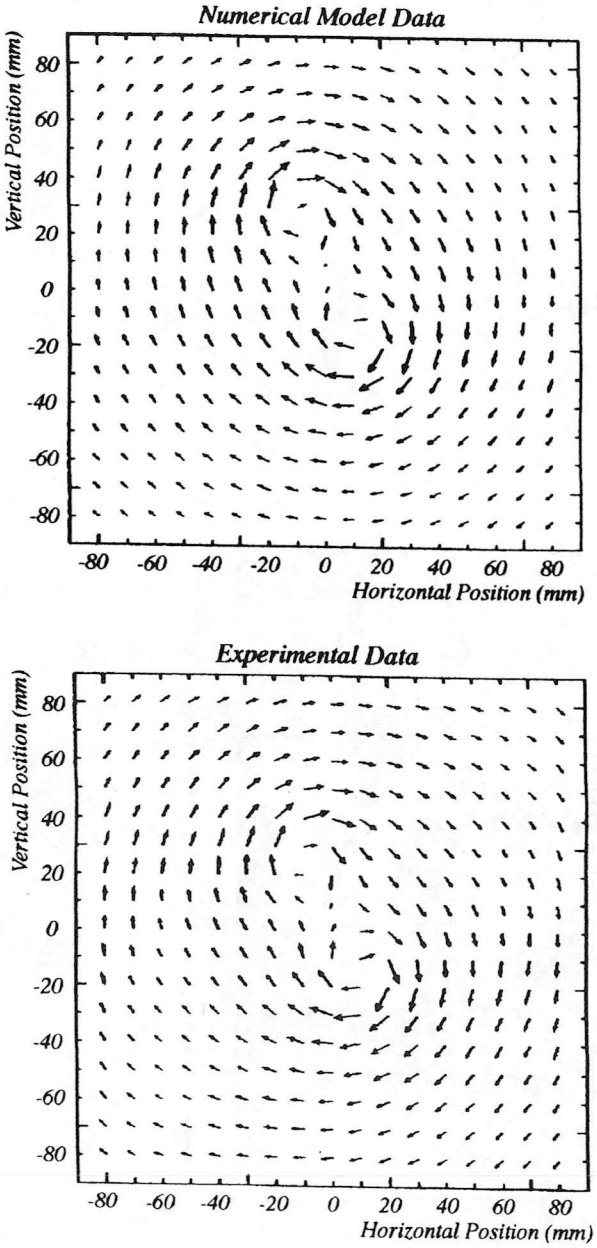


Fig. 4. Comparison of vector plots from numerical model and experimental data

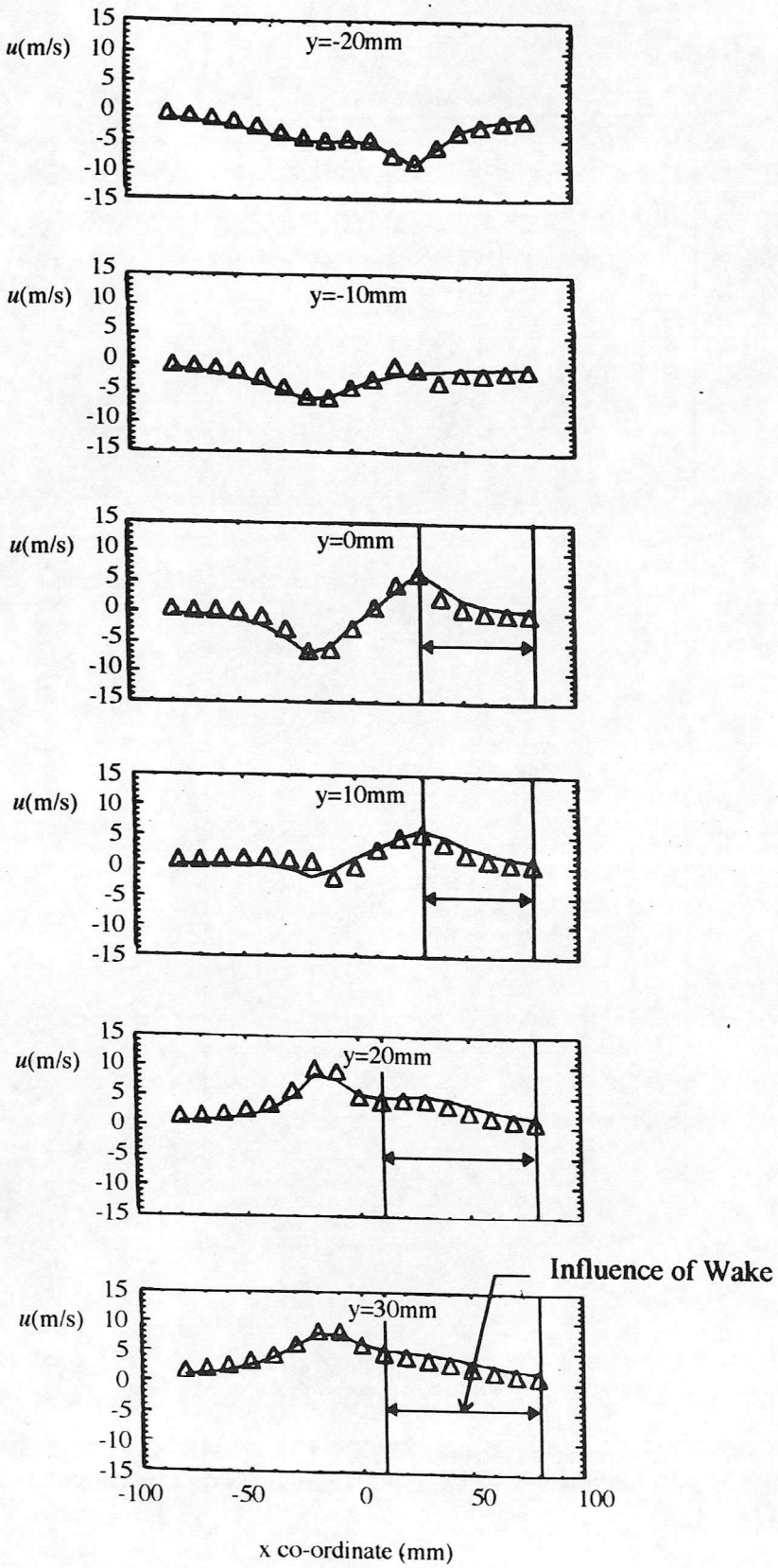


Fig. 5a. Comparison of experimental *u* (vertical ) velocity component with numerical model

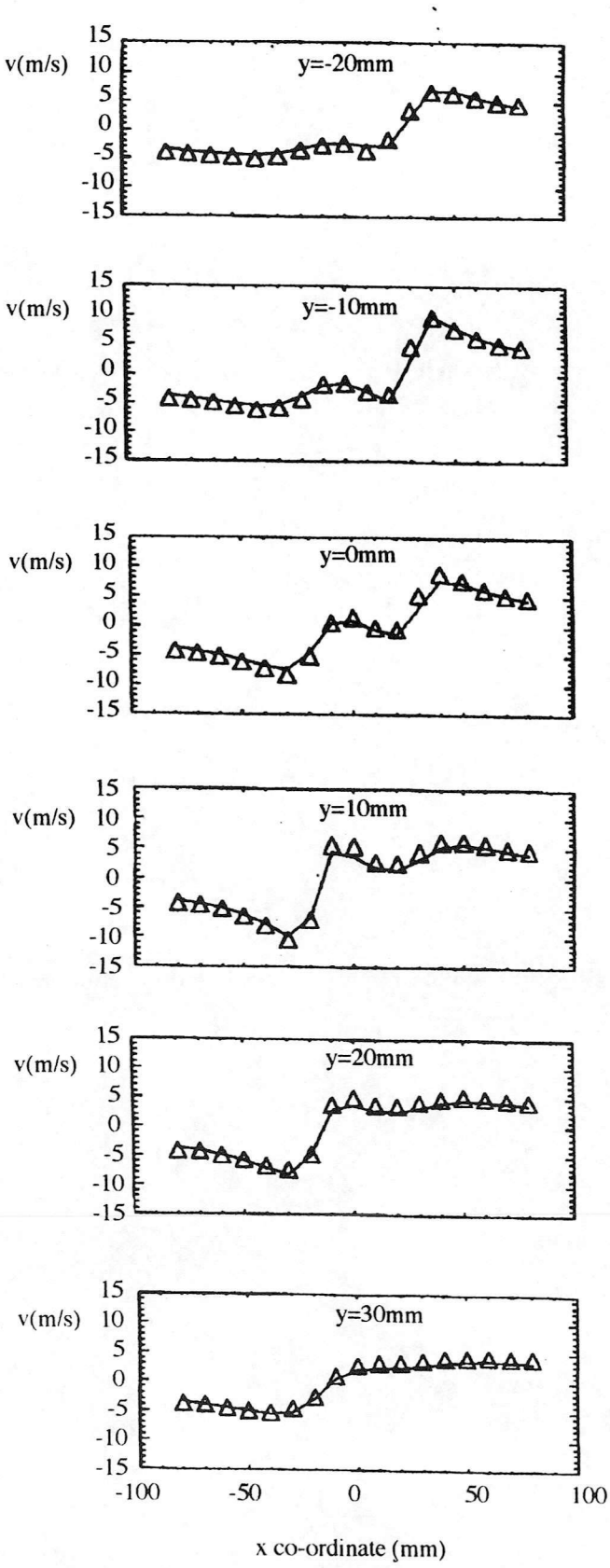


Fig. 5b. Comparison of experimental *v* (horizontal ) velocity component with numerical model

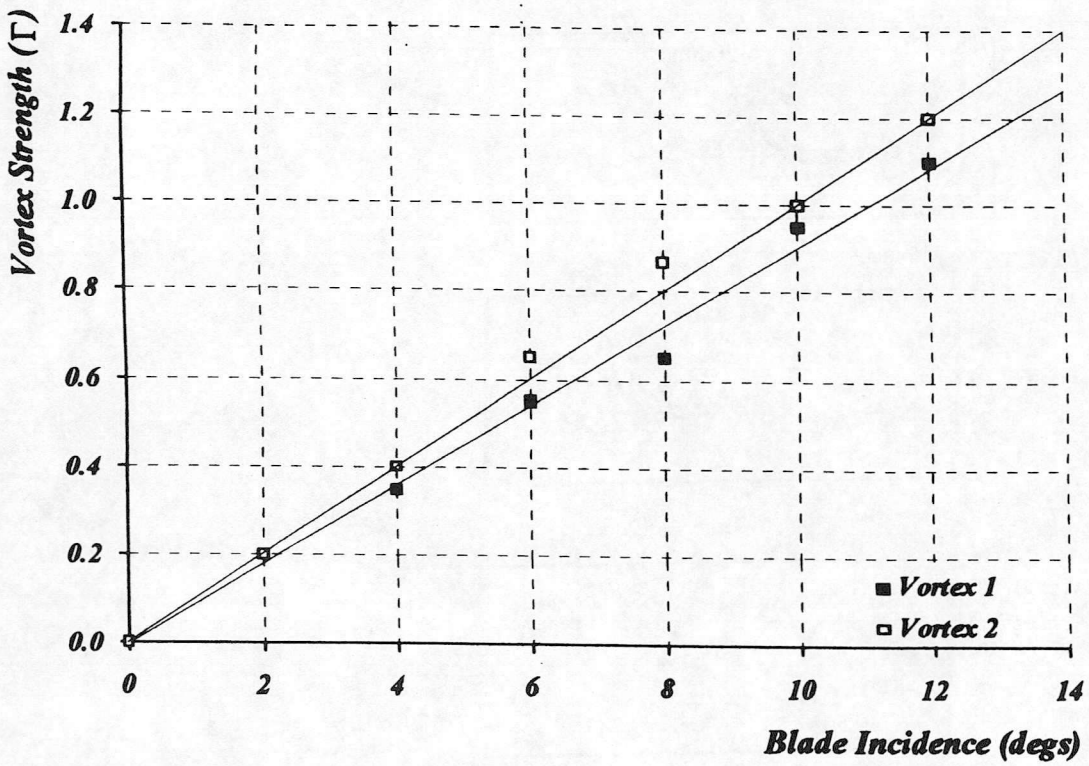


Fig. 6. Variation in vortex strength with change in incidence at 4.3c downstream of trailing edge

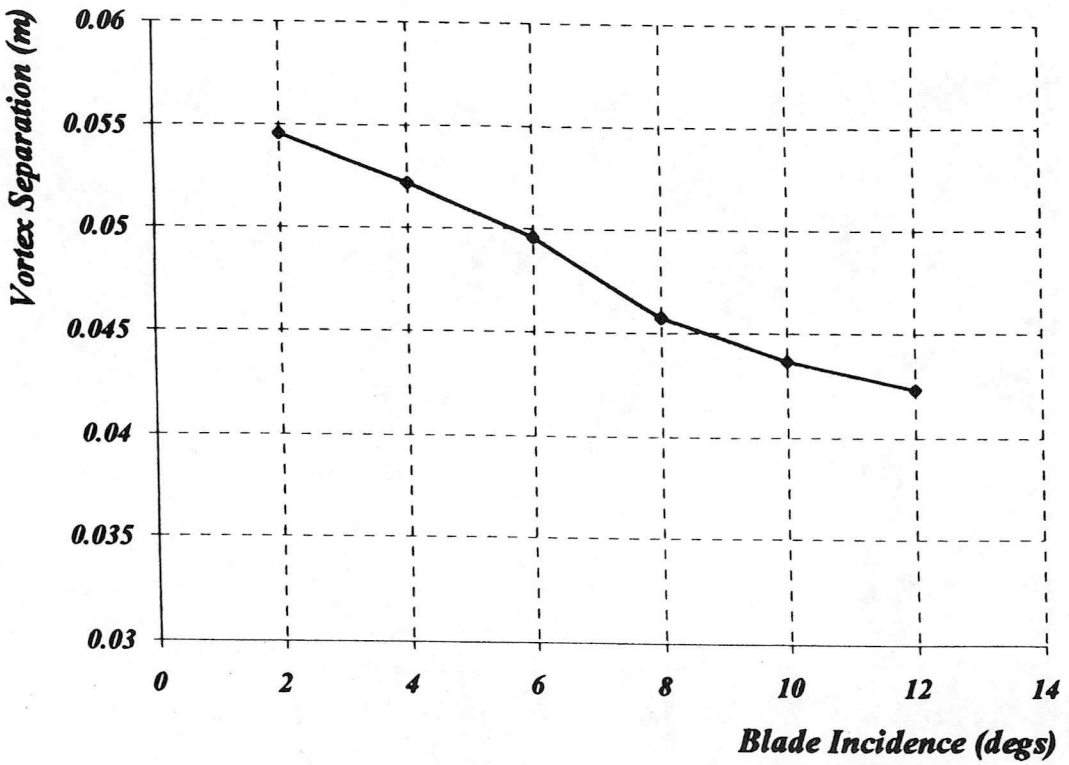


Fig. 7. Variation in vortex core separation with a change in incidence at 4.3c downstream

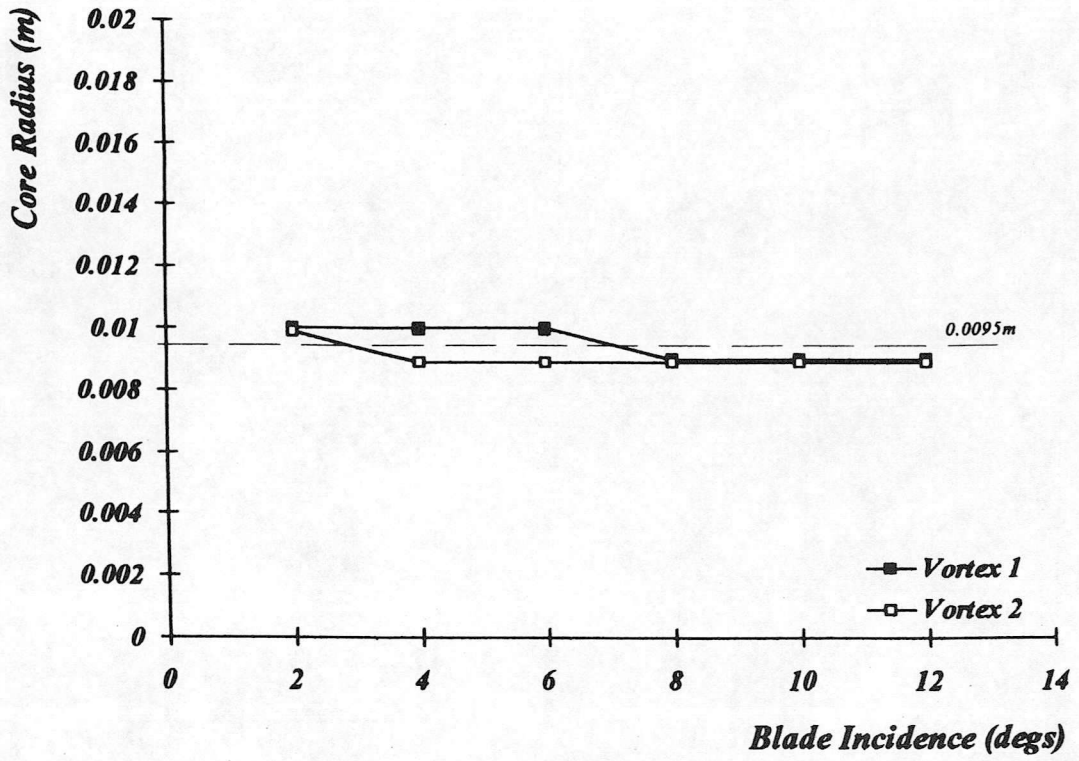


Fig. 8. Variation in core size with a change in incidence at 4.3c downstream

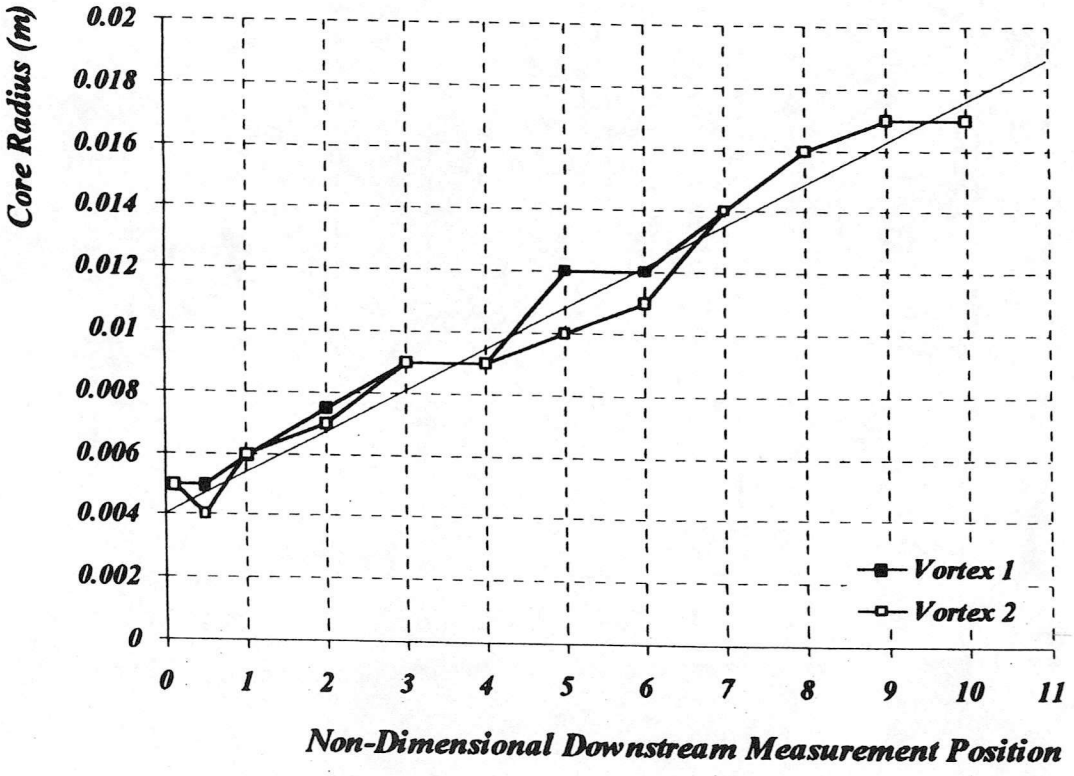


Fig. 9. Variation in core radius with downstream measurement position

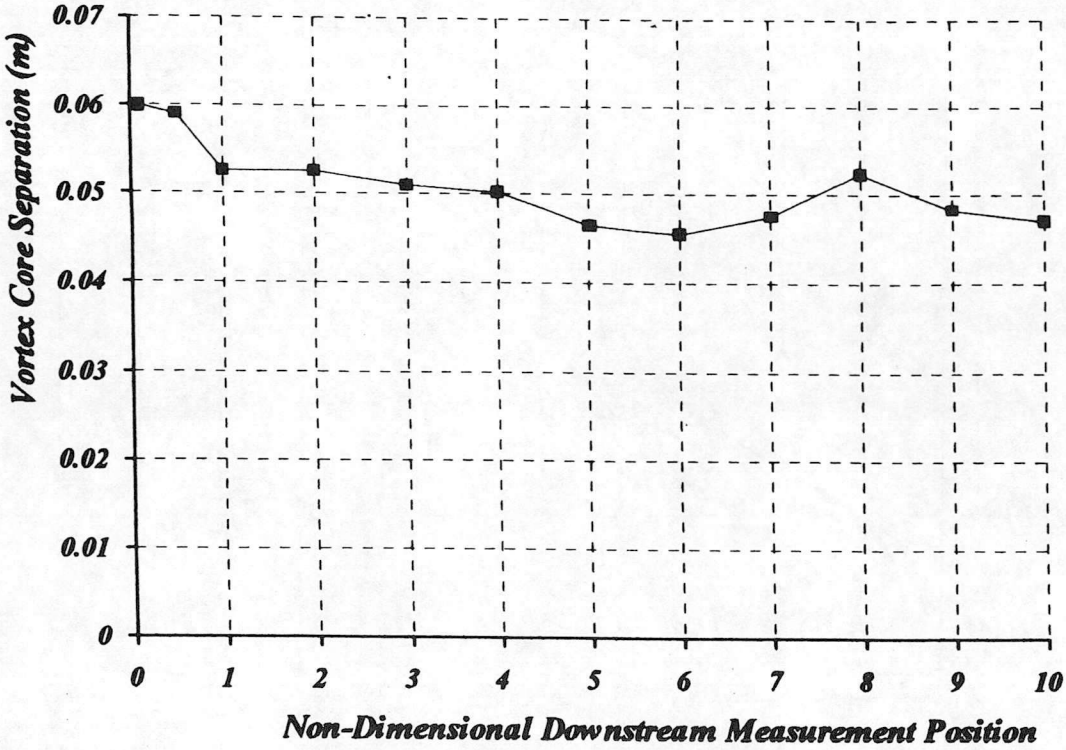


Fig. 10. Variation in vortex separation with downstream measurement position

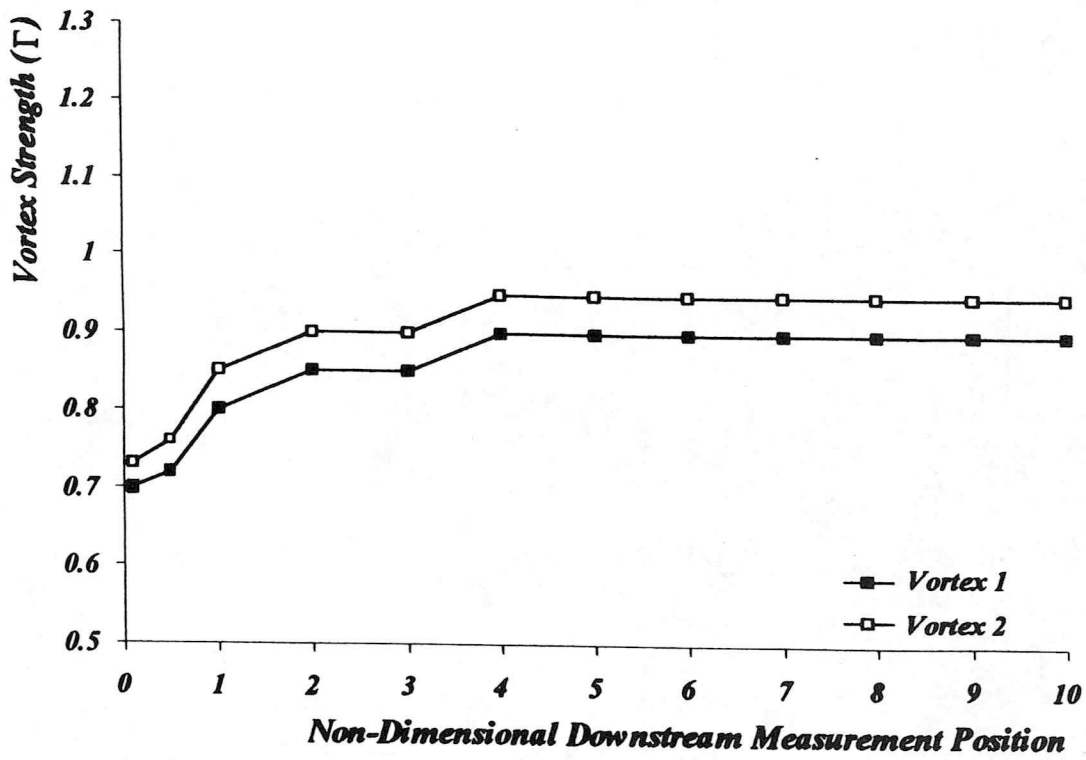


Fig. 11 Variation of vortex strength with downstream measurement position

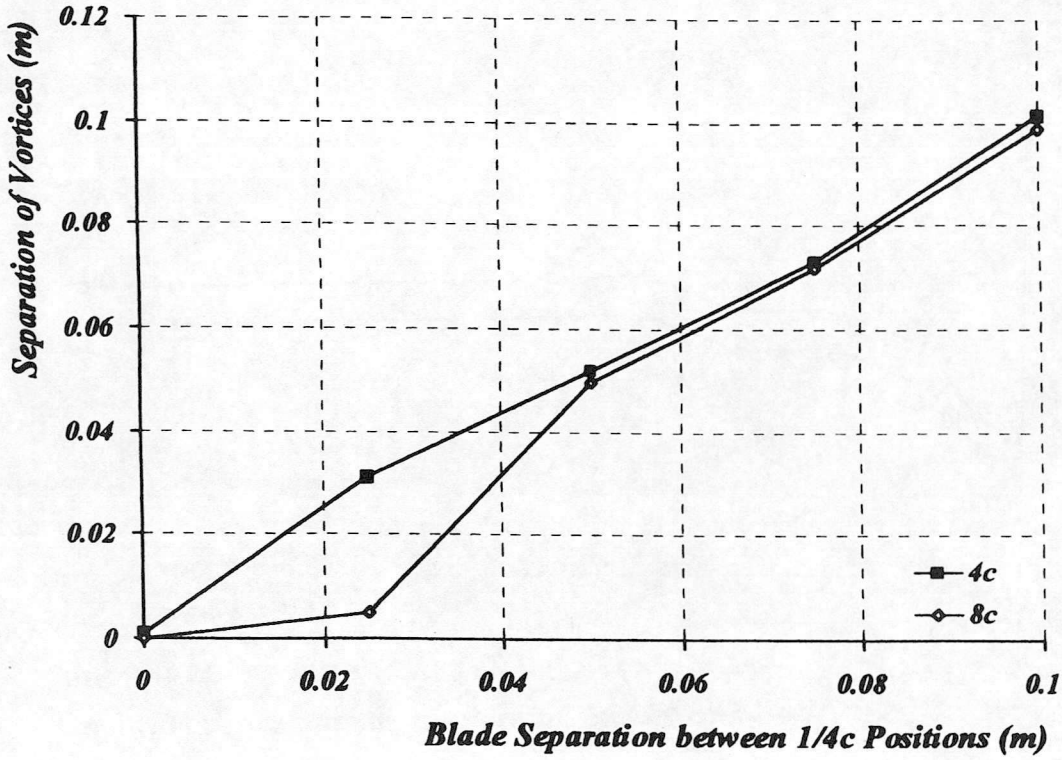


Fig. 12. Variation of vortex separation with respect to blade separation for downstream measurement positions of 4c and 8c.

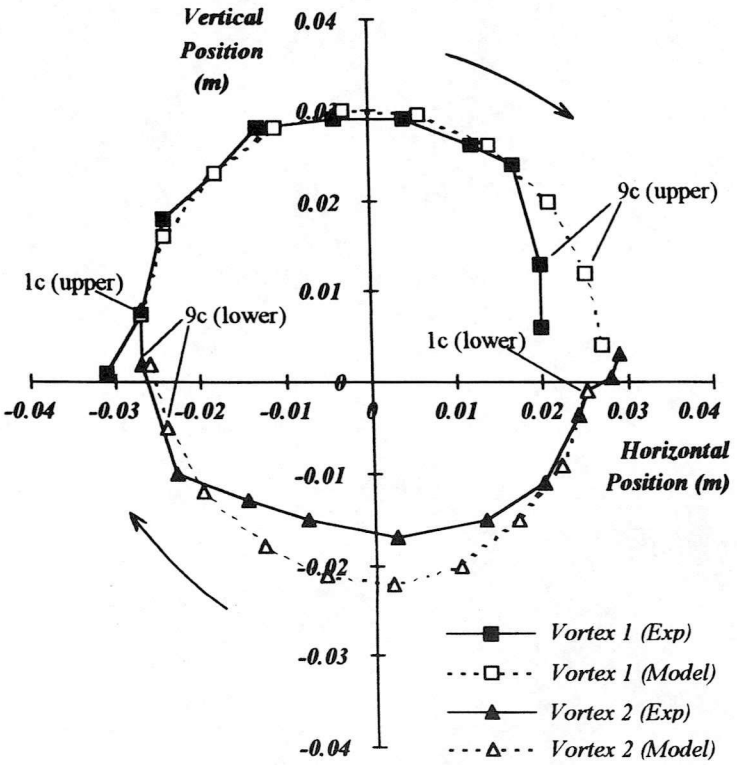


Fig. 13. Measured location of twin vortices with respect to test section centre for variation in downstream position and in comparison with numerical model

# Appendix 2

## USE OF NUMERICAL MODEL IN THE CONCEPTUAL DESIGN OF A NEW BLADE VORTEX INTERACTION FACILITY

by

C.M. Copland
F.N. Coton
R.A.McD. Galbraith

Glasgow University Aero. Report No. 9509

# USE OF A NUMERICAL MODEL IN THE CONCEPTUAL DESIGN OF A NEW BLADE VORTEX INTERACTION FACILITY

**By**

**C.M. Copland , F.N. Coton , R.A.McD. Galbraith**

**University of Glasgow**

**Department Of Aerospace Engineering**

**Internal Report Number 9509**

# Contents

# Nomenclature

| | |
|---|---|
| AOA1 | Geometric angle of incidence at ALP1 |
| AOA2 | Geometric angle of incidence at ALP2 |
| c | Rotor chord length |
| R | Rotor tip radius |
| X,Y | Position of rotor axis in wind tunnel coordinate system |
| Start Azi | Rotor start azimuth |
| AZI1 | Rotor position at end of initial acceletation |
| AZI2 | Rotor position at end of second acceleration or constant velocity phase. |
| Stop Azi | Rotor position at end of deceleration phase |
| Start Alp | Rotor position for start of pitch up |
| ALP1 | Rotor position with incidence at AOA1 |
| ALP2 | Rotor position with incidence at AOA2 |
| Stop Alp | Rotor position for end of pitch down |
| WS Vel | Working Section Velocity |
| TV1 | Specified tip velocity at AZI1 |
| TV2 | Specified tip velocity at AZI2 |
| tmax | Maximum time of simulation |
| tstep | Time step during simulation |
| nplot | Number of wake plots |

# Summary

This report describes and presents results from a numerical model developed to aid the preliminary design of a new wind tunnel based blade-vortex interaction (BVI) facility. The proposed facility will simulate tail rotor BVI by interacting a transverse vortex, produced by a single-bladed rotor situated in the wind tunnel contraction, with a blade mounted vertically in the tunnel working section. In the model a three dimensional source panel method is used to calculate the constrained flow through the low speed wind tunnel and a free wake vortex model represents the wake generated by the upstream rotor. Convection of the wake is then determined by superposition of the undisturbed tunnel velocity and the induced velocity components from the wake itself. Results, obtained via a parametric analysis, illustrate the geometry of the wake and tip vortex and their relation to basic design parameters. In particular, two possible operational strategies for the upstream rotor are examined with reference to developement of the experimental facility. It is concluded that, while a short duration finite rotor traverse may be the optimum vortex generation strategy, a continuous running rotor may be the most cost effective option.

# Introduction

The flow field around modern rotor craft is both highly complex and unsteady. Of considerable importance are the concentrated trailed tip vortices generated by the main rotor which may convect and interact with the other rotor blades, the tail rotor and the fuselage. In powered descent and vigorous manoeuvring these interactions become more distinct with the result of unwanted phenomena such as noise, vibration and, in the case of interactions with the tail rotor, unusual yaw handling and control problems. The need to reduce these effects requires a clear understanding of the fundamental fluid dynamic characteristics of blade-vortex interactions.

In certain flight cases the main rotor will experience multiple vortex interactions which occur when a main rotor blade interacts with the tip vortex of a preceding blade. The angle of the interactions varies from near parallel through what is commonly termed oblique interactions to near perpendicular. These interactions are all characterised by the interacting vortex lying in a plane parallel to the plane of the blade. This is not the case, however, with main rotor tip vortex /tail rotor interactions when the interacting vortex lies in a plane perpendicular to that of the blade. Experimental research has, to date, targeted the problem of interactions on the main rotor blade but there is currently a considerable dearth of information on interactions associated with the tail rotor environment.

A number of experimental studies have been carried out into the fundamental mechanism for a vortex approaching a rotating blade. In this respect the studies conducted by Surendraiah[1] and subsequently Padakannaya [2] using an upstream wing tip to generate a vortex that interacted with a downstream rotor are seminal work. This work enabled the gross features of the blade-vortex interaction to be illustrated. Researchers at NASA Ames[3] developed this approach further in the

eighties using a similar facility but with better resolution in the pressure data allowing a "convective disturbance" in the airfoil pressure distribution to be identified. Further studies at Glasgow University [4-6] improved on previous pressure and aerodynamic load measurements but also provided vital flow field information through the use of Particle Image Velocimetry (PIV). The PIV results provided high quality images of the local blade flow field at various stages of the interaction process.

In wind tunnel tests of a model MBB BO-105 rotor Van der Wall [10] successfully measured the pressure distribution around one instrumented rotating blade of a complete rotor system to concentrate on BVI locations and noise radiation. Test were conducted in high and low speed cases representing descent flight conditions with a high noise level. The low speed BVI case was characterised by very strong vortex interactions at the blade tip which produce an extreme noise producing state commonly known as blade slap. This enabled the BVI locations for the complete rotor to be determined and then comparison drawn to the aerodynamic lift and moment distributions. Whilst not concentrating on the fundamental fluid dynamic aspect of BVI, the study identified that, in the full rotor environment, many blade vortex interactions involve pairs of trailed vortices. These pairs of voritices occur on the advancing side of the rotor, rotating in different directions, in the high speed case. There is still a need for continued research into twin vortex interactions as, at present, only the mechanism for the generation has been noted and not the detailed influence on the local blade flowfield and noise radiation.

Other studies have used different experimental set-ups to investigate the fundamental aspects of blade vortex interactions, notably Seath et al. [7] and Straus et al. [8]. In these tests the pitching motion of an upstream aerofoil generated a nominally two-dimensional shed vortex which convected downstream to interact with a second (fixed) airfoil. These test do have the advantage of varying the orientation of the fixed blade enabling the vortex line to line to lie either perpendicular or parallel to the

blade surface. However, it is doubtful whether the structure of the shed vortex comprehensively mimics that of the trailing tip vortex of a main rotor.

Unfortunately there hve been few experimental studies conducted on main rotor /tail rotor interactions. Most notible was the in-flight study carried out by Ellin [11] on the DRA Research Lynx with an instrumented tail rotor designed to obtain pressure data. This study noted six distinct regions of main rotor/tail rotor interaction each corresponding to a different mechanism in the low speed envelope. The tests were carried out in hover, forward flight and in what is commonly termed quartering flight. Ellin stated that further experimental work was required into blade vortex interaction with the vortex perpendicular to the blade surface to investigate these phenomena.

Obviously, rotorcraft flight testing is an expensive and, to most, inaccessible method of examining tail rotor interaction. Consequently, wind tunnel based studies may provide the most appropriate means of enhancing contemporary understanding of BVI. The crucial factor in all experiments to date has been the manner in which the interacting vortices have been generated and their subsequent trajectory through the wind tunnel's working section. It is essential that the detailed structure of the interacting vortex and the vortex trajectory, its stability and tendency to "wander" from its mean path are known. This applies irrespective of the method of generation of the vortex.

The present study is primarily concerned with the design of a facility for the generation of a transverse trailed tip vortex in a low speed wind tunnel. The facility will consist of a single-bladed rotor positioned in the contraction of a low speed wind tunnel. The design of the experimental facility is in progress at present and a numerical model has been developed to assist. In particular the model has been used to determine the convection and geometry of the wake and related tip vortex produced by the rotor as they progress through the working section. The computational model

and selected results are discussed and related to the practical development of the new BVI facility. This facility, once developed, could be used to investigate fundamental aspects of many different vortex interactions but, in particular, interactions where the vortex orientation is perpendicular to a blade.

# Developement Plan Of Proposed Experimental Facility

The proposed experimental facility will consist of a single, variable pitch, rotating blade with a NACA0015 cross section. The blade will be positioned in the contraction (illustrated in fig.1) of the Department Of Aerospace Engineering's 3ft.x3ft low speed wind tunnel at the University Of Glasgow . As the blade rotates and pitches up, a vortical wake will be generated containing a strong trailed tip vortex. The wake will then convect downstream through the remainder of the contraction and into the working section. This will allow an instrumented blade to be place in the tunnel working section to examine blade-vortex interactions.

To gain some insight into the sizing of the drive and mechanical set-up for the rotor blade a numerical model of the wake produced by the vortex generator has been developed. This has provided valuable information to aid in the mechanical design which is currently underway. Once the vortex generator has been constructed, measurements will be made using hot-wire anemometry to determine the three dimensional convection, strength and geometry of the trailed tip vortex. The measurements will be taken using cross-wire porbes and a TSI Model IFA300 Constant Temperature Anemometer (CTA).

It is important to note that the primary objective of the study is to assess the feasibility of a specific technique for generating a transverse trailed tip vortex. If the facility proves to be successful, BVI studies will then be initiated.

# Outline Of Numerical Model.

## Introduction

Of particular interest in this study were the relevant geometric parameters and operating conditions of the blade and the wind tunnel to attain a good representation of a transverse vortex. The developed code, therefore, had to be adaptable to enable a comprehensive analysis of fundamental input parameters such as position, size and motion of the blade, and working section velocity. Results had to illustrate the three dimensional developement of the wake (and related tip vortex) through the wind tunnel with enough clarity to isolate the specific effects of a particular design parameter.

The features of the experimental facility that had to be modelled were the vortical wake structure from the rotating blade and the mainstream flow through the wind tunnel. The wake from the rotor was represented by a free wake model consisting of a lattice of shed and trailed vortex elements. The wake was generated using classical lifting line theory which enables the spanwise and temporal changes in bound circulation to be determined and hence the strength of the vortex elements. These elements were then convected through the contraction and working section of the wind tunnel with the superposition of the local velocity, calculated via a three dimensional source panel method, and the induced velocity components from the vortex elements. Due to the inviscid nature of the model no account has been taken for vortex dissipation and so there is no change in the vortex strength with time.

## Model Of Wind Tunnel

A source panel method was used to calculate the incompressible, inviscid, potential flow through a low speed wind tunnel. This was based on the work of Hess and Smith[12]. The method was chosen for its relative simplicity and adaptability to internal flows. A considerable amount of theory is available on panel methods[13] and the choice of which to use is determined primarily by the case in question and geometric limitations. Due to the simple geometry of the modelled portion of the wind tunnel and the non-lifting nature of the body, a plane quadrilateral element with constant source distribution was deemed sufficient in this case.

The internal surface of the wind tunnel was discretised into approximately 1000 individual quadrilateral elements representing the Settling Chamber, contraction, working section and diffuser. Since the accuracy of the calculation not only depends on the number of quadrilateral elements used but also on the manner in which these elements are distributed over the surface, a non-uniform distribution of panels was used. In particular, panels were concentrated in the regions of the contraction (area of high curvature) and the working section (area of interest).

Initially, the model requires the specified geometry of the tunnel and from this calculates the corner points of the quadrilateral elements. The control point of each panel, where the fluid velocity normal to the elements is required to vanish (Neumann boundary condition), is then determined. This then allows the induced velocity matrix to be calculated. This induced velocity matrix depends solely on the geometry of the quadrilateral elements and is independent of the onset flow. The matrix contains the components of velocity induced at a point in space by a plane quadrilateral having a constant unit value of source density. This is evaluated for the normal velocities induced by all the quadrilateral elements at each other's control points. Multiplying the normal velocity induced by an element at a particular control

point for a unit source density by the constant but unknown value of the source density on that element, summing over all elements, and repeating for each control point gives the set of total normal velocities at the control point due to the entire approximated body surface. The analytical expressions for this are given in refs. 12,13.

At this stage, the boundary conditions for the surface are now employed. This entails equating the induced normal velocities and the normal components of the onset flow at the control points of the panels to zero. The variation of onset velocity through the wind tunnel, as a result of the changing cross sectional area is obtained be application of the conservation of mass equation based on a specified working section velocity. Once the normal components of this onset flow have been calculated at each control point, the Neumann boundary condition is then applied. This results in a set of linear algebraic equations which is then solved for the required source density distribution using the Gauss-Seidel iterative method.

Once the source density distribution is known the three velocity components at any point in the contraction can be calculated. This is done in exactly the same way as for the induced velocities at the control points i.e. velocities induced by all the panels are calculated, and then added to the local onset flow velocity to get the final total velocity at the prescribed point.

## Model Of Rotor Blade and Wake

The model of the rotor blade and wake is based on the work of Coton and Iglesia[9]. Their work was developed to examine how a stream wise convecting vortex interacts with a rotating blade of fixed incidence running at a specified constant blade tip speed. For the present study, it was necessary to remove the convecting vortex and

make provision for variation of the blade incidenceand angular velocity. These features, together with the inclusion of the wind tunnel wall effect, were incorporated by substantial modification of the existing code.

The single blade rotor with a NACA 0015 profile is modelled using a lifting line positioned at the quarter chord line. This line is discretised into several sections and the bound circulation determined via two-dimensional lift curve data fot the aerofoil section. Shed vorticity appears as the variation of the bound circulation with time and trailed vorticity as the difference in circulation between two adjacent spanwise sections. This vorticity is represented in the wake by discrete trailed and shed vortex filaments which are added at each time step. The manner in which these wake filaments move is then determined by a free wake approach. In it, the wake shape is modified at each time step by integration of the velocity field according to the second order Adam's-Bashforth predictor equation. An essential feature of this approach is the calculation of the velocity induced at each node point by all wake filaments and bound vorticity elements. This, together with an increment in the angle of incidence induced at the blade by the wake, is evaluated by application of the Biot-Savart equation.

Within the numerical model, the blade is positioned relative to the wind tunnel co-ordinate system at a location in the contraction. All the rotor and wake calculations are relative to a hub fixed co-ordinate system but are easily transformed into a tunnel fixed co-ordinate system for calculation of the local velocity components. The model allows input specification of azimuthal blade tip velocity and geometric angle of incidence functions. There is also an option to run the blade continuously or for a short period with a specified acceleration/deceleration tip velocity profile. The blade is assumed to be rigid along its span and no allowance has been made for blade flap.

# Parameters In The Numerical Model

The numerical model initially reads in an input parameter file which contains all the relevent variables for use in the parametric analysis. The file simplifies alteration of test conditions when running numerous different cases. A discription of the parameters contained within this file is given below.

## Blade Axis Position

The rotor blade axis is positioned relative to the wind tunnel co-ordinate system (as indicated in fig.1) whose x-axis lies along the centreline of the tunnel and has the z-axis positive upwards. The origin of tunnel co-ordinate system is located at the entrance to the settling chamber which corresponds to the start of the modelled portion of the tunnel. Although the blade position could be varied in all three co-ordinate directions, only movement in the x-direction was considered in this study. Typical x-values ranged from 2.5 to 3.5 metres relative to the wind tunnel origin.

## Blade Geometry

The geometry of the blade is specified by the radius and the chord length. These are primarily determined from the maximum allowable radius available wherever the blade is positioned in the contraction. Values range between 0.8 and 0.55 metres. Changes in chord length provide adjustment of the circulation strength and hence the strength of the trailed tip vortex.

## Blade Tip Speed

The blade tip speed can be specified either as a constant for continuous running or as a tip velocity distribution in relation to azimuth. Thus, the blade can be accelerated and decelerated from a specified starting azimuth to a final stopping azimuth.

## Working Section Velocity

The working section velocity is specified and used to calculate the required source density. The source density distribution is then used to calculate the local velocities in the wake and on the lifting line due to the wind tunnel geometry. In the study the wind tunnel working section velocity was varied between 10 and 30 m/s which represent the operational limits of the low speed wind tunnel being modelled.

## Geometric Angle Of Incidence

The geometric angle of attack is specified at individual azimuthal positions to give an angle of attack distribution for one revolution. For the present application, this involves a pitch-up phase from zero incidence, a constant pitch or ramp down phase to control tip vortex strength and a final pitch down phase to zero incidence. Values up to a maximum of 10 deg were considered although, for the majority of cases, a maximum geometric angle of incidence of 5 degrees produced an adequate tip vortex.

## Azimuthal Positions Of Blade

It is necessary to specify a series of motion defining blade positions when the model is used in the acccelerating/decelerating configuration. The specified azimuthal positions correspond to the start and stop positions of the blade and the change over from acceleration to deceleration phases. In this way, three phases of motion can be defined. The first phase consists of an initial acceleration up to a specified tip speed which is sufficient to overcome reversed flow problems. In the second phase, the blade is either accelerated again or held at a constant tip speed. Finally, the blade is decelerated back down to rest.

## Rotor Blade Root Cut-Off

To eliminate any numerical instabilities caused by the rotor hub arrangement a root cut-off is required. This is set at 20 % of the rotor radius. In the experimental set-up

this portion of the blade will be taken up by the pitch mechanism and rotor hub, consequently, it will contribute little to the aerodynamic behaviour of the blade.

## Wake Core

A Scully vortex was adopted for the vortex elements with the vortex core radius set at 20 % of the blade chord. This corresponds to typical values obtained from experimental measurements carried out at Glasgow University.

## Influence Of Vortex Filaments

To enhance computational efficiency, there is a cut-off distance beyond which the influence of a vortex filament is assumed to be zero. This can be varied but a value of two metres was found to be optimum.

## Time Step and Duration Of simulation

For a given distance of wake travel, the duration of the simulation is related to the working section velocity, i.e. a slower working section velocity corresponds to a longer simulation time. Similarly, to retain a given level of detail in the rotor wake, the time step is necessarily related to the rotational speed of the blade.

# Results

## Introduction

In the course of the present study, a large number of possible configurations were considered. In this section selected results are presented to illustrate the main influences on geometric features of the tip vortex and wake. The results are presented in two sections corresponding to the modes of operation of the rotor i.e. the limited azimuthal range and continuous running cases. The figures show the plane of the wake and the tunnel walls as viewed from above. In each case, the blade axis is indicated and the blade rotates in a clockwise direction. Three dimensional views of the wake and tunnel are not presented as the wake lattice was found to exhibit little wander notably the cross sectional plane along which it convected.

Initial tests were conducted to determine the appropriate range of each parameter and to identify numerical instabilities in the model. These tests were carried out with the rotor at a fixed incidence and constant rotational speed. Initial results were poor as a consequence of the wake distribution induced by a strong vortex shed from the impulsively started blade. Further tests were, therefore, conducted using a prescribed variation of blade incidence. Thus, by setting the initial blade incidence value to zero and allowing it to increase thereafter, it was possible to eliminate the strong starting vortex.

## Acceleration/Deceleration Cases

The complete set of test cases which were investigated for this operational mode are given in figure 2. These cases are characterised by a specified function of tip speed

versus azimuth which may be sub-divided into three different phases of motion. Firstly, an acceleration at zero incidence brings the blade up to the necessary speed to avoid numerical instabilities associated with reversed flow. This is followed by a constant velocity or second acceleration phase corresponding to the blade crossing the entrance of the working section. Finally, the blade is brought to rest by a deceleration phase at zero incidence. These three phases of motion were initially confined to one revolution to minimise the disturbance which the rotor may have on the tip vortex but it is possible to extend the acceleration and deceleration phases if required. In each case the pitch motion did not have to have the same prescribed azimuthal break-points as the acceleration/ deceleration phases and was independantly prescribed in the input parameter file.

The analysis first concentrated on the variation of blade speed and working section velocity. Figure 4 illustrates one of the first cases examined. The blade tip speed was set at 70m/s using a blade of radius 0.6 metres positioned at 3.3 metres relative to the wind tunnel origin. This corresponds to a blade position close to the working section. The tip speed was held constant through the second phase of motion during which the blade incidence was set at 5 degrees. For this case, the working section velocity was set at 30 m/s which is the highest velocity attainable in the wind tunnel. From the figure, it is noticeable that the wake lattice is fairly sparse as a consequence of the large time step (0.0035 seconds) used in the calculation. This value was chosen purely to minimise computational time in the initial stages of the study. This value is, however, sufficient to provide enough detail to illustrate the effect which the blade speed and tunnel velocity have on the wake geometry. The figure shows that the wake structure is skewed because of its high convection speed. To study perpendicular BVI, a near symmetrical wake structure would be preferred. There are two possible ways of achieving this. It could be done by either increasing the blade tip speed or decreasing the working section velocity. It would be inadvisable to

increase the blade tip speed too much because of mechanical design considerations and so a reduction in the tunnel velocity would be the most appropriate action.

Figure 5 represents a similar case where the working section velocity is reduced to 20 m/s. All other parameters are unchanged from the previous analysis. As can be seen from the figure, the wake is more symmetrical and much less skewed. The tunnel velocity could be reduced further to 10 or 15 m/s but the time taken for the wake to convect through the working section would be higher. With due consideration being given to the practical problem of vortex dissipation with time, it was decided to fix the working section velocity at 20 m/s for future calculations using the same rotor radius.

Although the reduction in wind tunnel operating speed produced a more symmetric wake structure, it was evident that scope still existed to improve symmetry by varying the rotor speed. For thios reason, the next stage in the work was to alter the second phase of the blade motion from the constant tip velocity previously used to a linearly increasing velocity. Figure 6 illustrates one such case. The blade is accelerated up to 50 m/s then accelerated again across the entrance to the working section up to 90 m/s. For this calculation, the time step was decreased to 0.0025 seconds and so there is an increase in the number of vortex filaments in the figure. As before, the motion of the blade was restricted to one revolution during which the blade was pitched up to 5 degrees whilst accelerating, its incidence was then held constant until the blade was pointing approximately downstream, and then it was pitched down to zero degrees. As may be observed in the figure, the changing incidence generated a strong tip vortex on the right side of the wake with weaker tip vortex elements on the left.

As the blade changes from travelling with the flow to moving against it, the relative velocities which it experiences increase as a result of its orientation to the local flow velocity. Consequently, if the blade velocity was held constant across the working

section, there would be a stronger vortex strength on the left side of the wake compared with the right side. It may, therefore be concluded that obtaining a constant tip vortex strength across the working section whilst ensuring that the wake shape is symmetrical is only possible through control of the tip vortex strength by pitching the blade to counter the increase in relative velocities experienced by the blade. Subsequent analysis concentrated on determining this pitching motion profile so a constant tip vortex strength would span the working section.

Figure 7 is typical of results incorporating pitch down motion as the blade crosses the entrance of the working section. Here the blade is still accelerated in the second phase of motion but the final tip velocity is 100 m/s as compared to 90 m/s in the previous example. The blade axis has also been moved slightly forward from 3.3 to 3.45 metres. Since the blade axis has moved further into the contraction in this case, the increase in mainstream velocity at the blade has to be offset by an increase in tip velocity to counter wake skewing. Also, with the blade being positioned further forward and no reduction in the radius, there is less clearance between the blade tip and tunnel wall. This enables the wake to occupy more of the working section and creates a better tip vortex profile. For the case presented, the pitch profile is characterised by an initial increase to 5 degrees followed by a linear reduction to 2.75 degrees as the blade travels across the working section. The incidence is then finally reduced to zero and the blade brought to rest.. The tip vortex strength depicted in the diagram is now fairly constant across the width of the tunnel.

In figure 8 a larger blade of 0.75m was located slighlty further back in the contraction at 3.2m. The working section velocity was also reduced to 15m/s to improve the symmetry of the wake. The blade was initially accelerated up to 50m/s and, as in the previous case, accelerated again across the working section but only up to 90m/s before decelerating back to zero. Even though the tip velocity profile was not altered from previous examples, the increase in blade radius did reduce the rotational speed

of the blade. It is pertinent to note that the separation distance between the tunnel walls and the blade tip was small enough in this case that some doubt must be cast on the validity of the potential flow model within this region.

Before conducting the continual running cases, a single rotation case with a blade of 0.65 metres radius positioned at 3.45 metres was examined for a working section velocity of 20 m/s (figure 9). In this case the blade was accelerated up to a tip speed of 50 m/s which was then held constant across the working section before bringing the blade to rest. Once again, the pitching motion comprised an initial pitch-up to 5 degrees, then a reduction to 2.75 degrees across the working section and finally back to zero. Due to the lower resultant velocities incurred on the left side of the diagram by holding the tip velocity constant there is a lower tip vortex strength in this area compared with previous cases. It was evident from this result that the continual running case would not produce as good a transverse vortex as the single rotation but, as discussed later the mechanical advantages of such an arrangement may be significant.

## Continual Running Cases

The continual running cases are characterised by a series of wake lattice generated by each revolution of the blade. All continual running configurations are listed in figure 3. The main reason for concidering continuous running is to simplify the design of the actual facility. As in the previous section, it is necessary to determine the optimum position of the rotor and the most appropriate setting for the working section velocity. In this case, however, it is the influence which these have on the separation between each individual convecting wake which is of primary importance.

Figure 10 depicts a continuous running case with a constant tip speed of 50 m/s. All parameters are the same as the previous single rotation case although a larger time step has been used. This was necessary as a result of the increased computational time required to run the simulation over a longer duration together with the increased number of vortex filaments compared with the single rotation cases. The geometry of the lattice in Fig. 10 is consistent with the previous single rotation depicted in Fig. 9. In both cases, the incidence of the blade section varied linearly between 5 degrees and 2.75 degrees as it crossed the working section. This resulted in non-symmetry of the tip vortex strength which was subsequently overcome by keeping the blade incidence constant when crossing the working section. This also had the practical advantage of simplifying the pitch motion profile. It should be noted, however, that this does not, result in the generation of a constant strength trailed tip vortex. An exact function for incidence variation could be calculated for each azimuth position to attain a constant tip vortex strength but this would only result in a highly complex pitch/azimuth profile which would be difficult to implement experimentally.

Further continuous running cases concentrated on blade position. In figure 11 the blade was moved back to 2.5 metres. The diagram shows the distortion that occurs in the wake with the blade so far back in the contraction/settling chamber. This is exactly the same phenomenon that was noted in an earlier single rotation case. As may be observed, lower streamwise velocity in this region of the tunnel necessitates a lower tip velocity speed to avoid interaction of consecutive wakes. The convective velocity has to be high enough to produce an acceptable separation distance between wake formations. An increase in tunnel velocity to 30 m/s is illustrated in Fig. 12 but the resulting wake structure is unacceptable because of the high curvature of the vortex system in the working section.

Figure 13 illustrates the optimum continuous running case examined in this study. The parameters are chosen to reduce the high rotational speeds incurred in previous

cases and so ease the design criteria. A blade of radius 0.75 metres is positioned at 3.2 metres from the origin of the wind tunnel coordinate system which, interestingly, corresponds to the configuration of the best single rotation case. The tip velocity was again set at 50 m/s with a working section velocity of 20 m/s. The separation between tip vortices is approximately equal to the length of the working section and is sufficient to measure the vortex trajectory without significant influence from preceding vortical wake structures.

# Discussion

The results indicate that the wake geometry is primarily determined by the wind tunnel velocity, the blade rotational speed and the position of the hub axis. The relative magnitudes of the tunnel velocity and the rotational speed determine the extent to which the wake is skewed, and the hub position dictates the wake curvature and elongation. For the latter, it is important for the blade to be positioned close to the working section to minimise vortex dissipation and to ensure the generation of a well structured vortex with a high local convection velocity. These three parameters are critical irrespective of whether the blade is in a continuous running configuration or following an acceleration/deceleration profile over a specified azimuth range.

There are considerable differences between the single rotation (acceleration/deceleration profile) and the continual running cases. The single rotation configuration is characterised by a continually varying tip velocity profile representing the constant acceleration and deceleration of the rotating blade. This , in the majority of cases investigated, is contained within one revolution. In the numerical model the motion of the blade is represented by three distinct velocity variations. Initially, there is an acceleration from rest up to a specified tip velocity with the blade pitching up. The blade is then either accelerated again across the entrance to the working section or held at a constant tip velocity before deceleration back to rest. The critical phase of the motion is when the blade crosses the working section. Here, the pitch profile is varied to produce a near constant tip vortex strength. If the blade travels at a constant velocity, the incidence of the blade should be approximately constant, but if the blade is accelerated, the blade must be pitched down to balance the higher normal velocities experienced by the blade.

The continuous running configuration, on the other hand, does not require the complicated motion profiles of the single rotation cases. In fact , the blade operates at

constant rotational speed and only a pitch variation has to be specified. The pitching motion of the blade is, however, determined with reference to the same objective as the single rotation cases i.e. the generation of a constant tip vortex strength. With the blade traversing the working section, the magnitude of the normal velocity experienced by the blade is dominated by the component of velocity derived from the rotation of the blade. The local wind tunnel velocity does influence this value but the magnitude of the normal component on the blade from the tunnel is small compared to that of the rotating blade. Hence, it is appropriate to conclude that with an almost constant tip velocity profile in this region a constant pitch incidence would be acceptable to attain (approximately) a constant tip vortex strength.

From the two configurations investigated the results indicate that the best case configuration for the generation of a lateral vortex occurs in the acceleration/ deceleration case. This corresponds to a single rotation consisting of a rapid acceleration up to a tip speed of 50 m/s, followed by an acceleration phase across the working section up to 90 m/s and finally a rapid deceleration back to rest (figure 8) . In this case, the blade radius is 0.75 m and the hub is located at 3.2 m from the wind tunnel origin. To enable the generation of a constant tip vortex strength, the pitch motion of the blade consists of a ramp up to 5 degrees during the initial acceleration phase, followed by a ramp down to 2.75 degrees to balance the higher normal velocities, before the blade is returned to zero incidence during the deceleration phase.

By restricting the motion of the blade to one revolution, extremely high blade accelerations occur. Consequently, any mechanism to actuate the rotor must be able to impose very high torques to attain the prescribed accelerations. One possible way of ameliarating this requirement could be to extend the range of motion over two or more revolutions to reduce the high loads during the initial acceleration and final deceleration phases. Extending these phases does not adversely affect the wake

structure as long as the blade is held at zero incidence during the extended range of motion. The severe accelerations coould also be reduced by either increasing the blade radius or reducing the wind tunnel velocity (which enables a reduction in rotational speeds). The blade radius, however, is restricted by the contraction geometry and a reduction in tunnel velocity is not advisable due to the need for the vortex to have a high convection velocity. Unfortunately, there is no practical solution to reduce the extremely high loads in the critical phase when the blade is accelerating across the entrance to the working section.

In the continuous running cases the wake geometry is not significantly different to that produced in the corresponding single rotation acceleration/deceleration cases when the tip velocity is held constant across the working section (figs.9,10). Since, however, the blade now operates with a constant tip velocity around the azimuth, consideration focuses on the separation between the consecutive wake structures generated by each revolution rather than to what extent the wake geometry is skewed. This separation distance is dependant on the relationship between wind tunnel velocity and blade tip velocity. These, together with the rotor hub position, also determine the geometric features of the wake.

The design criteria for the rotating blade are considerably simpler for the continual running case. Since there are no stringent limitations with repect to blade travel, the blade could be run up to speed over a number of revolutions then left to wind-down after measurement. This would result in a considerable reduction in the loads required to rotate the blade.

There is no significant difference between the physical dimensions and position of the rotating blade in the best case continual running and single rotation cases. The difference between the two arises from the type of actuation that would be required to produce the torque for either the short period variable acceleration motion or the

long duration constant velocity motion. It is interesting to note that the tip speed of 50 m/s and radius of 0.75m corresponds to approximately 11 revolutions per second which is marginally higher than the 9 revolutions per second of the current Glasgow University BVI facility. That facility is driven by a geared down servo motor and has a larger blade with a higher inertia than the proposed rig. It should, therefore, be possible to utilise the existing motor or one similar as the actuation for the proposed facility if the continuous running mode were adopted. Initial estimates would indicate that for the acceleration/deceleration configuration, a hydraulic system, which would be prohibitively expensive, would be required to produce the prescribed motion profile over two revolutions. Since the geometry of the vortex structure is not significantly worse in the continual running configuration it would be difficult to justify the added expense that would be required to implement the acceleration/deceleration case.

The pitching motion of the blade would also be achieved more easily with the blade in the continuous running configuration. A prescribed incidence variation could be obtained using a simple swash-plate mechanism. This would provide the periodic wake generation depicted in the results. Another option may be to incorporate a motor within the hub. Whilst this would provide ease of control and adaptability to different pitch profiles, it would inevitably be more difficult to implement and incur higher costs. This would be unavoidable if the short period acceleration/deceleration mode was implemented as the optimum prescribed pitch profile is non-periodic.

Practical consideration must also be given to the proximity of the blade tip to the tunnel wall during the rotation of the blade. The numerical model takes no account of the viscous effects that would be experienced in this region. This is not a feature when the blade crosses the working section but must be considered when the blade initially pitches up to generate the wake. Viscous interaction with the wall may result in vortex dissipation and produce unwanted phenomena in the convecting vortex

structure. If this does occur then alteration of the radius of the blade would probably be required.

## Conclusions

A numerical model has been used in the conceptual design of a new blade vortex interaction facility. The model showed the convecting wake geometry was dependant on the wind tunnel velocity, the tip velocity profile and the pitching motion of the rotating blade. Two independent cases for the motion of the blade were investigated, a single rotation acceleration/deceleration motion and a continuous running motion with constant tip velocity. The single rotation case, with an acceleration across the entrance to the working section , produced the optimum wake geometry for the generation of a lateral vortex but may be impractical to implement due to the excessively high torques required to accelerate and decelerate the blade. The continuous running configuration produces a wake geometry which is not significantly worse than the single rotation case but would have the advantages of being considerably easier to implement.

## Further Work

This will involve the design and construction of the facility and subsequent measurement of the convecting trailed tip vortex. Construction will be based on the continuously rotating blade configuration . The hot-wire measurement system will be set-up and initial calibration and bench mark tests will be conducted.

# References

1. Surendraiah, M. "An Experimental Study of Rotor Blade-Vortex Interaction.", M.S. Thesis, The Pennsylvaia State University, December 1969.

2. Padakannaya, R. "Experimental Study of Rotor Unsteady Airloads due to Blade-Vortex Interaction.", NASA CR-1909, November 1971.

3. Caradonna, F.X., Lautenschlager, J.L., Silva, M.J., "An Experimental Study of Rotor-Vortex Interaction." AIAA Paper 88-0045, AIAA 26th Aerospace Sciences Meeting, Reno, Nevada, Jan 1988.

4. Horner, M.H., Saliveros, E., Galbraith, R.A.McD., "An Experimental Investigation of the Oblique Blade-Vortex Interaction.", 17th European Rotorcraft and Powered Lift Aircraft Forum, Berlin, Germany, Sept 1991.

5. Horner, M.H., Saliveros, E., Galbraith, R.A.McD., "An Examination of Vortex Convection Effects During Blade-Vortex Interaction.", AHS/RAeS Technical Specialists Meeting on Rotorcraft Acoustics and Rotor Flight Dynamics, Philadelphia, U.S.A.,Oct 1991.

6. Horner, M.H., Stewart, J.N.,, Galbraith,R.A.McD., Grant, I., Coton, F.N., Smith, G.H. "Preliminary Results from a Particle Image Velocimetry Study of Blade-Vortex Interaction." 19th European Rotorcraft Forum, Cernobbio, Italy, Sept 1993.

7. Seath, D.D., Kim, J.M., Wilson, D.R. "An Invesigation of the Parallel Blade-Vortex Interaction in a Low-Speed Wind Tunnel.", AIAA Paper 87-1345, 19th Fluid Dynamics, Plasma Dynamics and Lasers Conference, Honolulu, Hawaii, June 1987.

8. Straus, J., Renzoni, O., Mayle, R.E. "Airfoil Pressure Measurements During a Blade-Vortex Interaction and Comparison with Theory.", AIAA Paper 88-0669, 26th Aerospace Sciences Meeting, Reno, Nevada, Jan 1988.

9. Coton, F.N., De la Iglesia, F. "A Three-Dimensional Model Of Low Speed Blade-Vortex Interaction." 20th European Rotorcraft Forum, Amsterdam, Oct 1994.

10. Wall, B.G., van der "CP-ROT, First Results from Pressure Instrumented BO-105 Hingeless Model Rotor Tests" 19th European Rotorcraft Forum, Cernobbio, Italy, Sept 1993.

11. Ellin, A.D.S. "An In-Flight Investigation of Lynx AH MK5 Main Rotor/Tail Rotor Interactions.", 19th European Rotorcraft Forum, Cernobbio, Italy, Sept 1993.

12. Hess, J.L.,Smith, A.M.O. "Calculation of Potential Flow About Arbitrary Bodies." Progress in Aeronautical Sciences, vol. 8, pp. 1-138 , 1967.

13. Katz, J., Plotkin, A. "Low-speed Aerodynamics-From Wing Thoery to Panel Methods."McGraw-Hill Publications Inc., 1991

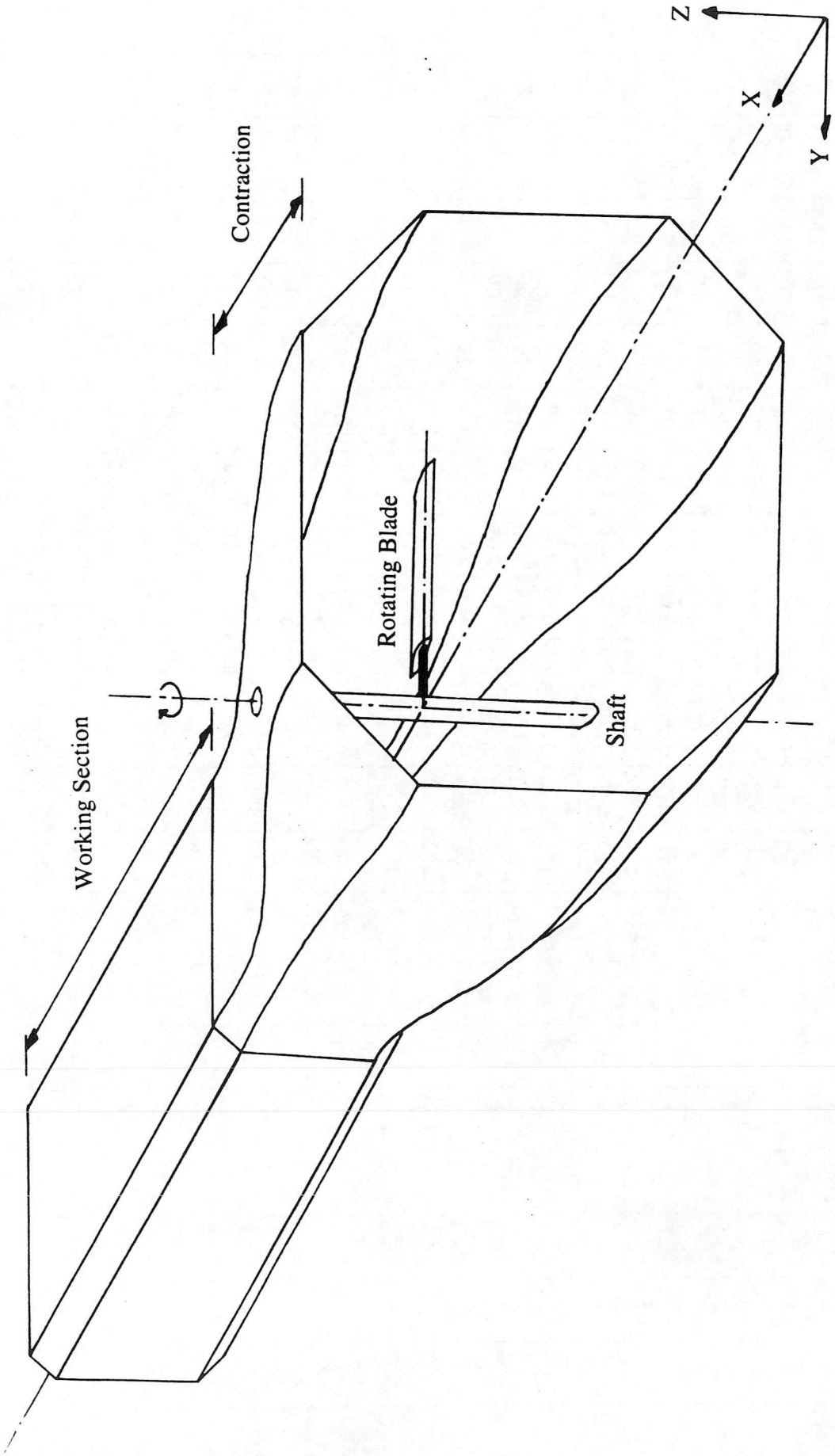


Fig.1 Diagram of experimental set-up indicating the wind tunnel co-ordinate system.

| Case | AOA1 | AOA2 | c | R | X | Y | Start Azi | AZI1 | AZI2 | Stop Azi | Start Alp | ALP1 | ALP2 | Stop Alp | WS Vel | TV1 | TV2 | tmax | tstep | nplot |
|---|---|---|---|---|---|---|---|---|---|---|---|---|---|---|---|---|---|---|---|---|
| 1 | 5 | 5 | 0.09 | 0.7 | 3 | 0 | 225 | 300 | 420 | 500 | 270 | 315 | 390 | 450 | 20 | 70 | 70 | 0.15 | 0.0035 | 15 |
| 2 | 5 | 5 | 0.09 | 0.6 | 3.3 | 0 | 225 | 300 | 420 | 500 | 270 | 315 | 390 | 450 | 20 | 70 | 70 | 0.15 | 0.0035 | 13 |
| 3 | 5 | 5 | 0.09 | 0.6 | 3.3 | 0 | 225 | 300 | 420 | 500 | 270 | 315 | 390 | 450 | 30 | 70 | 70 | 0.15 | 0.0035 | 15 |
| 4 | 5 | 5 | 0.09 | 0.6 | 3.3 | 0 | 225 | 300 | 420 | 500 | 270 | 315 | 390 | 450 | 30 | 50 | 70 | 0.17 | 0.0035 | 20 |
| 5 | 5 | 5 | 0.09 | 0.6 | 3.3 | 0.1 | 225 | 300 | 420 | 500 | 270 | 315 | 390 | 450 | 30 | 50 | 70 | 0.17 | 0.0035 | 20 |
| 6 | 5 | 5 | 0.09 | 0.6 | 3.3 | 0 | 225 | 300 | 420 | 500 | 270 | 315 | 390 | 450 | 20 | 50 | 70 | 0.2 | 0.0035 | 20 |
| 7 | 5 | 5 | 0.09 | 0.6 | 3.3 | 0 | 225 | 300 | 420 | 500 | 270 | 315 | 390 | 450 | 20 | 50 | 90 | 0.2 | 0.0035 | 20 |
| 8 | 5 | 5 | 0.09 | 0.6 | 3.3 | 0 | 225 | 300 | 420 | 500 | 270 | 315 | 390 | 450 | 25 | 50 | 90 | 0.2 | 0.0035 | 15 |
| 9 | 5 | 5 | 0.09 | 0.6 | 3.3 | 0 | 180 | 270 | 345 | 500 | 270 | 315 | 350 | 400 | 25 | 50 | 90 | 0.2 | 0.0035 | 15 |
| 10 | 5 | 5 | 0.09 | 0.6 | 3.3 | 0 | 180 | 270 | 345 | 500 | 270 | 315 | 350 | 450 | 20 | 50 | 90 | 0.2 | 0.0035 | 20 |
| 11 | 5 | 5 | 0.09 | 0.6 | 3.3 | 0 | 180 | 270 | 370 | 500 | 270 | 315 | 350 | 450 | 20 | 50 | 90 | 0.2 | 0.0025 | 20 |
| 12 | 5 | 5 | 0.09 | 0.6 | 3.3 | 0 | 180 | 270 | 390 | 500 | 270 | 315 | 350 | 450 | 20 | 70 | 110 | 0.2 | 0.0025 | 20 |
| 13 | 5 | 5 | 0.09 | 0.6 | 3.3 | 0 | 180 | 300 | 390 | 500 | 270 | 315 | 350 | 450 | 20 | 50 | 100 | 0.2 | 0.0025 | 20 |
| 14 | 5 | 5 | 0.09 | 0.55 | 3.3 | -0.2 | 180 | 300 | 390 | 540 | 270 | 315 | 350 | 450 | 20 | 50 | 100 | 0.2 | 0.0025 | 20 |
| 15 | 5 | 5 | 0.09 | 0.6 | 3.3 | 0 | 180 | 300 | 390 | 540 | 250 | 300 | 405 | 540 | 20 | 50 | 100 | 0.2 | 0.0025 | 20 |
| 16 | 5 | 5 | 0.09 | 0.6 | 3.3 | 0 | 180 | 300 | 390 | 540 | 250 | 300 | 405 | 540 | 20 | 50 | 100 | 0.2 | 0.0025 | 20 |
| 17 | 5 | 5 | 0.09 | 0.6 | 3.3 | 0 | 180 | 300 | 390 | 540 | 250 | 300 | 450 | 540 | 20 | 50 | 100 | 0.2 | 0.0025 | 20 |
| 18 | 5 | 5 | 0.09 | 0.6 | 3.2 | 0 | 180 | 300 | 390 | 540 | 250 | 300 | 450 | 540 | 20 | 50 | 100 | 0.2 | 0.0025 | 20 |
| 19 | 5 | 2 | 0.09 | 0.6 | 3.2 | 0 | 180 | 300 | 390 | 540 | 250 | 300 | 390 | 540 | 20 | 50 | 100 | 0.2 | 0.0025 | 20 |
| 20 | 5 | 2.5 | 0.09 | 0.6 | 3.3 | 0 | 180 | 300 | 390 | 540 | 250 | 300 | 390 | 540 | 20 | 50 | 100 | 0.2 | 0.0025 | 20 |
| 21 | 5 | 3 | 0.09 | 0.6 | 3.4 | 0 | 180 | 300 | 390 | 540 | 250 | 300 | 390 | 540 | 20 | 50 | 100 | 0.2 | 0.0025 | 20 |
| 22 | 5 | 2.75 | 0.09 | 0.6 | 3.45 | 0 | 180 | 300 | 420 | 540 | 250 | 300 | 390 | 490 | 20 | 50 | 100 | 0.2 | 0.0025 | 20 |
| 23 | 5 | 2.75 | 0.09 | 0.6 | 3.45 | 0 | 180 | 300 | 440 | 540 | 250 | 300 | 390 | 490 | 20 | 50 | 100 | 0.2 | 0.0025 | 20 |
| 24 | 5 | 2.75 | 0.09 | 0.6 | 3.45 | 0 | 0 | 300 | 440 | 720 | 250 | 300 | 390 | 490 | 20 | 50 | 100 | 0.4 | 0.0035 | 20 |
| 25 | 5 | 2.75 | 0.09 | 0.6 | 3.45 | 0 | 180 | 300 | 420 | 540 | 250 | 300 | 390 | 490 | 15 | 60 | 100 | 0.2 | 0.0025 | 20 |
| 26 | 5 | 2.75 | 0.09 | 0.6 | 3.45 | 0 | 180 | 300 | 420 | 540 | 250 | 300 | 390 | 490 | 20 | 60 | 100 | 0.2 | 0.0025 | 20 |
| 27 | 5 | 2.75 | 0.09 | 0.8 | 3 | 0 | 180 | 300 | 420 | 540 | 280 | 320 | 400 | 450 | 20 | 30 | 60 | 0.4 | 0.0035 | 20 |
| 28 | 10 | 5 | 0.09 | 0.6 | 3.45 | 0 | 180 | 300 | 420 | 540 | 280 | 330 | 400 | 450 | 20 | 50 | 100 | 0.2 | 0.0025 | 20 |
| 29 | 5 | 2.75 | 0.09 | 0.75 | 3.2 | 0 | 180 | 300 | 420 | 540 | 280 | 330 | 400 | 450 | 20 | 50 | 90 | 0.2 | 0.0025 | 20 |
| 30 | 5 | 2.75 | 0.09 | 0.75 | 3.2 | 0 | 180 | 300 | 420 | 540 | 280 | 330 | 400 | 450 | 15 | 50 | 90 | 0.35 | 0.003 | 20 |

Fig.2 Table of acceleration/deceleration cases.

| Case | AOA1 | AOA2 | c | R | X | Y | Start Azi | AZI1 | AZI2 | Stop Azi | Start Alp | ALP1 | ALP2 | Stop Alp | WS Vel | TV1 | TV2 | tmax | tstep | nplot |
|---|---|---|---|---|---|---|---|---|---|---|---|---|---|---|---|---|---|---|---|---|
| 31 | 5 | 2.75 | 0.1 | 0.6 | 3.45 | 0 | 0 | 300 | 420 | 730 | 250 | 330 | 380 | 490 | 20 | 50 | 50 | 0.3 | 0.0025 | 20 |
| 32 | 5 | 2.75 | 0.1 | 0.6 | 3.45 | 0 | 0 | 300 | 420 | 730 | 250 | 330 | 380 | 440 | 20 | 35 | 50 | 0.2 | 0.0015 | 20 |
| 33 | 5 | 2.75 | 0.1 | 0.6 | 3.45 | 0 | 0 | 300 | 420 | 730 | 250 | 330 | 380 | 440 | 20 | 50 | 50 | 0.2 | 0.0015 | 20 |
| 34 | 5 | 2.75 | 0.1 | 0.65 | 3.45 | 0 | 0 | 300 | 420 | 730 | 250 | 330 | 380 | 440 | 20 | 50 | 50 | 0.2 | 0.0015 | 20 |

Fig.2 Table of acceleration/deceleration cases (continued).

| Case | AOA1 | AOA2 | c | R | X | Y | Start Azi | AZI1 | AZI2 | Stop Azi | Start Alp | ALP1 | ALP2 | Stop Alp | WS Vel | TV1 | TV2 | tmax | tstep | nplot |
|---|---|---|---|---|---|---|---|---|---|---|---|---|---|---|---|---|---|---|---|---|
| 35 | 5 | 2.75 | 0.15 | 0.65 | 3.45 | 0 | 0 | - | - | - | 250 | 330 | 380 | 440 | 20 | 50 | - | 0.4 | 0.0025 | 20 |
| 36 | 5 | 2.75 | 0.15 | 0.7 | 3 | 0 | 0 | - | - | - | 250 | 330 | 380 | 440 | 20 | 50 | - | 0.4 | 0.0025 | 20 |
| 37 | 5 | 2.75 | 0.15 | 0.8 | 2.5 | 0 | 0 | - | - | - | 250 | 330 | 380 | 440 | 20 | 50 | - | 0.3 | 0.0035 | 20 |
| 38 | 5 | 2.75 | 0.15 | 0.8 | 2.5 | 0 | 0 | - | - | - | 250 | 330 | 380 | 440 | 30 | 50 | - | 0.3 | 0.0035 | 20 |
| 39 | 5 | 2.75 | 0.15 | 0.75 | 3.2 | 0 | 0 | - | - | - | 250 | 330 | 380 | 440 | 30 | 50 | - | 0.3 | 0.003 | 20 |
| 40 | 5 | 2.75 | 0.15 | 0.75 | 2.8 | 0 | 0 | - | - | - | 250 | 330 | 380 | 440 | 30 | 50 | - | 0.3 | 0.003 | 20 |
| 41 | 5 | 2.75 | 0.15 | 0.75 | 2.8 | 0 | 0 | - | - | - | 250 | 330 | 380 | 440 | 20 | 50 | - | 0.3 | 0.003 | 20 |
| 42 | 5 | 2.75 | 0.15 | 0.75 | 3.2 | 0 | 0 | - | - | - | 250 | 330 | 380 | 440 | 20 | 50 | - | 0.3 | 0.003 | 20 |
| 43 | 5 | 2.75 | 0.09 | 0.75 | 3.2 | 0 | 0 | - | - | - | 250 | 330 | 380 | 440 | 20 | 50 | - | 0.3 | 0.003 | 20 |
| 44 | 8 | 4 | 0.09 | 0.75 | 3.2 | 0 | 0 | - | - | - | 250 | 330 | 380 | 440 | 20 | 50 | - | 0.3 | 0.003 | 20 |
| 45 | 10 | 5 | 0.09 | 0.75 | 3.2 | 0 | 0 | - | - | - | 250 | 330 | 380 | 440 | 20 | 50 | - | 0.3 | 0.003 | 20 |
| 46 | 10 | 10 | 0.09 | 0.75 | 3.2 | 0 | 0 | - | - | - | 250 | 330 | 380 | 440 | 20 | 50 | - | 0.3 | 0.003 | 20 |
| 47 | 5 | 5 | 0.15 | 0.75 | 3.2 | 0 | 0 | - | - | - | 250 | 330 | 380 | 440 | 20 | 50 | - | 0.3 | 0.003 | 20 |
| 48 | 10 | 10 | 0.15 | 0.75 | 3.1 | 0 | 0 | - | - | - | 250 | 330 | 380 | 440 | 20 | 50 | - | 0.3 | 0.003 | 20 |
| 49 | 5 | 5 | 0.15 | 0.75 | 3.1 | 0 | 0 | - | - | - | 250 | 330 | 380 | 440 | 20 | 50 | - | 0.3 | 0.003 | 20 |
| 50 | 5 | 5 | 0.09 | 0.75 | 3.1 | 0 | 0 | - | - | - | 250 | 330 | 380 | 440 | 20 | 50 | - | 0.3 | 0.003 | 20 |

Fig.3 Table of continuous running cases.

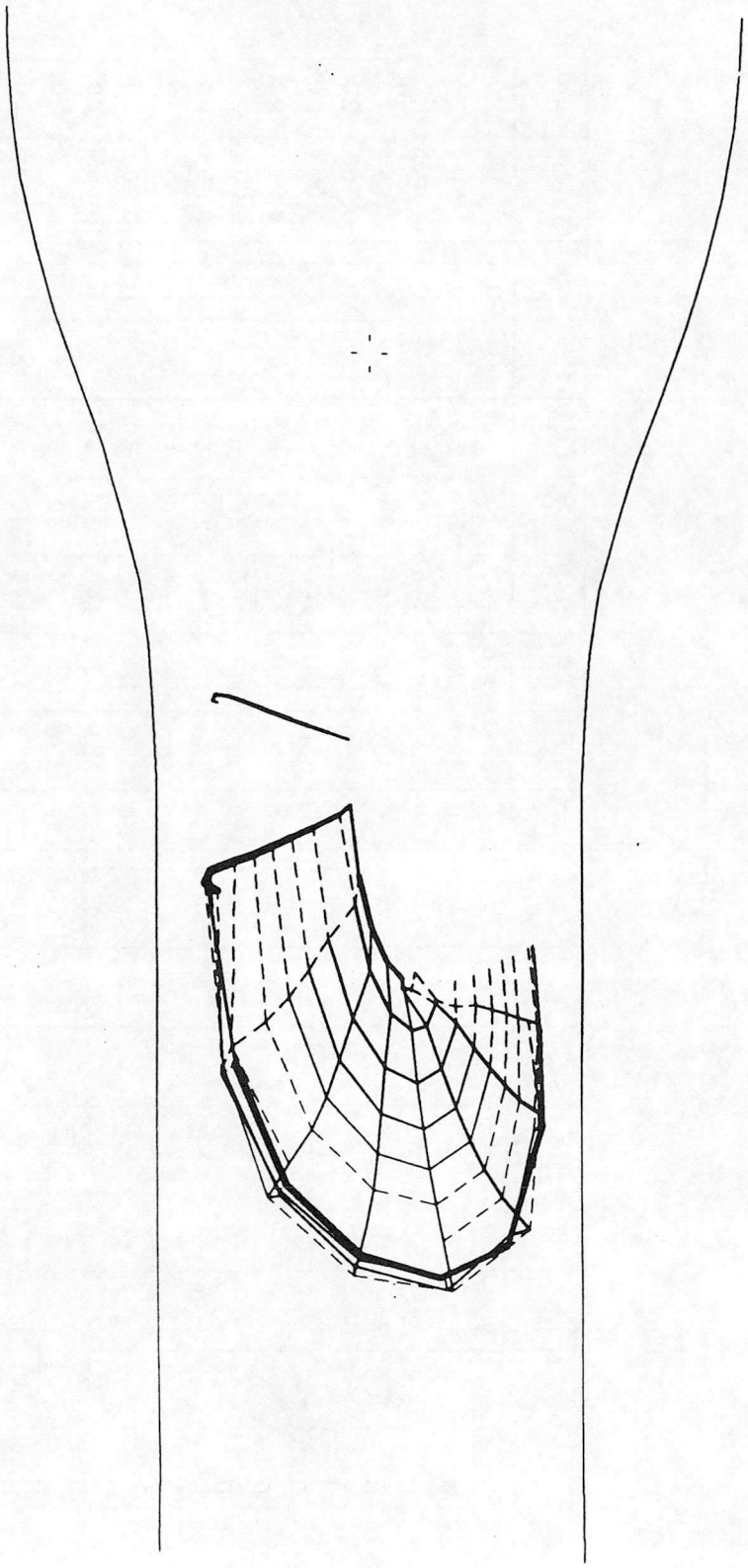

Fig.4 Single rotation convecting wake with working section velocity at 30 m/s, tip velocity constant at 70 m/s across working section.

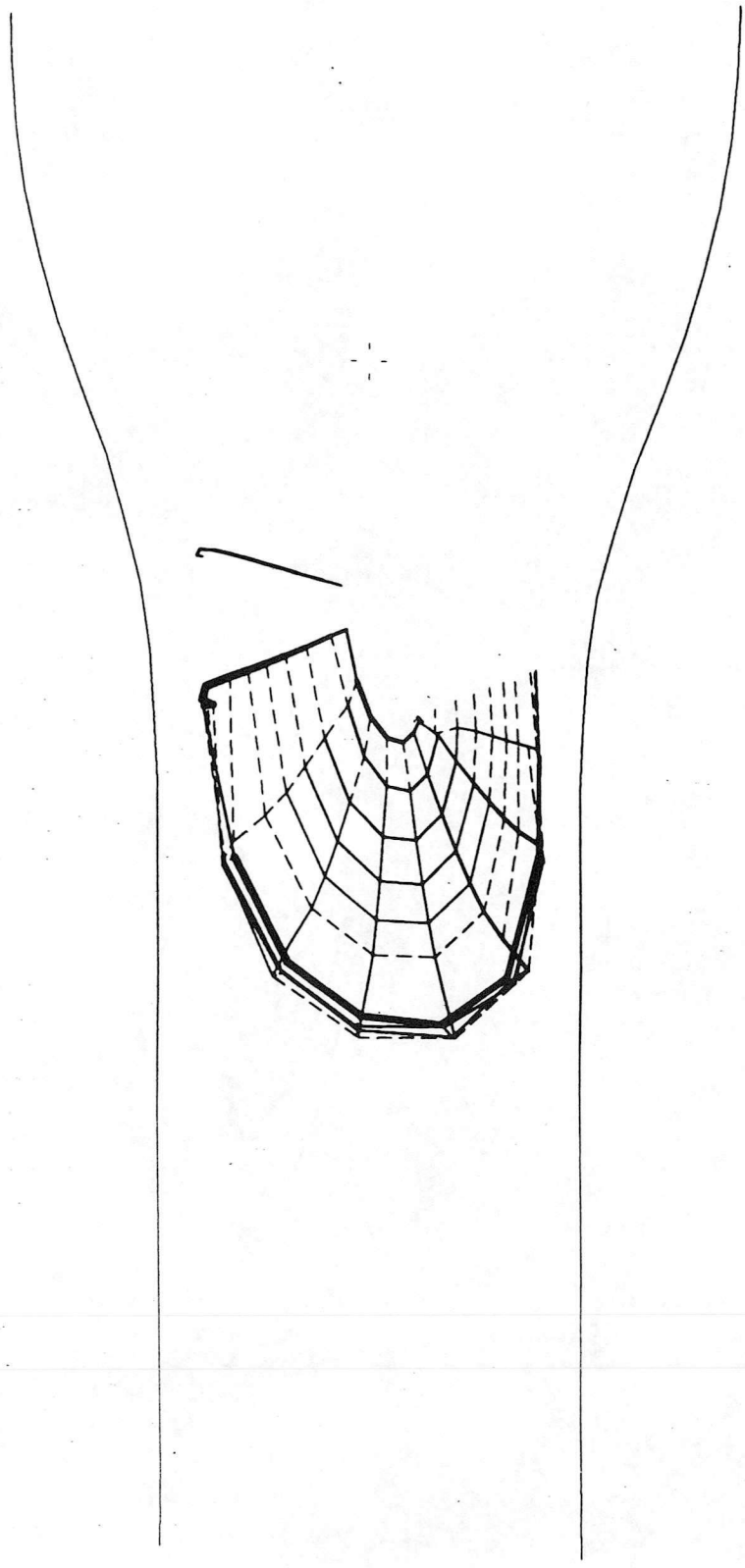

Fig.5 Single rotation convecting wake with working section velocity at 20 m/s, tip velocity constant at 70 m/s across working section.

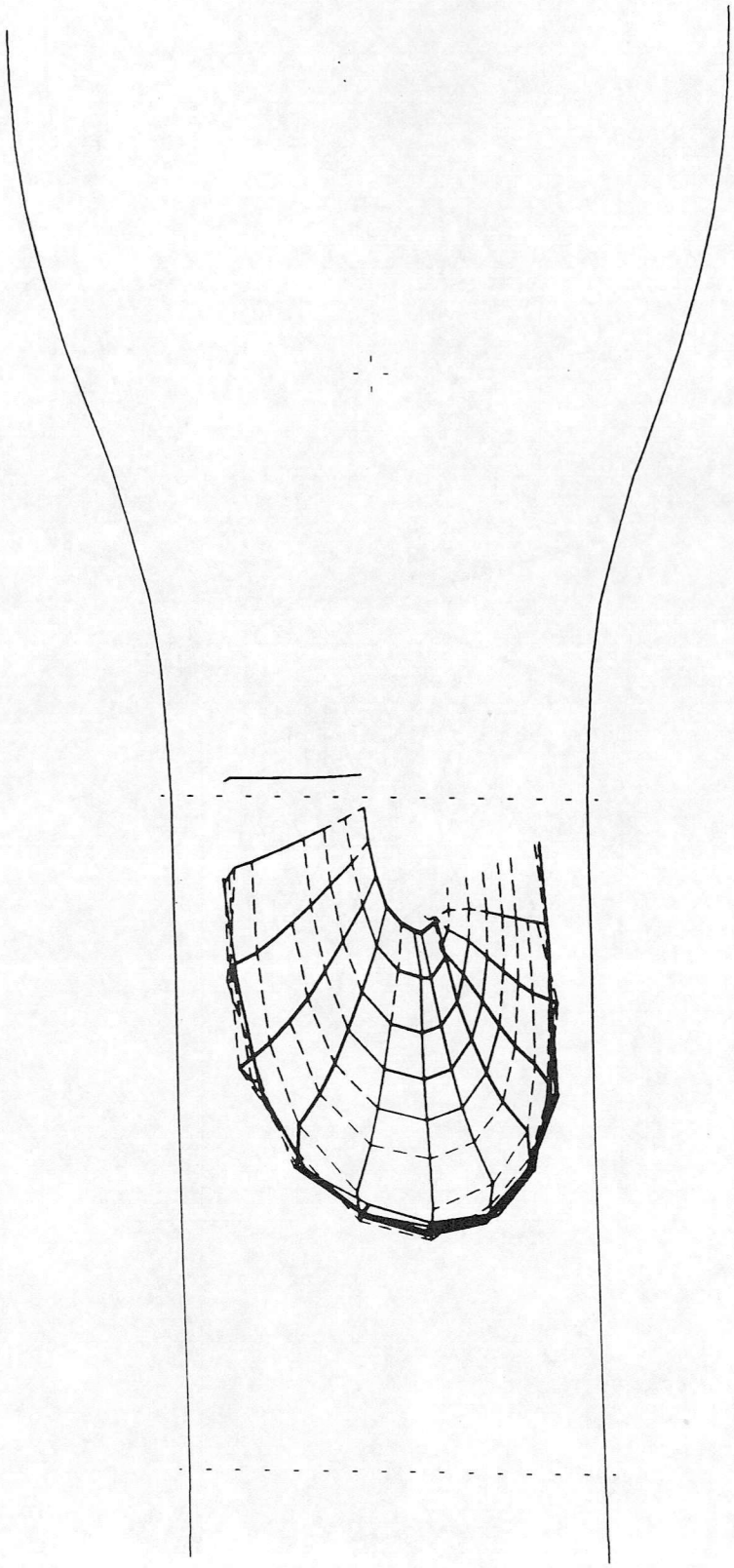

Fig.6 Single rotation convecting wake with working section velocity at 20 m/s, tip velocity increasing from 50 m/s to 90 m/s across working section, incidence held constant at 5 deg.

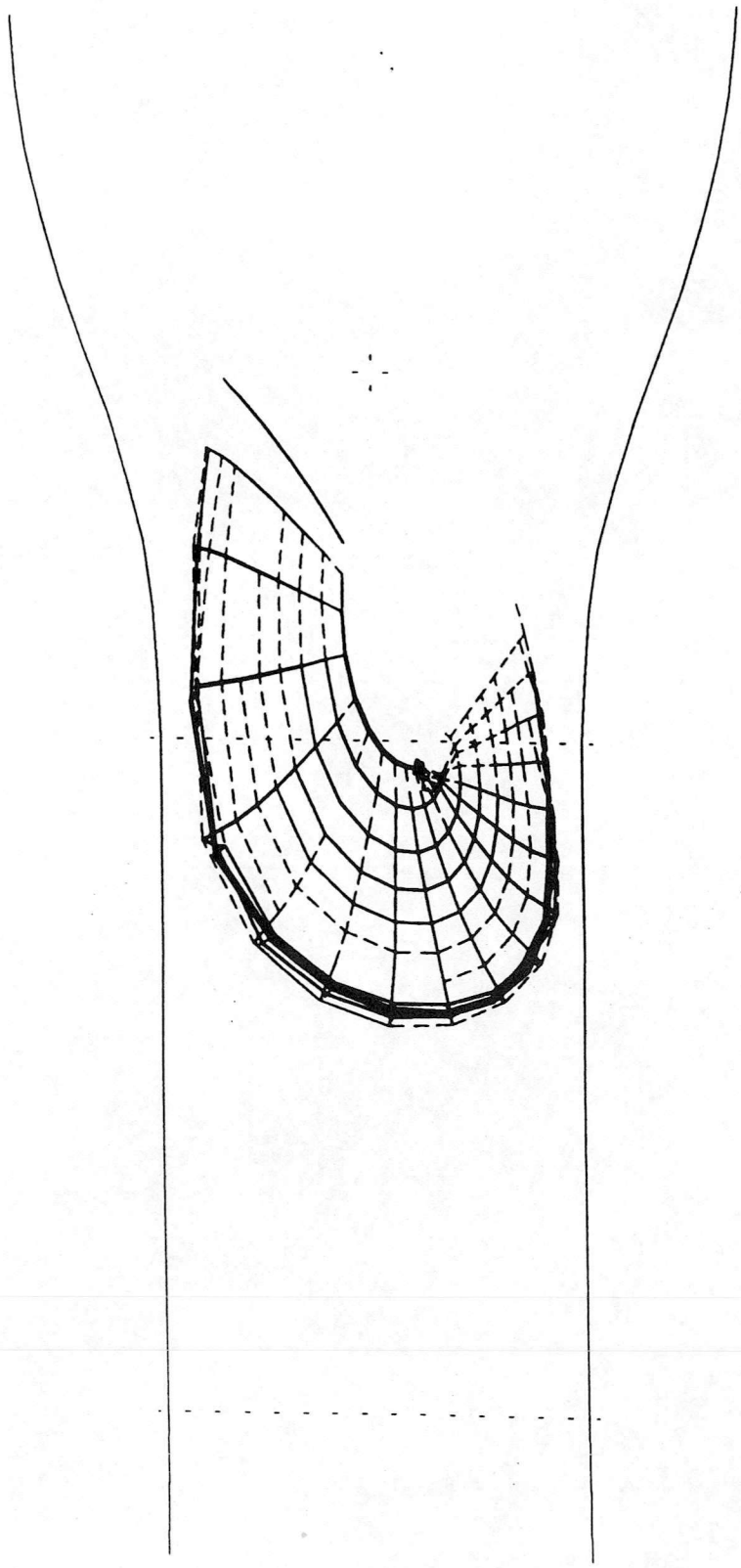

Fig.7 Single rotation convecting wake, tip velocity increasing from 50 m/s to 90 m/s across working section with pitch down from 5 deg. to 2.75 deg.

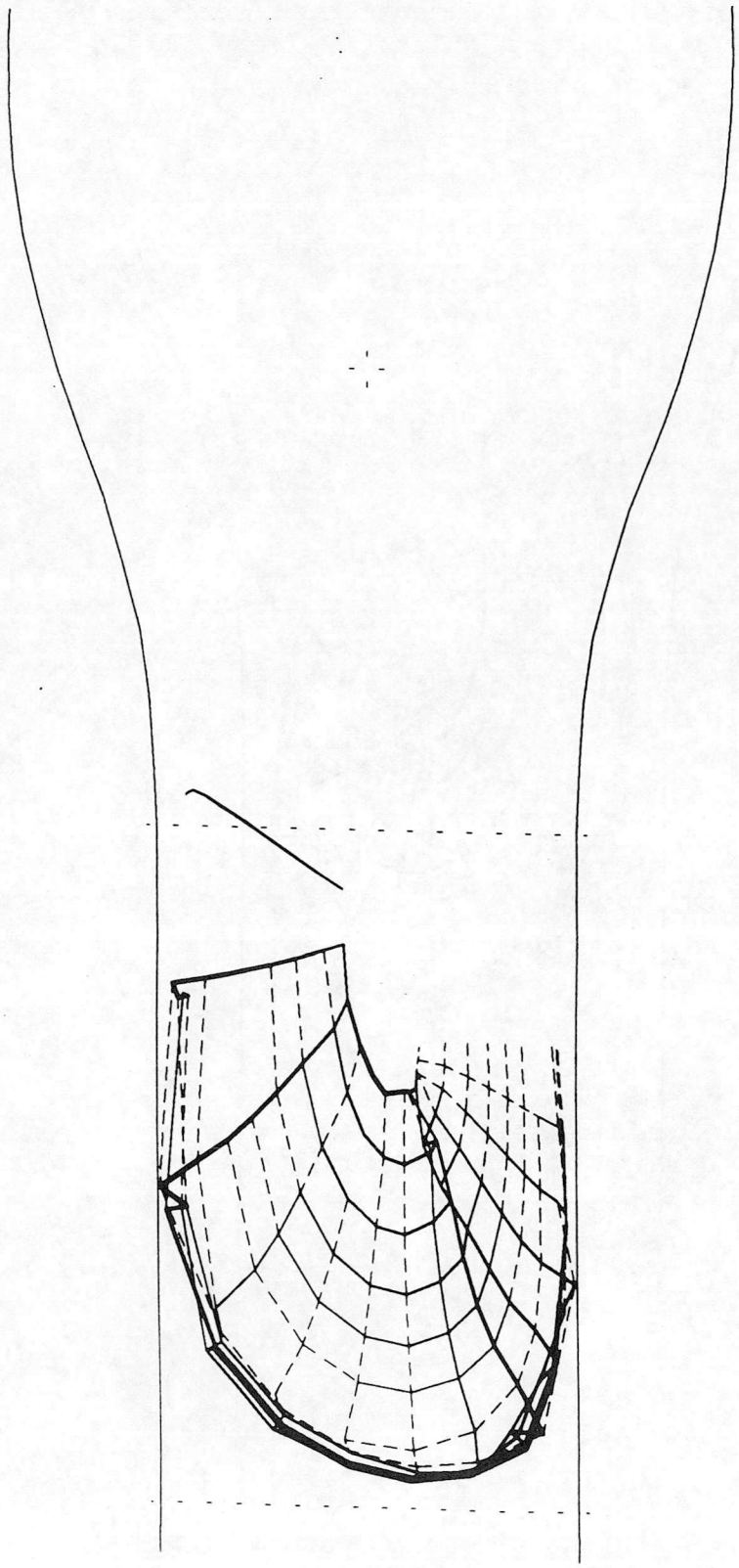

Fig.8 Single rotation convecting wake with a blade of radius 0.75m positioned at 3.2m from tunnel origin, working section velocity 15m/s.

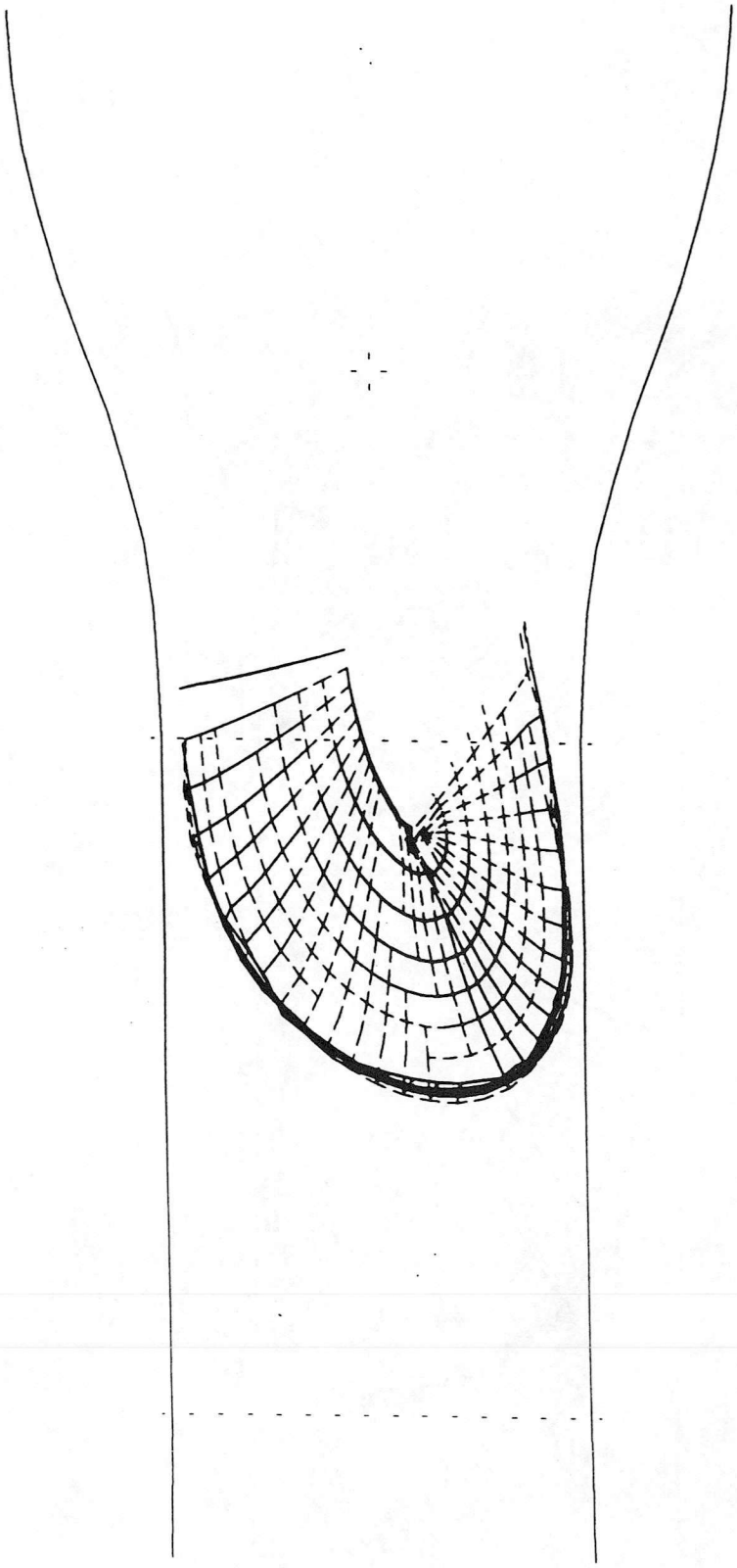

Fig.9 Single rotation convecting wake with tip velocity constant at 50 m/s across working section, blade radius 0.65m positioned at 3.45m from origin.

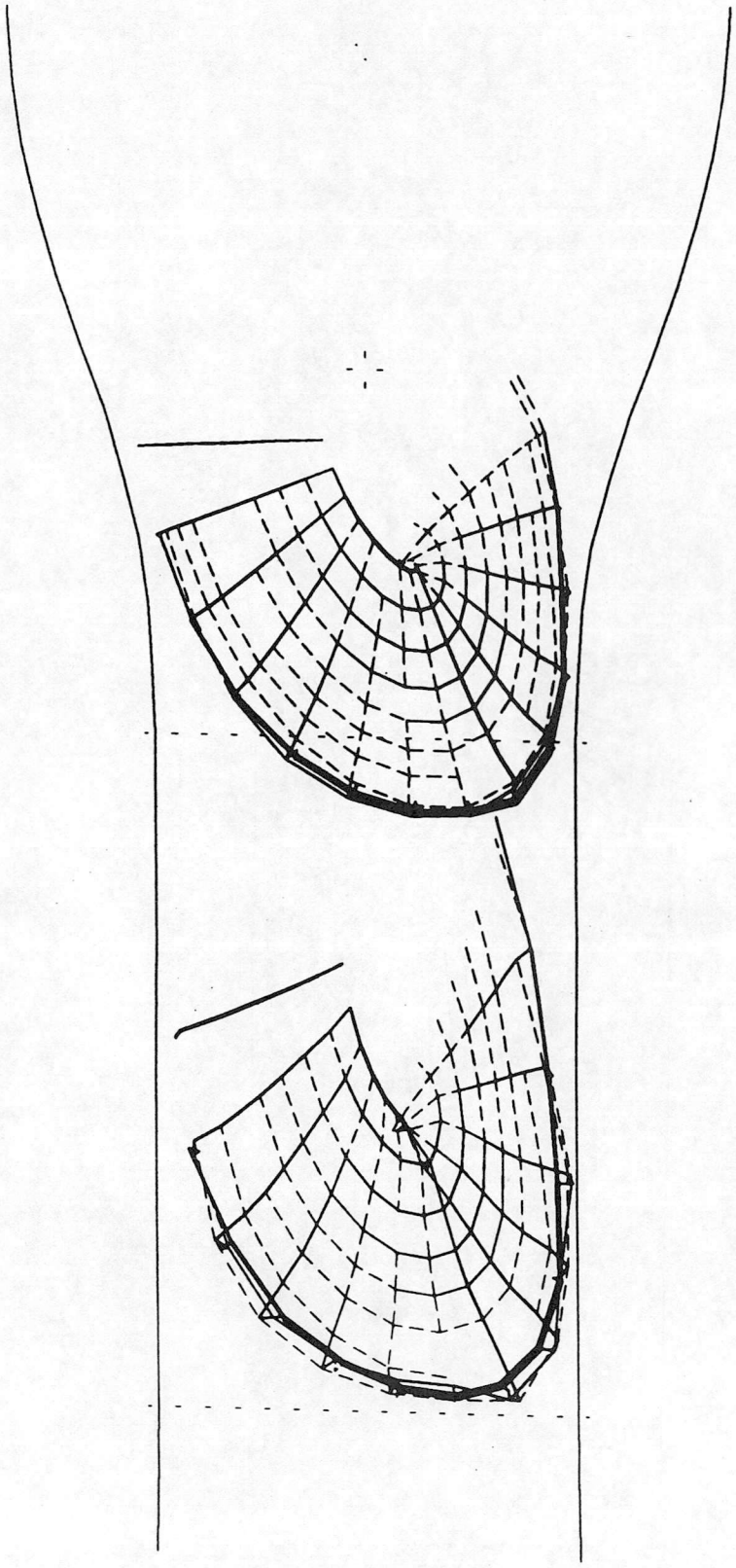

Fig.10 Continuous running wake development with a blade of radius 0.65m positioned at 3.45m from tunnel origin.

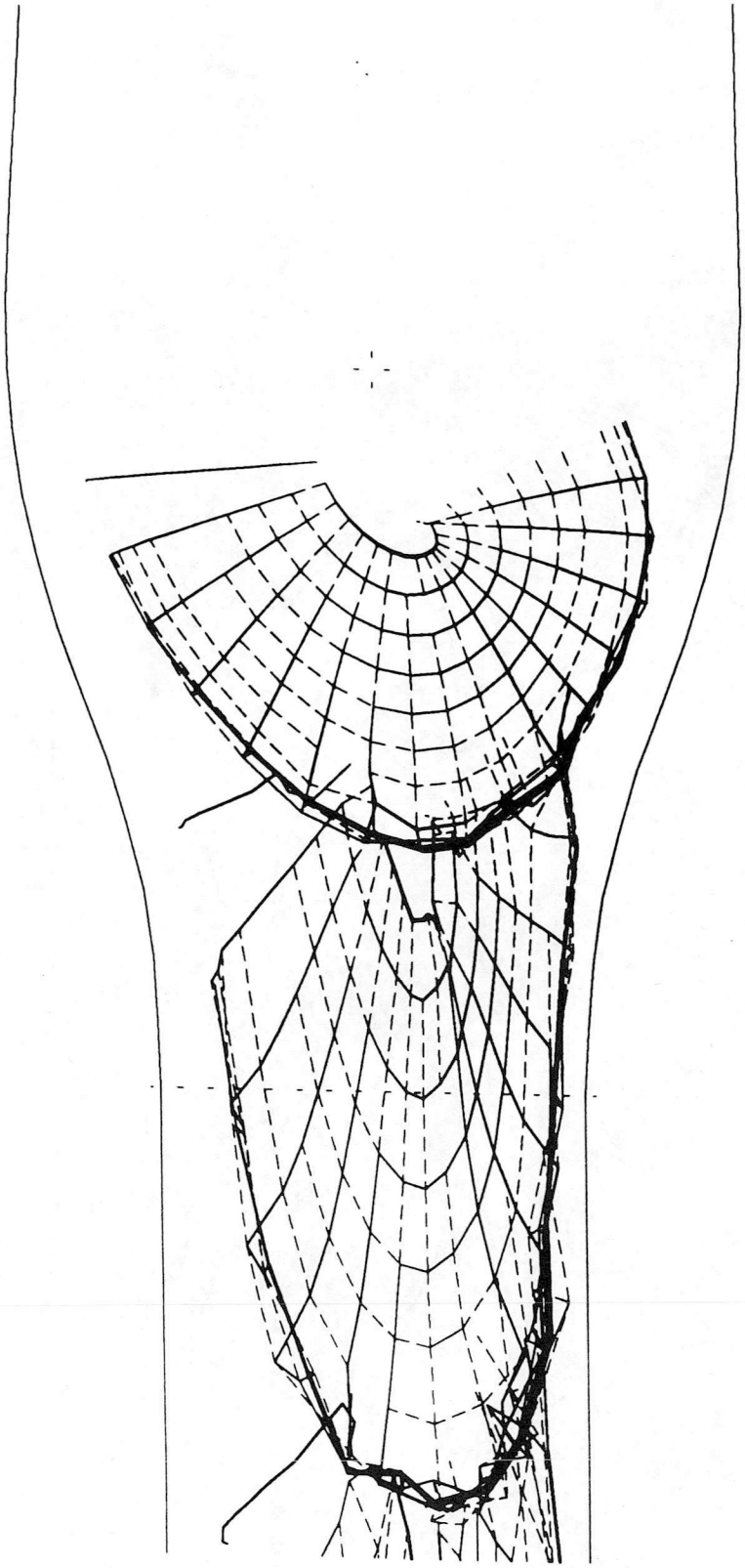

Fig.11 Continuous running wake development with a blade of radius 0.8m positioned at 2.5m from tunnel origin, working section velocity 20 m/s.

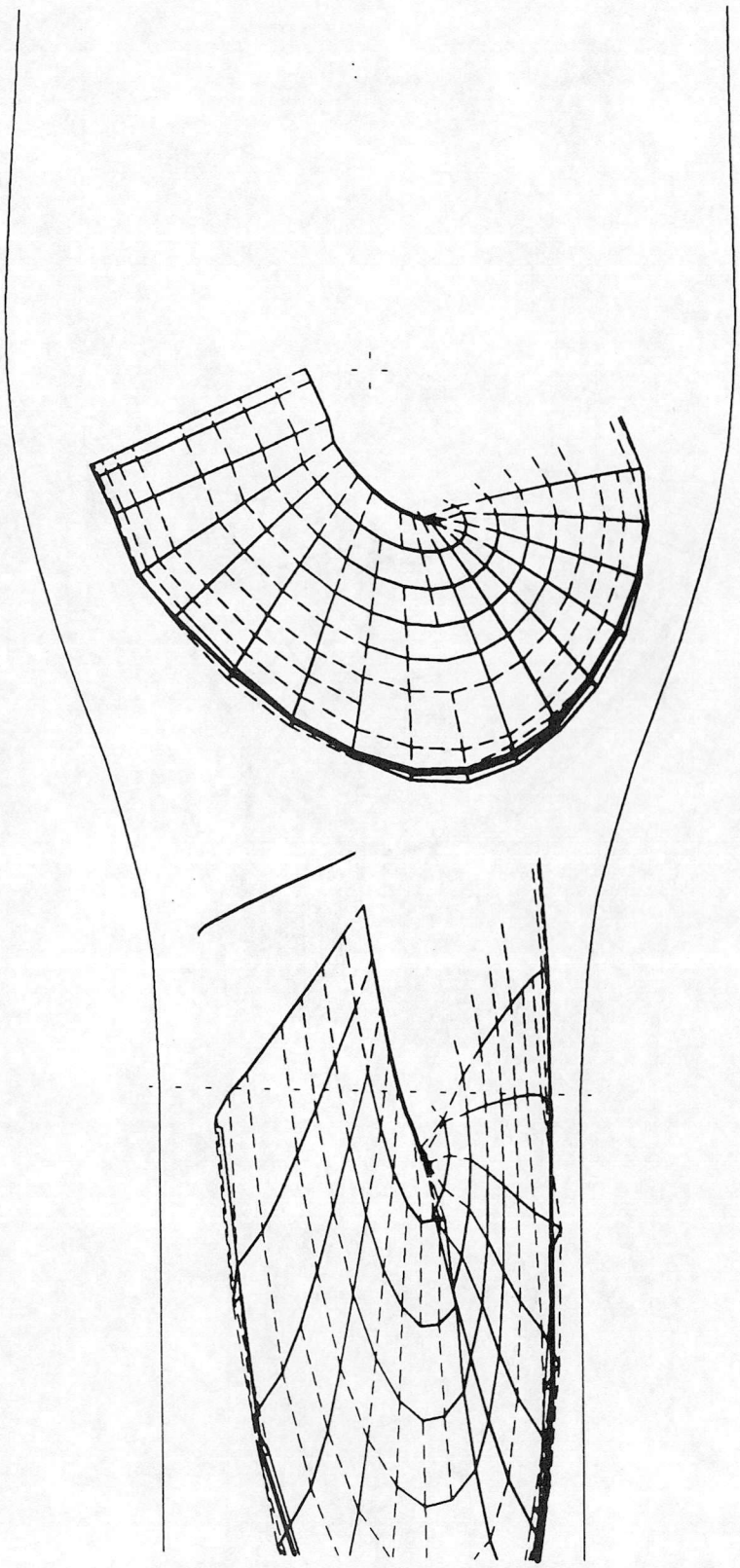

Fig.12 Continuous running wake development with a blade of radius 0.8m positioned at 2.5m from tunnel origin, working section velocity 30m/s.

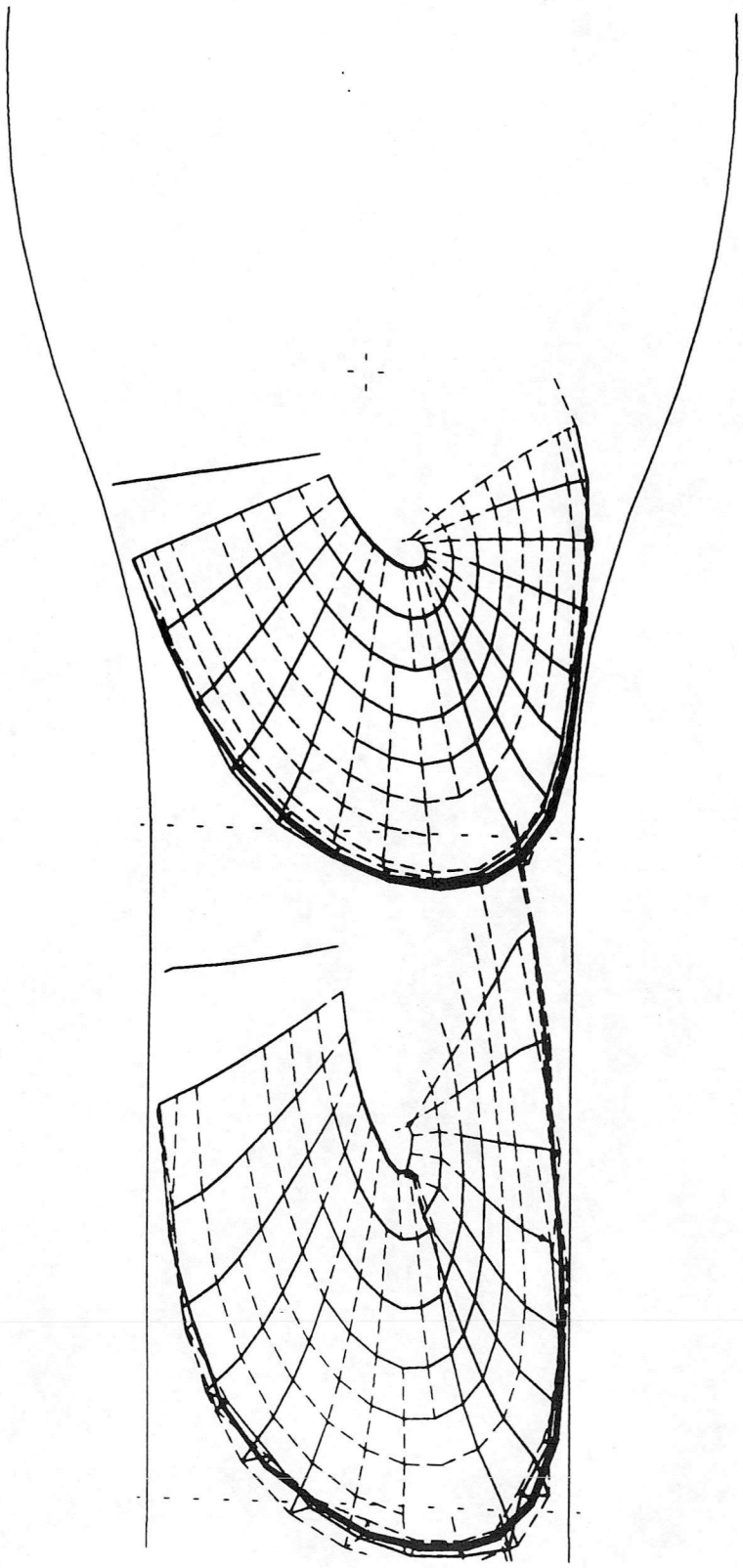

Fig.13 Continuous running wake development with a blade of radius 0.75m positioned at 3.2m from tunnel origin.

# Appendix 3

## A STUDY OF HELICOPTER TAIL ROTOR INTERACTION: PHASE 1 - PROOF OF CONCEPT

by

C.M. Copland
F.N. Coton
R.A.McD. Galbraith

Presented at the 24th European Rotorcraft Forum, Marseilles, 1998

**Reference : Aerodynamics AE 03**

# *A Study of Helicopter Tail Rotor Interaction:*

# *Phase 1 - Proof of Concept*

**C.M. Copland, F.N. Coton, R.A.McD. Galbraith**
Department of Aerospace Engineering,
The University of Glasgow,
Glasgow, G12 8QQ
Scotland

This paper describes the design, development and initial testing of a new facility for the generation of transverse vortices for use in a wind tunnel based study of helicopter tail rotor blade-vortex interaction. The facility consists of a single-bladed pitching rotor, positioned in the contraction of a low speed wind tunnel, which generates a transverse vortex representative of the idealised vortex system associated with a rotor blade. The manner in which a numerical model was utilised during the design process, to provide an accurate means of determining design parameters such as vortex generator position, rotational speed, working section velocity and blade pitch profile, is described. Initial hot-wire measurements, which were made downstream of the generator and document the periodic motion of the convecting vortex structure, are also presented. Finally, the remaining stages of the research programme are outlined.

## *Introduction*

The interactional aerodynamics of tail rotors have been minimally researched in comparison to those of main rotors[1,2,3]. There is, consequently, a universal lack of understanding of the many interactional mechanisms that affect helicopter tail rotor performance. Inevitably, there are significant differences between interactions where the vortex path lies in, or close to, the plane of the main rotor blade (Fig. 1), i.e. the common conception of Blade Vortex Interaction (BVI), and interactions associated with the tail rotor environment where the vortex is orthogonal to the tail rotor blade (Fig. 2).

Despite the importance of BVI being recognised for many years[4-7] and being the focus of several experimental[8-14] and numerical[15,16] studies, very few studies have investigated tail rotor interactional effects. Possibly the most notable was the in-flight study of Ellin[1], which considered the interaction of the main rotor wake with the tail rotor for a range of flight conditions. Ellin stated that the isolated convecting main rotor vortex can interact with the tail rotor itself (Fig. 2. Position 1), or with its wake both during the roll-up of the trailing tail rotor tip vortex (Fig. 2. Position 2) and with the fully rolled up tip vortex(Fig. 2. Position 3). Unfortunately, there is no apparent work documented on the specific mechanisms that are associated with these particular phenomena.

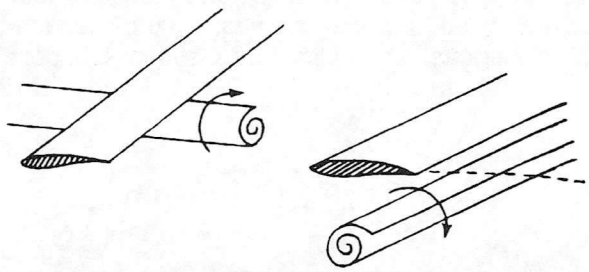

**Fig.1- Illustration of the vortical flow field associated main rotor BVI.**

It is well known that a helicopter in forward flight can generate a flow field similar to that of a fixed wing aircraft (Fig. 3). These vortices are generated from the individual blade tip vortices rolling around each other to form larger trailed structures. In addition to these structures, a series of connecting transverse tip vortex segments are produced by the passage of the rotor blades around the forward and aft regions of the rotor disk. Thus, in forward flight the tail rotor will be in the centre of the main rotor wake and will cut each of these transverse vortex segments in sequence as they are trailed

from the rear of the disc. In quartering flight (Fig. 4), however, the tail rotor can become immersed in the large rolled up vortex structures trailed from the edge of the main rotor disc. This flight condition has the most significant effect on tail

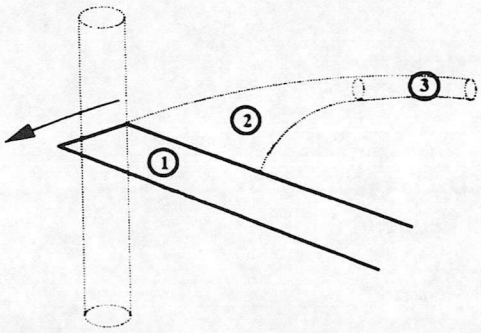


**Fig.2- Illustration of the vortical flow field associated with tail rotor BVI.**

rotor performance. Depending on the relative rotation of the vortices and tail rotor, the net effect can be a dramatic loss in tail rotor performance.

It is well known that the direction of the rotor rotation, the type (pusher or puller) and the position relative to the main rotor disk, all have a significant effect on tail rotor performance. It is likely that all these design factors are related to the interaction with the main rotor tip vortices and wake. It is not understood why this is the case. The evolution of a specific helicopter tail rotor design has followed a trial and error approach but the general consensus is top blade forward gives the best tail rotor performance. In many cases it is only when the yaw handling of a helicopter is unsatisfactory that research has been carried out[17]. Although understanding of the tail rotor has improved over the years, the fundamental orthogonal interactions are still not understood.

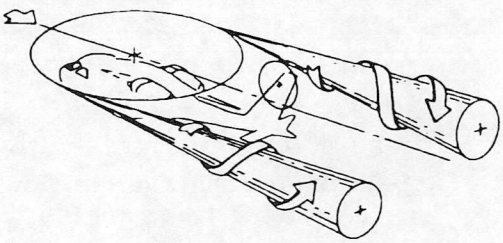

**Fig.3- Illustration of the flow field associated with a helicopter in forward flight.**

In his study, Ellin concluded that the furtherance of the understanding of main rotor/tail rotor interactions would benefit from two particular areas of research;

1) An experimental investigation of interactions where the vortex is orthogonal to the blade leading edge
2) An experimental investigation of blade vortex interaction with the vortex perpendicular to the blade chord.

This paper documents the first stage of a research programme to address the latter of these two topics and goes on to describe the remaining stages of the programme.

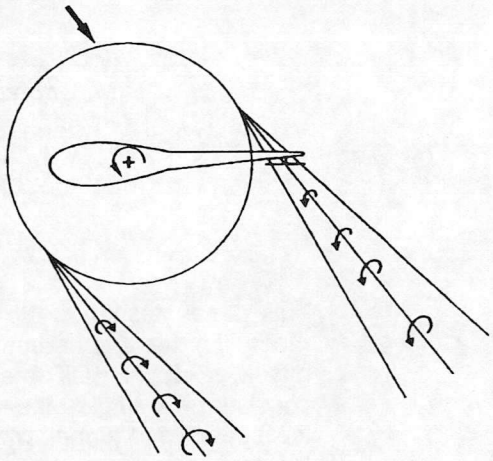

**Fig.4- Illustration of a helicopter in quartering flight.**

Previous experimental studies of main rotor BVI have been predominantly wind tunnel based and have utilised a variety of test geometry's to create the BVI phenomenon. Early studies attempted to isolate single interactions in the hope that a clear description of the process would be forthcoming. Unfortunately, these tests were often hampered by problems associated with vortex generation or poor measurement resolution. In recent years, improvements in instrumentation technology have allowed more detailed studies of BVI, both as an isolated phenomenon and also in the full rotor domain to be conducted. In the surface pressure measurement and flow visualisation work of Horner et al.[12,13,14] a vortex generator was located upstream of a single-bladed rotor in the working section of a low-speed wind tunnel. During the interaction of the vortex with the rotor blade, unsteady surface pressures were measured and Particle Image Velocimetry was used to obtain quantitative flow field information.

Other studies have used different experimental set-ups to investigate the fundamental aspects of blade vortex interactions. Booth et al.[8,9,10] utilised an oscillating aerofoil to generate transverse vortices. However, the wake behind the aerofoil contained pairs of vortices which resembled a Karman vortex street. It was pointed out that there are some inherent limitations in this experimental method. Firstly, the vortex pairs cannot be considered to be exactly equivalent to an isolated tip vortex encountering a rotor blade on a

helicopter. Since the vortices occur in pairs, they influence each other. Secondly, in the presence of a blade, the spacing between the filaments becomes important. The blade can be said to have an isolated encounter only if the spacing between the vortices is greater than the blade model chord. Such a requirement may conflict with the need for a well defined vortex and consequently the condition for an isolated encounter is not always met.

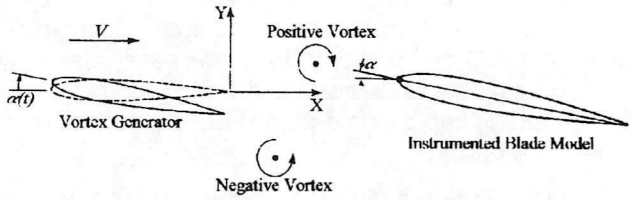


**Fig.5- Illustration of the vortex system associated with an oscillating wing (Ref.8)**

Straus et al. utilised a similar facility to Booth but limited the pitching motion to a single ramp up profile rather than a continuously oscillating motion. The aerofoil was rapidly pitched to try and obtain a single two-dimensional shed vortex. However, as stated by Straus, the response time of the pitching system is crucial to produce a single rolled-up shed vortex. The required time of motion of the pitching aerofoil should be less than the time it takes the air to travel one chord length. If the time is too long the shed vorticity will not roll-up into the required vortex. As expected, at low velocities the time to pitch the aerofoil is short - a threshold time of 21ms is quoted at a freestream velocity of 12.2 m/s. However, if the freestream velocity were to be increased, the threshold time to attain a single vortex would decrease and so mechanical actuation limits may be reached which could limit the operational range of the generator. Flow separation may also occur which could result in the generation of another vortex of opposite sense to the original shed vortex. It is also difficult to vary the size and strength of the generated vortex.

It may, therefore, be concluded that the crucial factor in all experiments to date has been the manner in which the interacting vortices have been generated and their subsequent trajectory through the wind tunnel's working section. These two features are of critical importance in interpreting the resultant data collected and in the application of such interpretations to real aircraft. When data pertaining to blade vortex interactions are acquired from experiments in which the generation of the interacting vortex differs, there are clear differences in the flow development. How important these differences are is not clear, and it may be that they simply affect the peripheral response and not the fundamental interaction. Nonetheless, whatever system is used, it is essential that the detailed structure of the interacting vortex is known. It is also important to have a good knowledge of the vortex trajectory, stability and tendency to wander from its mean path. This applies irrespective of the method of generation.

To mimic the convection of a main rotor tip vortex requires the generation of a transverse vortex which will travel in a stable fashion through the wind tunnel's working section. As discussed previously, the conventional generation method for such a vortex is to place an aerofoil at the entrance of the working section and subject it to a rapid change in incidence. Although this procedure is fraught with difficulty, it does produce a vortex, but one in which the structure may not comprehensively mimic the trailing vortex from the tip of a rotor. Accordingly, it was decided to investigate the generation of a tip vortex via the alternative method of a rotor placed in the settling chamber of a wind tunnel. The first stage of the present study was to establish the feasibility of this method of vortex generation.

This paper examines the method of generation and subsequent behaviour of a transverse vortex in a wind tunnel environment. The initial parametric design of the vortex generator, using a numerical model, is presented along with the mechanical design of the facility. Preliminary results, obtained using hot-wire anemometry, which document both the clarity of the vortex structure and its downstream movement are also presented and discussed. Finally, the remaining phases of the experimental programme, which are currently underway, are outlined.

## *Numerical Modelling*

To aid in the experimental design, development and verification of the experimental facility, it was initially decided to model the convecting vortex numerically. This model was then used to determine design parameters for the subsequent manufacture of the test facility.

The transverse vortex was to be produced by a rotating blade placed in the contraction a low speed wind tunnel. This configuration posed a number of complex problems that could only be overcome with the aid of the numerical model. The first, and most significant problem, was the accelerating flow field associated with the contraction of the tunnel. This had to be modelled to determine the effect of the velocity gradient on the convecting tip vortex and wake.

Also of interest at this stage were the relevant geometrical parameters of the blade, and the operating conditions of the blade and wind tunnel,

to attain a good representation of a transverse vortex. The developed code, therefore, had to be adaptable to enable a comprehensive analysis of the fundamental input parameters such as position, size and motion of the blade, and working section velocity. Results had to illustrate the three dimensional development of the wake (and related tip vortex) through the wind tunnel with enough clarity to isolate the specific effects of a particular design parameter.

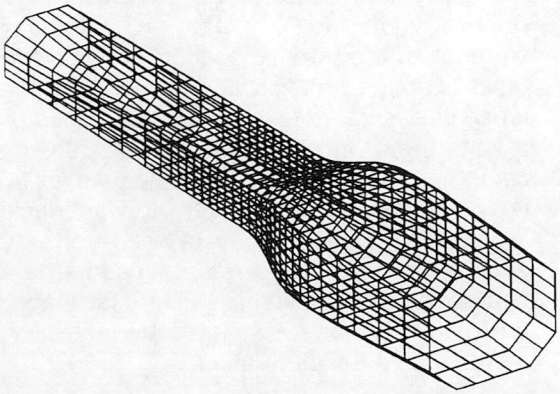

**Fig.6- Illustration of the discretised tunnel geometry used as input to the 3 dimensional panel method.**

The features of the experimental facility that had to be modelled were the vortical wake structure generated from the rotating blade and the main flow through the wind tunnel. The rotor wake was represented by a free wake vortex model consisting of a lattice of shed and trailed vortex elements which were generated using classical lifting line theory. This vortex system was then convected through the contraction and working section of the wind tunnel with the superposition of the local velocity, calculated via a three dimensional source panel method, and the induced velocity components from the vortex elements. Due to the inviscid nature of this model, no account was taken of vortex dissipation or the change in vortex strength due to deformation of the vortex element, and so the strength of each vortex element was invariant with time.

A source panel method was used to represent the constraining effects of the wind tunnel walls. The method adopted was based on the work of Hess and Smith and was chosen for its relative simplicity and adaptability to internal flows. Due to the simple geometry of the modelled portion of the wind tunnel and the non-lifting nature of the body, it was deemed sufficient to represent the wall surfaces using plane quadrilateral elements with constant source distributions.

The internal surface of the wind tunnel was discretised into approximately 1000 individual quadrilateral elements representing the settling chamber, contraction, working section and diffuser (Fig.6). This representation gave sufficient distance upstream of the vortex generator location to be out of its disturbance environment, and extended far enough downstream to allow the vortex system to convect through and out of the working section. Since the accuracy of such calculations can depend not only on the number of quadrilateral elements used but also on the manner in which these elements are distributed over the surface, a non-uniform distribution of panels was used. In particular, panels were concentrated in the region of the contraction (area of high curvature) and the working section (area of interest).

The panel method and the wake model were loosely coupled in that the induced velocities from the wake were not taken into account when calculating the source strengths of the panels. This was done for efficiency since strongly linking the two models, by calculating the induced velocities from the wake at each panel collocation point, would have significantly increased the computational time and so limited the range of cases which could have been considered in the parametric study. This approach was considered acceptable due to the low blockage presented by the generator assembly.

## *Parametric Design Study*

Two possible operating strategies were investigated for the vortex generator. Both involved the blade undergoing a specified variation in pitch angle with azimuth position. The intention was to have zero pitch on the upwind pass of the blade and then a variation of pitch angle on the downwind pass where the desired vortex structure would be produced. The aim was to produce an interacting vortex whose strength was as constant as possible along its length.

The first operating strategy involved the rotating blade accelerating from rest up to a specified speed and then being returned to rest; all within one rotor rotation. This had the advantage of producing one clean vortex structure which could be very carefully controlled by variations in rotational velocity and pitch profile.

The alternative strategy was to use a blade rotating continuously at constant speed. This approach did not require the complicated motion profiles of the single rotation cases. In fact, with the blade operating at constant rotational speed, only a pitch variation has to be specified. It is worthy of note that, while the blade traverses the area ahead of the working section, the magnitude of the normal velocity component on the blade from the tunnel flow is small compared to that of

the rotating blade itself. Hence, it is appropriate to conclude that with an almost constant tip velocity profile in this region, a constant pitch incidence would be acceptable to attain (approximately) a constant tip vortex strength.

Preliminary analysis indicated that the wind tunnel velocity, the blade rotational speed, and the position of the hub axis primarily determine the wake geometry. The relative magnitudes of the tunnel velocity and the rotational speed determine the extent to which the wake is skewed and, in the continuous running case, the separation between each consecutive convecting wake structure. The rotor hub position, on the other hand, dictates the wake curvature and elongation. For the latter, it is important for the blade to be positioned close to the working section to minimise vortex dissipation and to ensure the generation of a well-structured vortex with a high local convective velocity. These three parameters are critical for the generation of a tip vortex which is suitable for interaction experiments.

Investigation of the two operating strategies indicated that the optimum theoretical configuration for the generation of a lateral vortex was a single revolution acceleration/deceleration case. To achieve this at even moderate wind speeds necessitated very high rotational accelerations of the blade and, hence, high actuation loads. In fact, these loads were such that design of an appropriate actuation system proved impractical. Attention was, therefore, focused on the continuous running strategy.

Figure 7 depicts three examples of continuous running cases which illustrate some of the effects predicted by the numerical model. In all the cases presented, the rotational speed of the blade is such that the blade tip speed is a constant 50m/s. In Fig. 7a the blade rotational axis is a considerable distance upstream from the working section. The diagram illustrates the distortion that occurs in the wake with the blade at this location in the contraction/settling chamber. As may be observed, lower streamwise velocity in this region of the tunnel necessitates a lower tip speed to avoid interaction of consecutive wakes.

An increase in wind tunnel velocity to 30 m/s is illustrated in Fig. 7b. It is interesting to note that each wake structure is now well separated from those around it but its general form is still unacceptable because of the high curvature of the vortex system in the working section.

Figure 7c illustrates the optimum continuous running case examined in this study. As in Fig. 7a the wind tunnel velocity is 20m/s but this time the rotor hub is located much closer to the working section of the tunnel. This has the effect of reducing the wake curvature and, thus, increasing the separation distance between consecutive wake structures. In fact, the separation between tip vortices is approximately equal to the length of the working section and is sufficient to measure the vortex trajectory without significant influence from preceding vortical wake structure. For this case, the rotor had a of radius 0.75 metres.

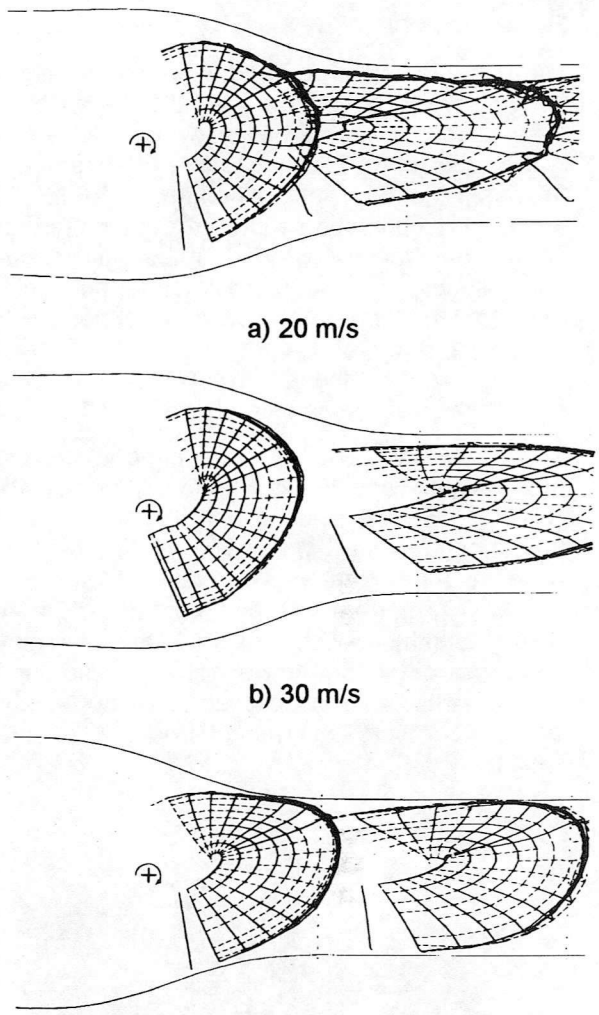


**Fig.7- Illustration of Calculated Rotor Wake Shapes**

Practical consideration must also be given to the proximity of the blade tip to the tunnel wall during the rotation of the blade. The numerical model takes no account of the viscous effects that would be experienced in this region. This is not a feature when the blade crosses the working section, but must be considered when the blade initially pitches up to generate the wake. Viscous interaction with the wall may result in vortex dissipation and produce unwanted phenomena in the convecting vortex structure. If this does occur then alteration of the radius of the blade would probably be required.

The strength of the tip vortex produced by the generator depends, to a large extent, on the pitch profile which the blade is subject to. If this profile is expressed non-dimensionally, the magnitude of the interacting vortex is simply related to the maximum pitch of the blade.

### *Experimental Facility and Apparatus*

The experiments were conducted in the 1.15m x 0.85m low speed wind tunnel of the Department of Aerospace Engineering, Glasgow University. This is a closed return facility capable of speeds up to 33 m/s. The test section length is 1.8m. The tunnel is equipped with an automated two component traverse which can be wall mounted vertically or on a support structure horizontally. The traverse is actuated via stepper motors controlled through a data acquisition board by software written under Labview. The positional error of the traverse is of the order of 0.5%.

The transverse vortex generator facility consisted of a single, variable pitch, rotating blade with a NACA 0015 cross section, positioned in the wind tunnel contraction (Fig 8). The rotating blade had a rectangular planform of chord 0.1m and tip radius 0.75m from the hub centre (0.66m total blade length). This resulted in a minimum clearance of 0.025m between the rotor tip and the tunnel wall. As discussed previously, these parameters were determined from the numerical model.

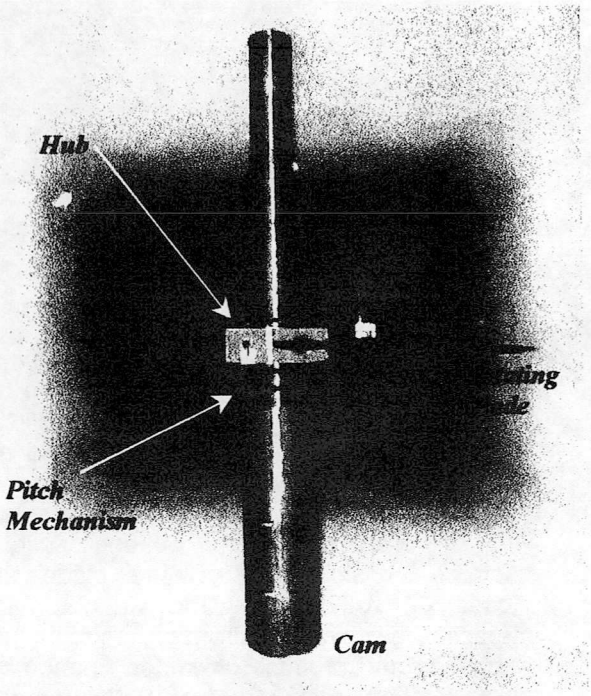


**Fig.8- Illustration of Experimental Set-Up.**

The rotor configuration adopted was that of a rigid blade with no flap and lag hinges. A flap hinge would have alleviated the root stresses and moments transferred to the hub by allowing out of plane motion. However, the vertical location of the tip could possibly have varied causing the position of the generated tip vortex to be uncertain. Also, if a flap hinge had been employed the motion of the blade would have introduced aerodynamic and inertial forces in the plane of the rotor and so, a corresponding lag hinge would probably have been required (as is the case with helicopter rotors). These hinges would have increased the complexity of the apparatus significantly and therefore the cost. Adaptation of the numerical model may also have to have been made for comparative purposes. In the rigid blade design, the aerodynamic forces generated on the blade were transferred through the hub and shaft to the external support structure.

The required blade pitch profile was produced by a spring-loaded pitch link mechanism connected to a roller which was designed to follow an appropriately shaped non-rotating cam. This cam took the form of a shroud around the lower section of the rotating shaft assembly which was isolated from the rotating shaft and bolted to a mounting plate below the wind tunnel floor. The actual pitch profile was machined along the top edge of the shroud. Thus, as the blade hub rotated, the roller followed the cam profile causing the pitch link to be displaced vertically which, in turn, produced the pitching motion of the blade.

The cam profile was such that zero degrees blade incidence, occurred when the blade was pointing into the settling chamber (45 degrees azimuthal travel on either side of the centre line). In this phase, the roller was at its lowest position. In the next 90 degree phase of motion, the blade was pitched up to 10 degrees. In this phase, the constraining arm and pitch arm return to the horizontal and the spring internally housed in the hub is compressed. After this, the blade crossed the working section at a constant incidence of 10 degrees (azimuthal position 45 degrees either side of the centre line). In the final 90 degree phase, the blade returned to zero degrees. In this phase, the spring forced the roller to remain in contact with the cam. Due to the roller being 90 degrees ahead of the rotating blade, the cam was necessarily 90 degrees out of phase with the blade.

The rotor rig was equipped with two sensors. The first optical sensor provided a measurement of the rpm of the rotating blade to enable the rotational speed of the blade to be controlled. The second sensor provided an external trigger for the hot-wire system via a 16 channel BNC input board for the internal A/D Converter.

Measurements of the magnitude and associated direction of the time-dependent velocities, produced in the wind tunnel working section by the wake passage, were obtained using a cross-wire probe connected to a TSI IFA-300 three-channel constant temperature anemometer system. For a single cross-wire, the maximum sampling rate for this system is 400 kHz. The cross-wire probes used in this study were DANTEC 55P61 probes. The sensor wires on these probes are 5*mm* diameter platinum plated tungsten wires with a length/diameter ratio of 250, which form a measuring volume of approximately 0.8mm in diameter and 0.5mm in height. The wires are orientated perpendicular to each other corresponding to 45 degrees from the freestream direction which gives the best angular resolution. An additional temperature probe was used to correct the anemometer output voltages for any variation in ambient flow temperature.

For probe calibration, an open jet vertical wind tunnel with a maximum operating velocity of 43 m/s was used. A support allowed the sensors of X-wire probe to be rotated by 30 degs in the plane of the sensors. Variation of the flow velocity and yaw angle then enabled the coefficients of the effective velocity method to be determined.

## Description of Tests

The main variables in the tests conducted were the working section velocity and rotor rotational speed. In addition the measurement position, sampling time and sampling frequency were also varied. However, a constant sampling frequency of 5000 Hz and a sampling time of 0.8 seconds was used for the majority of tests. All tests reported here were conducted with the x-wire probe situated 1.65 m downstream of the rotating axis.

Table 1 details the initial tests which were conducted at the two extremes of the operating range to investigate the actual existence of a periodic signal representative of a transverse vortex. Tests 1 and 2 were conducted at low working section velocity and rotational speed settings (10 m/s and 400 rpm respectively) and tests 3 and 4 at high wind tunnel and rotational speed settings (20 m/s and 520rpm (test3), 600 rpm(test4)). All measurements were made at position 30mm to the right of the wind tunnel centre line (when looking upstream into the settling chamber). This position was largely free of disturbances produced in the wake of the rotor hub. The vertical position of the probe was determined by traversing the probe vertically until a signal indicative of a vortex was detected. The position corresponding to the maximum response varied, as would be expected, with the operating parameters of the rig. For consistency between tests, however, a fixed location 30mm below the rotor plane was used.

**Table 1 – Initial test cases conducted.**

| Test Case | Freestream Velocity (m/s) | Rotational Speed (rpm) | Sampling Time (secs) |
|---|---|---|---|
| 1 | 10 | 400 | 0.4 |
| 2 | 10 | 400 | 0.8 |
| 3 | 20 | 520 | 0.4 |
| 4 | 20 | 600 | 0.8 |

A further series of tests were conducted at a constant working section velocity of 10 m/s. In these tests, the relationship between the rotational speed setting and the periodic nature of the convecting vortex was investigated as was the dependency of the measured signal on the horizontal measurement location. These tests were then repeated for working section velocities of 20 and 15 m/s.

All the tests documented here used a manual trigger to obtain a time history containing the signature of several vortex systems. These were sufficient to both identify and document the characteristics of the periodic vortex passage.

## Discussion of Experimental Results

The hot-wire results are presented in this section in the form of time series for the streamwise ($u$) and the vertical ($v$) velocity components. Figure 9 illustrates the orientation of the probe in relation to a convecting vortex when looking horizontally through the working section and indicates the associated sign convention used for the velocity components.

In Fig. 10a, the streamwise and vertical velocity time series for Test 1 are presented As can be seen, there is a strong periodic signal indicative of a vortex in both time series, with three vortices evident in the 0.4 second sample time. The period between each vortex is approximately 0.15 seconds which corresponds exactly to the prescribed rotational speed of 400 rpm. This corresponds to a vortex spacing of 1.5m.

The first two vortex passes are characterised by a sharp rise in the measured streamwise velocity component as the vortex approaches the probe. Subsequently, the velocity peaks and then returns to the freestream level as the vortex moves downstream of the probe. In both cases, the peak

in the streamwise velocity component is coincident with a sign change in the vertical component.

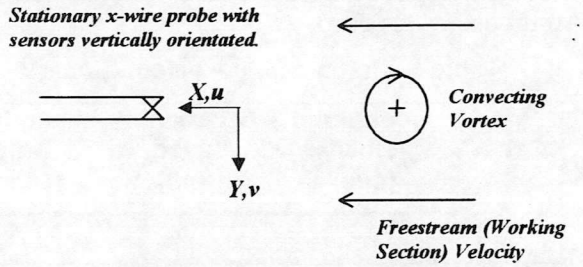


**Fig.9- Illustration of probe orientation with respect to convecting vortex.**

As may be observed in Fig.9, if the vortex were to pass above the probe, the superposition of the freestream velocity with the induced velocity from the convecting vortex would result in the observed sharp increase in streamwise velocity as the vortex passes the measurement location. This increase would reach a maximum value if the vortex were to pass exactly one core radius above the probe. If, on the other hand, the probe were to move upwards into the vortex core, the magnitude of the response of the streamwise velocity would decrease rapidly. Continuing this trend, if the vortex were to pass below the probe, the response of the streamwise velocity component would reverse to become a decrease in velocity.

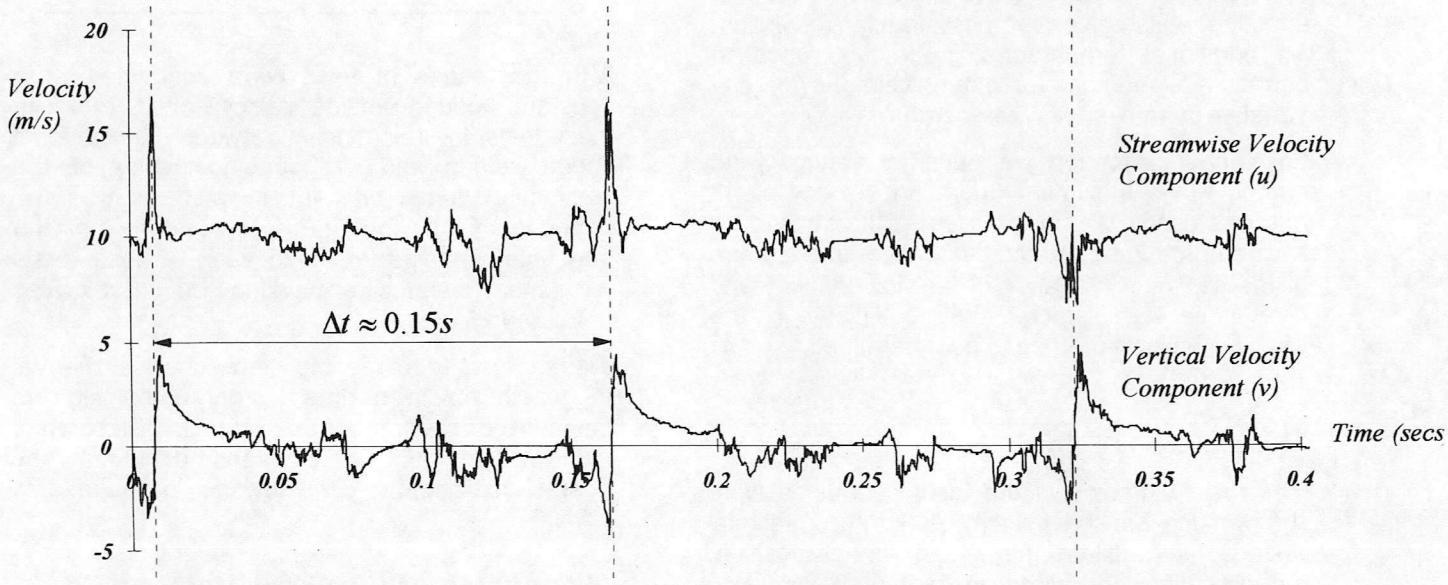


**Figure 10a – Time series for initial test case 1 depicting the periodic convecting vortex.**

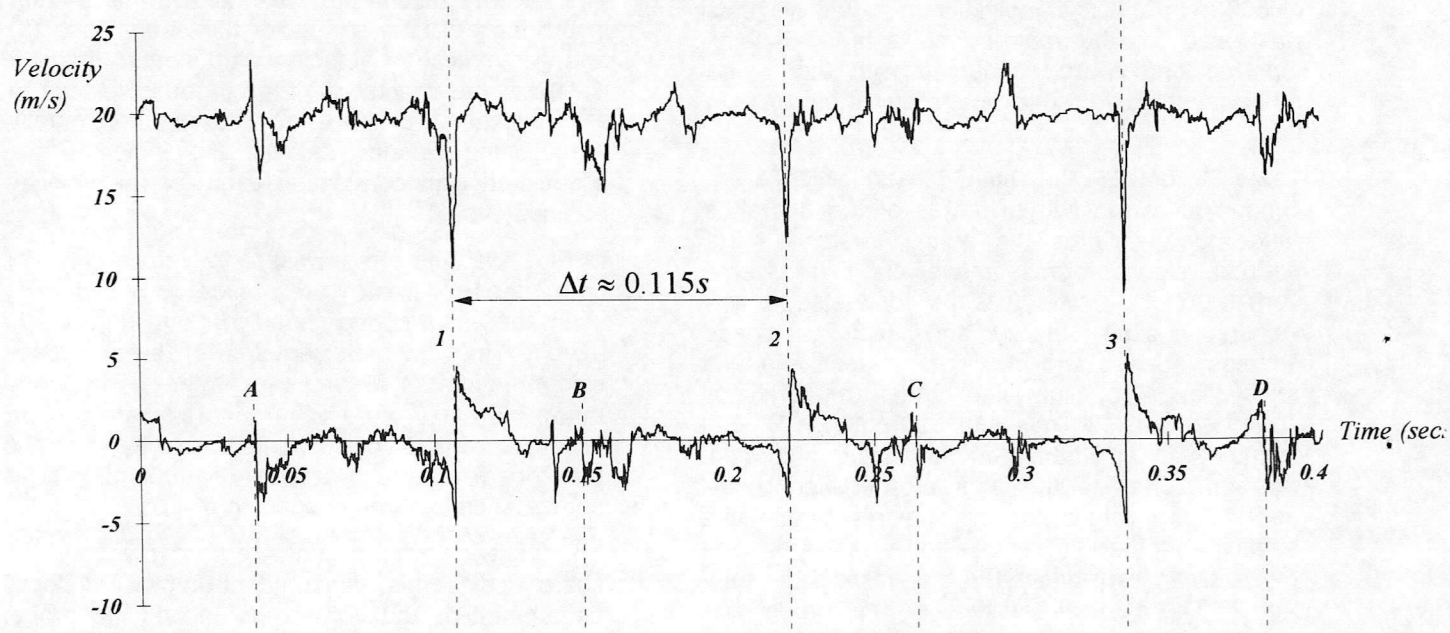


**Figure 10b – Time series for initial test case 3 depicting the periodic convecting vortex.**

In contrast to the above, the expected response of the vertical velocity component depends only on the distance of the probe from the vortex centre. As the probe is moved out from the vortex centre, the peak to peak change measured during the vortex passage would gradually decrease. This trend would continue up to and beyond the edge of the vortex core.

Given the expected behaviour of the two velocity components, it is possible to formulate an explanation for the measured response during the passage of the third vortex in Fig. 10a. The streamwise response is consistent with the vortex passing below the probe by an amount greater than the vortex core radius. Consequently, the magnitude of the vertical velocity change is slightly smaller than the previous cases.

In Fig. 10b, the freestream velocity has been increased to 20 m/s which was the maximum design speed of the facility. The rotational speed of the blade has also been increased to a value of 520 rpm. Again, the period between convecting vortices (0.115 secs) is consistent with the rotational speed of the blade. This figure depicts three convecting vortices, numbered 1,2 and 3, which, due to the greater downwash from the rotor, pass below the probe. In addition, however, there appears to be a second weak periodic signal between each vortex pass. This signal is characteristic of a vortex of the opposite sign to the strong transverse tip vortex and is identified in the figure by the letters A,B,C and D. As may be observed in Fig. 7c, which is a similar case calculated using the numerical model, there is a strong root vortex which exists to the right of the centre line; In Fig. 7, the vortex strength is indicated by the line thickness. This corresponds to the same location as the measurement probe and so this second periodic signal could be a rolled up root vortex. The response, however, could also be due to a coalescing of the shed vorticity produced during the pitching of the rotor blade. More detailed tests would be required to fully investigate the operating conditions which generate this secondary periodic signal and the measurement locations where it is evident. However, this may be complicated by the fact that this weak signal is clearly severely affected by turbulence.

The results presented above are illustrative of the basic features apparent in all of the measured hot-wire signals. In each case, the measurements, confirmed the findings of the earlier numerical study in terms of vortex position and phasing. Generally, as may be expected, the clearest and most consistent vortex signatures were obtained at the highest rotor speeds. As indicated in the numerical study, this is consistent with the production of a wake geometry suitable for interaction experiments, when the rotor is in its optimum position.

## Conclusions and Future Work

The new vortex generator facility has proved to be successful in the generation of a transverse vortex which convects through the working section of a low speed wind tunnel. It is, therefore, intended to use this technique for an experimental investigation into Blade Vortex Interaction with the vortex orthogonal to the plane of the aerofoil.

The next phase of the work will involve interacting the convecting vortex with a stationary blade located in the working section of the wind tunnel used for the present study. This blade will be instrumented with miniature pressure transducers to measure the change in surface pressure distribution during the interaction. In addition, hot-wire measurements will be made in the vicinity of the blade surface to measure the distortion of the vortex as it passes the blade.

Following this, the new vortex generation technique will be implemented in the larger 2.6mx2.1m low speed wind tunnel at Glasgow University. Once installed, the generator will be used for interaction studies on a stationary blade which will be instrumented with a large number of surface pressure transducers. Then, the stationary blade will be replaced by a tail rotor model which will have, in addition to basic force instrumentation, blades fitted with miniature pressure transducers. These two test programmes should make a significant contribution to contemporary understanding of both the pure orthogonal interaction and the more complex interactional environment of the tail rotor. The work should also compliment research planned at DERA within the HELIFLOW project to investigate quartering flight. This will use the DERA Mach scaled rotor rig together with a new tail rotor model.

## Acknowledgements

The authors would like to acknowledge the support of the British Ministry of Defence through the Defence Evaluation Research Agency (DERA). The work was funded by the DERA under extra-mural agreement ASF/2163U.

## References

1. Ellin A.D.S., "An In-Flight Investigation of Lynx AH Mk5 Main Rotor/Tail Rotor Interactions", 19th European Rotorcraft Forum, Cernobbio, Italy, Sept. 1993.

2. Wiesner W., Kohler G., "Tail Rotor Performance in Presence of Main Rotor, Ground and Winds", 29th Ann. Forum of the Amer. Heli. Soc., May 1973.

3. Leverton J.W., Pollard J.S., Wills C.R.," Main Rotor Wake/Tail Rotor Interaction", 1st European Rotorcraft & Powered Lift Forum, Sept 1975.

4. Lowson M.V., "Progress Towards Quieter Civil Helicopters", Aero. J. , 209-23, June/July 1992.

5. Sternfeld H., "Recent Developments in Helicopter Noise Reduction", 11th Congress of the International Council of the Aero. Sciences , Lisbon, Sept. 1978.

6. Tyler D.J., Vincent A.H., "Future Rotorcraft Technology Developments", Aero. J., 451-60, Dec.1996.

7. Sheridan P.F., Smith R.P., "Interactional Aerodynamics - A New Challenge to Helicopter Technology", 35th Ann. Forum of the Amer. Heli. Soc., May 1979.

8. Booth E.R., Yu J.C., "Two Dimensional Blade-Vortex Interaction Flow Visualisation Investigation", AIAA Paper 84-2307, Oct. 1984.

9. Booth E.R., "Surface Pressure Measurement During Low Speed Two-Dimensional Blade-Vortex Interaction", AIAA Paper 86-1856, July 1986.

10. Booth E.R., Yu J.C., "New Technique for Experimental Generation of Two-Dimensional Blade-Vortex Interaction at Low Reynolds Number", NASA TP-2551, March 1986.

11. Straus J., Renzoni P., Mayle R.E., "Airfoil Pressure Measurements During a Blade-Vortex Interaction and a Comparison with Theory", AIAA Paper 88-0669, Jan. 1988. (Also AIAA J. 28,222-8,Feb. 1990)

12. Horner M.B., Saliveros E., Galbraith R.A.McD., "An Experimental Investigation of the Oblique Blade-Vortex Interaction", 17th European Rotorcraft Forum, Berlin, Germany, Sept. 1991.

13. Horner M.B., Stewart J.N., Galbraith R.A.McD., Grant I., Coton F., Smith G.H., "Preliminary Results from a Particle Image Velocimetry Study of Blade-Vortex Interaction", 19th European Rotorcraft Forum, Cernobbio, Italy, Sept. 1993.

14. Horner M.B., Stewart J.N., Galbraith R.A.McD., Grant I., Coton F., "An Examination of Vortex Deformation during Blade-Vortex Interaction Utilising Particle Image Velocimetry", 19th Congress of the International Council of the Aero. Sciences, Anaheim, California, Sept 1994.

15. Coton F.N., De la Iglesia F., Galbraith R.A.McD., Horner M.B., "A Three-Dimensional Model of Low Speed Blade-Vortex Interaction", 20th European Rotorcraft Forum, Amsterdam, The Netherlands, Oct 1994.

16. Jones, H.E., Caradonna, F.X., "Full Potential Modelling of Blade Vortex Interactions", Vertica, Vol. 12, pp 129-145, 1988

17. Srinivas V., Chopra I., Haas D., McCool K.," Prediction of Yaw Control Effectiveness and Tail Rotor Loads", 19th European Rotorcraft Forum, Cernobbio, Italy, Sept. 1993.

# Appendix 4

## AN EXPERIMENTAL INVESTIGATION OF VORTEX CONVECTION EFFECTS ON A LOADED BLADE INTERACTING WITH A SINGLE VORTEX

by

C.A. Masson
R.B. Green
R.A.McD. Galbraith
F.N. Coton

Presented at the 16th AIAA Applied Aerodynamics Conference, Albuquerque, June 1998

# An Experimental Investigation of Vortex Convection Effects on a Loaded Blade Interacting with a Single Vortex[1]

by

C.A.Masson* ; R.B.Green† ; R.A.Galbraith‡ ; F.N.Coton§
Department of Aerospace Engineering
University of Glasgow
Glasgow
G12 8QQ

## ABSTRACT

**Presented in this paper are the preliminary vortex convection rate measurements recorded from a Blade Vortex Interaction (BVI) test series conducted in the University of Glasgow 1.61m × 2.13m, closed return, low speed wind tunnel, in which a single vortex interaction with a rigid, loaded rotor blade was studied. This work is an extension of that by Horner & Galbraith[3] which described the flow phenomena present during single vortex interaction with an unloaded blade. The paper presents local vortex convection effects using blade surface pressure data recorded at the 0.785 span location. A correlation of the integrated convection effects is also given using Cn and $Cm_{1/4}$ data derived from the local Cp data. The effects of pitch and vortex strength on vortex convection are also presented.**

## NOMENCLATURE

| | |
|---|---|
| Cn | sectional normal force coefficient ($= N/\frac{1}{2}\rho V_{TIP}^2 c$) |
| $Cm_{1/4}$ | sectional ¼ chord moment coefficient ($= M_{1/4}/\frac{1}{2}\rho V_{TIP}^2 c^2$) |
| Cp | sectional pressure coefficient ($= \Delta P/\frac{1}{2}\rho V_{TIP}^2$) |
| c | blade chord, 0.1524 m |
| r/R | non-dimensional span position |
| x/c | chordwise pressure transducer locations |
| $x_v$ | perpendicular horizontal distance between the leading edge pressure transducer and vortex generator (m) |
| $y_v$ | geometric height of single generator above or below rotor disk |
| $z_v$ | geometric lateral position of single generator from the tunnel centreline |
| $u_v$ | vortex convection speed (m/s) |
| $u_\infty$ | wind tunnel velocity (m/s) |
| $u_v / u_\infty$ | vortex convection ratio |
| $V_{tip}$ | rotor tip velocity ($= \Omega R$) |
| $\Delta P$ | difference in pressure between the blade surface and freestream ($N/m^2$) |
| $\theta$ | rotor pitch setting (°) |
| $\rho$ | air density ($kg/m^3$) |
| $\Gamma$ | vortex strength, ($m^2/s$) |
| $\psi$ | blade azimuth angle (°) |

## 1. INTRODUCTION

The problems associated with main rotor wake interactions have been one of the main aerodynamic areas of concern for the helicopter community. In particular, the vibratory and acoustic problems associated with the interaction of the tip vortices generated by individual blades with following blades in the rotor disk have been the main sources of aerodynamic induced problems still dogging the helicopter community. Considerable effort has been expended both in the past and present (the current investigation included) to try and better understand the phenomena. In addition, with the development of computational codes the requirement for code validation data has increased. With this in mind the present investigation has attempted to both enhance the understanding of the single BVI event by considering the vortex convection effects and hopefully provide an additional store of aerodynamic validation data.

Research into the BVI phenomena has involved both experimental[1-13] and computational[14-16] studies. (A large body of this work is reviewed in Reference 17). Relating to the experimental investigations, these studies have been performed both in-flight[1] and in the wind tunnel[2-6]. Of particular relevance to the present study are the tests performed in Refs. 2-4 in which unsteady surface pressure measurements were taken and which used a similar test set-up to the present study. This test set-up was first



* Research Assistant
† Lecturer
‡ Professor, Head of Department
§ Senior Lecturer

developed by McCormick and Surendraiah[2] and used a vortex generator positioned upstream of the rotor. This allowed far better control of the interaction parameters (height, obliqueness etc.) than could be obtained for a rotor generated BVI.

A number of experiments have also been performed in which detailed flow field data have been obtained during a BVI event. Techniques utilised have included Laser Doppler Velocimetry[7] (LDV) and Particle Image Velocimetry[8,9] (PIV). As a result the fundamental fluid phenomena associated with a BVI event has been clarified greatly.

Central to the study of BVI is the structure and behaviour of the interacting vortex[9-12] during a BVI. Following the identification of a vortex convective disturbance by Carradona et al[4] and subsequent work by Horner et al[3], investigations have progressed into the fundamental effects of the vortex as it convects over (or under) an unloaded (zero pitch) rotor blade. In particular, the work by Horner et al[3] revealed the importance of the vortex convection effects on the integrated Cn and $Cm_{1/4}$ data as the vortex approaches and then leaves the trailing edge of the blade. The present study is an extension of this work to consider vortex convection effects on a loaded blade. Both 'local' effects through a presentation of Cp data and 'integrated' effects from inspection of the Cn and $Cm_{1/4}$ trends are discussed. Finally, initial results from measurements of the vortex convection rate are presented and the effects of pitch and vortex strength on these values discussed.

## 2. EXPERIMENTAL DETAILS

### 2.1 MODEL AND TEST SET-UP

All tests were performed in the University of Glasgow 1.61 m x 2.13 m low speed, atmospheric pressure, closed return 'Handley Page' wind tunnel. Figure 1 illustrates the basic test set-up which consisted of a vortex generator located upstream of a rigid, untwisted single rotor blade. This arrangement is similar to that used by Horner & Galbraith[3].

A vortex generator was manufactured to produce a single trailing vortex. The vortex generator consisted of two NACA 0015 section cantilever wings of chord 0.1524m and was manufactured from suitably shaped aluminium spars enclosed in glass fibre skins. These wings were positioned at the roof and floor of the mouth of the working section and set at equal and opposite incidences to produce vortices of the required strength and rotational sense. The generator wing pair was pinned at the blade intersection and was of sufficient length to pass through the tunnel roof and floor. Due to the proximity of the pinned intersection a single vortex was formed. The resulting vortex system was then convected downstream by the tunnel flow to interact with the rotor, rotating clockwise when viewed from above as shown in Figure 1.

Vertical positioning of the single vortex generator was achieved automatically via a servo motor/lead screw arrangement located beneath the tunnel. Pneumatic clamps were also provided, synchronised to an electromagnetic brake on the motor to provide further stiffening following a vertical movement. Lateral positions were set manually.

Figure 2 shows the rotor blade and hub arrangement.

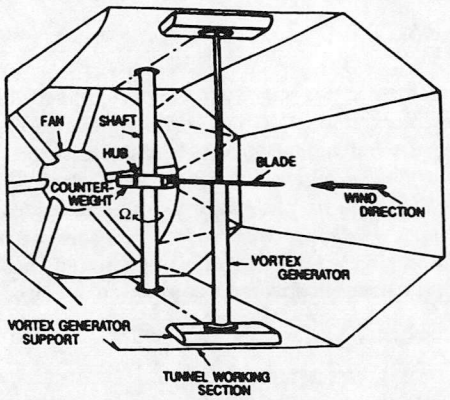


**Figure 1 : University of Glasgow BVI Facility**

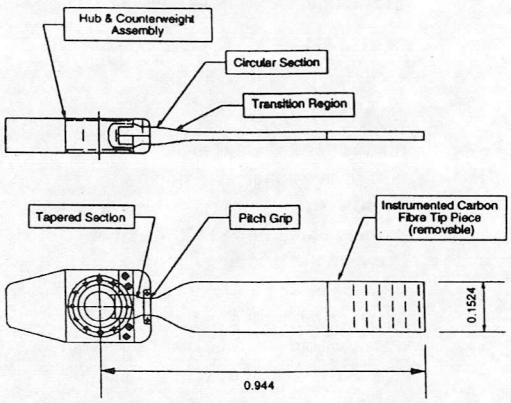


**Figure 2 : Model Blade and Hub Arrangement**

The blade, of NACA 0015 cross-section, was manufactured from carbon fibre using a purpose built Nylatron mould and had a chord of 0.1524m and a span of 0.944m (based on rotor disk radius) resulting in an aspect ratio of 6.19. The blade merged to a tapered circular section at the root located within the aluminium hub and counterweight assembly. The tapered section provided the centrifugal pull-out load reaction force, whilst the circular section and pitch grip clamp allowed the rotor pitch angle to be set at discrete values. A removable tip pod was constructed to house 72 miniature Kulite pressure transducers located at spanwise locations as shown in Table 1 and by the dashed lines in Figure 2. This allowed detailed chordwise and spanwise pressure data to be collected along the blade during a BVI event.

The rotor blade, hub and counterweight were mounted on a hollow cylindrical drive shaft located vertically in the test section and passing through the tunnel roof and floor (Figure 1). The rotor was driven at 600 rpm (10 Hz) by a DC electric motor and bevel gear arrangement located on the tunnel roof. The electrical wiring from the pressure transducers was passed through the drive shaft, and the signals were collected via a slipring set by a BE256 data logger. All data were recorded over a 144° capture angle at 50 kHz sampling rate with 32,000 samples being logged per channel, per run, over 16 revolutions. The resulting azimuth angle resolution between samples was 0.072° .

| 0.785 r/R, 0.985 r/R | | 0.825 r/R, 0.865 r/R, 0.905 r/R, 0.945 r/R |
|---|---|---|
| upper | lower | upper |
| 0 | | 0 |
| 0.009 | 0.011 | 0.501 |
| 0.029 | 0.037 | 0.948 |
| 0.059 | 0.069 | |
| 0.099 | 0.118 | |
| 0.145 | 0.183 | |
| 0.177 | 0.276 | |
| 0.224 | 0.387 | |
| 0.303 | 0.502 | |
| 0.401 | 0.630 | |
| 0.501 | 0.778 | |
| 0.578 | 0.861 | |
| 0.650 | 0.925 | |
| 0.714 | | |
| 0.775 | | |
| 0.834 | | |
| 0.895 | | |
| 0.948 | | |

**Table 1: Chordwise Distributions, x/c, of pressure transducers on the upper and lower surfaces for a given span location.**

The resultant rotor speed provided a tip Mach number of 0.17 and a nominal tip Reynolds number of 600,000. In addition, all aerodynamic data were non-dimensionalised using the rotor tip velocity, $V_{tip}$. This resulted in comparable aerodynamic scaling between the rotor and vortex generator.

## 2.2. TEST GEOMETRY

The test geometry used for the single BVI investigations is illustrated in Figure 3. All parameters were taken relative to the vortex generator wing junction located 2.1 rotor radii upstream of the rotor. Parameter $z_v$ was used as a measure of the lateral offset of this junction from the tunnel centreline. Figure 3 illustrates this for a 2nd quadrant oblique interaction.

In order to provide a temporal reference frame for a BVI interaction, the $x_v$ parameter was used. This provided a measure of the perpendicular distance between the generator wing junction and the leading edge pressure transducer at a particular station. Therefore $x_v$ was a function of both blade station, r/R, and blade azimuth angle, $\psi$. Henceforth, the ratio $x_v/c$ will be referred to as non-dimensional time.

The vertical position of the vortex generator junction above and below the rotor disk was set by the $y_v$ parameter. This is illustrated in section A-A of Figure 3 for a positive vortex. Note that the rotor disk coincides with the plane containing the mid-chord location of the pitched blade. Also note that all the above parameters are geometrical in origin and do not account for the effects of vortex meander.

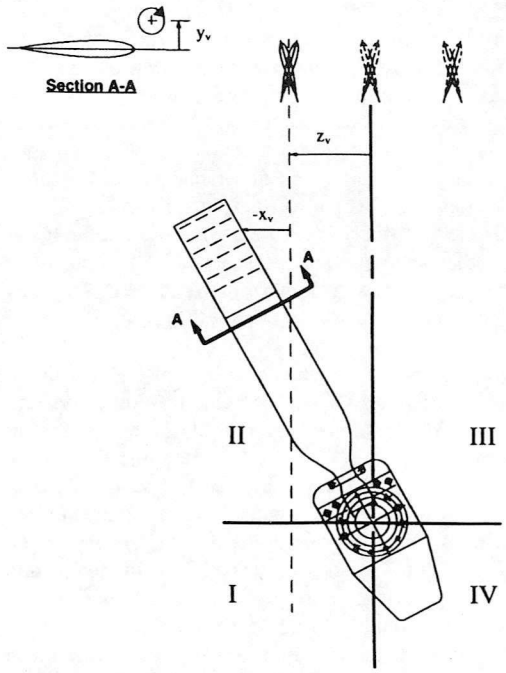


**Figure 3: Single Vortex Interactions - Test Geometry**

## 2.3. TEST PROGRAMME

Details of the single vortex test programme are shown in Table 2 from which it can be seen that five rotor pitch angle settings were considered. For each of these pitch angles a parallel interaction ($z_v/c = 0$) and two oblique interactions ($z_v/c = \pm 2$) were studied. For the zero pitch case the generator heights were set at 33 positions in steps of 0.1c over the $-1c < y_v < -0.2c$ and $0.2c < y_v < 1c$ ranges, and in steps of 0.025c over the range $-0.2c < y_v < 0.2c$. At all other pitch settings the generator heights were set at 13 positions:

$$y_v/c = \pm 1, \pm 0.8, \pm 0.6, \pm 0.4, \pm 0.2, \pm 0.1, 0$$

| Rotor Pitch , $\theta$ (degrees) | $Z_v/c$ | Vortex Strength, $\Gamma$ ($m^2/s$) |
|---|---|---|
| 0 | -2 | 5.8 |
| | 0 | 5.8 |
| | 2 | 5.8 |
| 3,6,9,12 | -2 | ± 5.8<br>± 3.7 |
| | 0 | ± 5.8<br>± 4.6<br>± 3.2<br>± 2.6 |
| | +2 | ± 5.8<br>± 5.2 |

**Table 2: Single Vortex Interactions - Test Matrix.**

## 3. EXPERIMENTAL ERRORS

Owing to the automatic gain adjustment feature on the data acquisition system, the pressure measurements during a given run were recorded at the maximum accuracy of the system. Removal of offsets from the pressure measurements required particular care, however. The total offset consisted of a static contribution and a dynamic contribution. The static contribution was removed automatically prior to a run, but since the dynamic contribution was caused by the effect of blade rotation on the transducer medium, this offset had to be measured and subtracted as part of the post-processing. To do this the transducer holes were covered, and the blade was then spun up to its test speed with the tunnel off. The transducer signals were then recorded. This was repeated for every blade pitch setting.

The overall accuracy of the non-dimensional pressure is high. When the discretization errors and calibration factors are considered, the uncertainty in each Cp value is estimated to be some 0.5%. The blade pitch could be set to an accuracy of better than $0.25^{\circ}$, while vortex strengths were determined by hot wire tests, and were accurate to some 2%. By far the largest source of error in the tests was in the position of the vortex, however. Although the vortex generator could be positioned to better than 0.5mm, the vortex itself was found to meander. This effect was due to the 10Hz forcing of the rotating blade, since in the vortex strength measurement tests the vortex core was found to be steady. The meandering effect during BVI tests has been observed in particle image velocimetry tests using a similar facility at Glasgow (Horner et al. [8,9]). The amplitude of meander from the PIV tests is estimated to be one quarter of the blade chord, although the mean meander is less than this. The primary effect is that of a change in vortex height. However, the 16 interactions recorded per test case permits a good estimation of the mean pressure data for a given nominal vortex height. In addition, pressure data were sampled during some of the above described PIV tests, which were then compared with the data for the nominal vortex height. On the strength of these previous investigations, the individual interactions presented in this paper are therefore believed to be representative data for the nominal vortex position. It is stressed that vortex meander effects are often reported in BVI experiments, and methods of accounting for the vortex meander during analysis are the subject of further research.

## 4. PRESENTATION AND DISCUSSION OF RESULTS

In each of the discussions below a detailed description of the salient features for a vortex traversing the upper surface of a 6° pitched blade is first given. This is then followed by a discussion of a BVI in which the vortex traverses the lower surface of the blade.

### 4.1.1 Local Vortex Effects - Pressure Data

Figure 4 illustrates typical reduced pressure data recorded on the upper surface during a parallel interaction ($z_v/c = 0$) with a clockwise rotating vortex of strength, $\Gamma = 5.8 m^2/s$ at the inboard ($r/R = 0.785$) station for a pitch of 6°. The plot shows -Cp data on the vertical axis plotted against the transducer chord position, x/c, and non-dimensional time, $x_v/c$, in the foreground. For this case the geometric interaction height, $y_v/c$, was set at 0.1 which resulted in a vortex trajectory above the rotor disk. Furthermore, in order to provide sufficient clarity in the pressure data presented, only every 3rd sample is plotted.

Figure 4 shows the characteristic slow increase in leading edge suction peak associated with the flow field induced by the approaching vortex. This is followed by a rapid collapse of this peak as the vortex moves onto and over the leading portions of the blade in the $0 < x_v/c < 0.35$ region. After this point, a more clearly defined low pressure ridge associated with the vortex convection over the aft portions of the blade is seen, until the vortex finally leaves the blade at approximately $x_v/c = 0.91$.

A disturbed region is also seen at the trailing edge of the blade. The origin of this signal is thought to be due to the effects of the vortex. PIV work at Glasgow[4,19] has shown that the following the passage of the vortex off the trailing edge, the rear most portions of the blade remain in a highly disturbed flow field as the vortex initially moves downwards and then upwards in the blade wake. A second possibility may be due to the physical restrictions in placing the transducers at the trailing edge of the blade. This resulted in complex interconnecting geometry's in the short tube lengths used between the surface tappings and transducer orifices. However, a computational analysis of these tubes revealed that transducer ringing would occur in the 1.5kHz region. As a consequence, all transducers were filtered at 1kHz to remove these high frequency components.

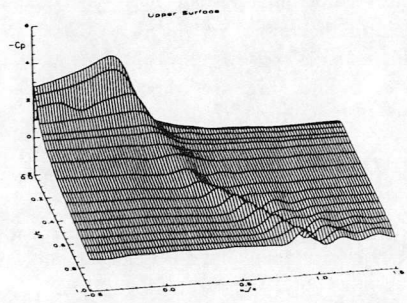


**Figure 4: Typical Pressure Data obtained at r/R= 0.785 and θ = 6° for a parallel upper surface vortex passage. ($y_v/c = 0.1$, $z_v/c = 0$ and $\Gamma$=5.8 $m^2/s$).**

For completeness in the discussion, Figure 5 is presented showing a typical lower surface pressure plot obtained from a vortex convecting below a 12°

pitched rotor blade during a BVI event. Note that due to the larger scale on the $x_v/c$ axis only every 4th sample is plotted.

Due to the sense of the vortex in Figure 5, the flow velocities on the lower surface of the blade are inhibited and no large suction region occurs as the vortex approaches the blade. The relatively large suction pressures recorded at the front two transducers are indicative of the rearward shift in the stagnation point on the lower surface.

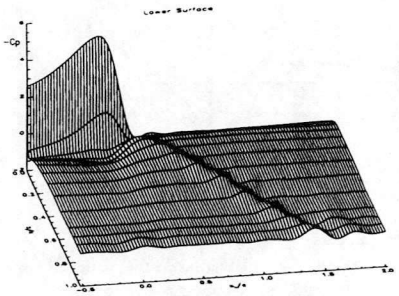


**Figure 5: Typical Pressure data obtained at r/R = 0.785 and θ = 12°, for a lower surface vortex passage. ($y_v/c = 0$, $z_v/c = 0$ and $\Gamma = 5.8$ m²/s).**

The remaining pressures recorded on the forward portion of the lower surface increase slightly as the vortex approaches the blade in the $x_v/c = 0$ region. This region of overpressure continues until approximately the $x_v/c = 0.3$ position. Furthermore, Figure 5 reveals a delay in the appearance of the low pressure ridge associated with the vortex convection below the blade until the $x_v/c = 0.3$ region. At present it is not clear if the region of overpressure slows the approaching vortex, hence delaying the start of the vortex convection ridge. This will be the subject of future investigations. A recovery in the lower surface suction pressures is then seen as the low pressures associated with the impinging vortex begin to dominate.

As a result of the absence of large leading edge suction pressures, the vortex convection ridge is more visible over a larger part of the chord on the lower surface than on the upper surface. In addition, due to the competing influences of the vortex and surface flows at this interaction height, it is evident from Figure 5 that the vortex takes longer to convect off the lower surface of the blade. Similar features were also found at other pitch settings for a vortex convecting below the rotor disk.

### 4.1.2 'Integrated' Vortex Effects - Cn data

Figure 6 illustrates the sectional normal force coefficient non-dimensional time histories obtained by integrating the upper and lower surface pressures of the 0.785 span station presented in Figure 4.

Figure 6 shows the results for the θ = 6° case from which it can be seen that the Cn data increases to a maximum value in the $x_v/c = 0$ region. Following this point the normal force abruptly decreases, flattens, and then following a sudden decrease in Cn near $x_v/c = 1$, approaches zero as the blade azimuth increases.

Comparison of this plot with that in Figure 4 reveals that this trend follows closely the vortex induced effects on the Cp data. In particular, the initial rise followed by the sudden reversal in Cn occurs as the vortex first approaches and then convects over the front section of the blade. The resulting suction peak produces the corresponding maximum Cn value in the $x_v/c = 0$ region. Following this, the collapse in suction pressures on the forward portion of the blade noted in Figure 4, results in the 'sloped' loss of upward force.

In the $x_v/c = 0.35$ region the leading edge suction peak has collapsed. Here, the relatively constant upward force increment associated with the low pressure vortex convection ridge, halts the drop in normal force data. This causes the Cn values to level off until the $x_v/c = 0.91$ timing line. This timing line (shown dashed) was extracted from Figure 4 and corresponds to the point at which the vortex convects off the trailing edge of the blade. The following negative spike corresponds to the loss of vortex induced upward force on the rotor as the low pressure vortex convects off the blade. In addition, the vortex flow field also causes a corresponding increase in the pressures recorded at the trailing edge of the lower surface which further contributes to the magnitude of this spike. This induced effect then decreases as the vortex convects away from the blade, and the Cn data returns gradually to a zero value.

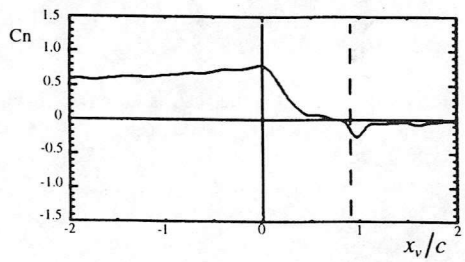


**Figure 6: Cn data obtained at r/R = 0.785 and θ = 6° parallel, upper surface vortex passage. ($y_v/c = 0.1$, $z_v/c = 0$ and $\Gamma = 5.8$ m²/s).**

Figure 7 presents the integrated Cn values obtained for the run shown in Figure 5, where the vortex convects below the blade. Note that the increased magnitude of the Cn data seen in the $x_v/c < 0$ region is due to the choice of the rotor tip velocity, $V_{tip}$, for non-dimensionalising the aerodynamic data. As a result, the wind tunnel velocity has not been scaled out of the resultant non-dimensional data. This produces the relatively high Cn values recorded in the second quadrant ($x_v/c < 0$).

Clearly, the Cn plot is still dominated by the increase and collapse in the leading edge suction region on the upper surface as the vortex approaches and then passes under the rotor. However, the low

pressures associated with the vortex result in an increased downward force acting on the blade as the vortex convects along the lower surface.

The collapse of the upper surface suction region, and the relatively constant force generated by the vortex convection ridge, result in a flattening of the Cn data up until the vortex leaves the blade at the $x_v/c$ = 1.41 timing line (extracted from Figure 5). This slower moving vortex leaving the trailing edge of the blade causes a reduced localised spike in the Cn data but in the opposite sense to that detailed above for the overhead vortex passage. This is thought to be due to the effect of the increased downwash at the trailing edge of the blade which deflects the vortex downwards, away from the rotor disk, and hence reduces the influence of the low pressure vortex on the upper surface.

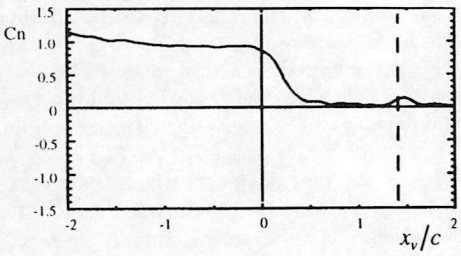


**Figure 7: Cn data obtained at r/R = 0.785 and θ = 12°, for a lower surface vortex passage. ($y_v/c$ = 0, $z_v/c$ = 0 and Γ = 5.8 $m^2/s$).**

### 4.1.3 'Integrated' Vortex Effects – $Cm_{1/4}$ data

Figure 8 presents the quarter chord sectional moment data obtained by integration of the upper and lower surface pressure distribution at the 0.785 span station presented in Figure 4.

This figure illustrates the results obtained for the θ = 6° case. The trend shows that as the vortex approaches the blade it experiences an increasing nose-up pitching moment until the $x_v/c$ = 0.1 region. Thereafter, the $Cm_{1/4}$ value reduces in magnitude as the vortex passes over the upper surface of the blade before a final, fast acting nose-up pitching moment occurs at the $x_v/c$ = 0.91 position. Following this point, the $Cm_{1/4}$ data peaks before returning to a negative value which slowly tends towards zero. Again, comparison of this plot with that in Figure 4 reveals that the $Cm_{1/4}$ corresponds closely with the vortex induced effects on the Cp data.

As indicated above, the approach of the vortex causes an increase in the nose up moment which continues past the $x_v/c$ = 0 region. This delay in recording the maximum $Cm_{1/4}$ value is thought to be due to a greater net suction pressure occurring on the forward portion of the blade as the low pressure vortex first convects onto the rotor.

The $Cm_{1/4}$ values then drop as the vortex convects past the quarter chord. This effect is produced by the low pressure vortex convection ridge which generates an increasing negative nose down pitching moment, as its moment arm increases during its movement towards the trailing edge. This continues until the vortex convects off the blade near the $x_v/c$ = 0.91 timing line. As the vortex spills off the blade, the sudden gain in negative Cn described above and the large moment arm combine to produce a fast acting surge in $Cm_{1/4}$. This then reverses as the vortex moves away from the blade. As the blade continues to move, this influence is further reduced and the pitching moment slowly returns to a zero value.

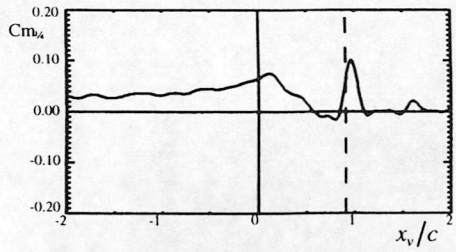


**Figure 8 : $Cm_{1/4}$ data obtained at r/R = 0.785 for a parallel upper surface vortex passage. ($y_v/c$ = 0.1, $z_v/c$ = 0 and Γ = 5.8 $m^2/s$).**

Figure 9 illustrates the $Cm_{1/4}$ history for the case when the vortex passes below the rotor blade. For this case a smaller increase in the $Cm_{1/4}$ values is experienced as the vortex approaches the blade. This is due to the presence of high suction pressures on the front portion of the lower surface which reduce the effect of the nose-up moment generated by the upper surface pressures. Following this point, the low pressures associated with the convection ridge maintain the nose up moment acting on the blade.

Finally, as the vortex convects off the underside of the blade at $x_v/c$ = 1.41, the induced moment spike is reversed in sign and is also of smaller magnitude. This is due to the reduced Cn spike noted above in Figure 7.

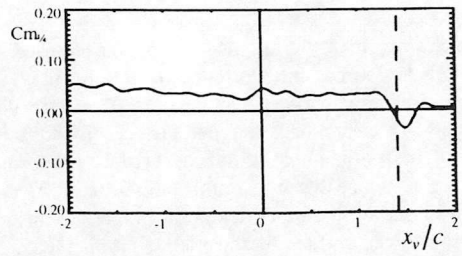


**Figure 9: $Cm_{1/4}$ data obtained at r/R = 0.785, and θ= 12°, for a parallel lower surface vortex passage. ($y_v/c$=0, $z_v/c$ =0 and Γ = 5.8 $m^2/s$).**

### 4.2 Vortex Convection Rate Effects

Although in principle the vortex convection rate is straightforward to measure, it is difficult to produce definitive quantitative results for the vortex convection rates. The reason for this is the true $y_v/c$ location of the vortex (as opposed to the geometric

$y_v/c$ value defined in section 2.1) is a function of the 10Hz forcing frequency of the blade and the initial starting position of the vortex. This variation in true $y_v/c$ results in considerable variation in the radial distance between the vortex core and blade surface and consequently large variations in the local velocities at the blade - especially at true $y_v/c$ values close to the vortex core radius. Furthermore, any vortex deformation (Horner et al[9]) will further accentuate these velocities.

The following study is an attempt to provide a qualitative discussion of the actual vortex convection rates as a function of vortex height, blade pitch and vortex strength. The methodology adopted in calculating the vortex convection rate is discussed in the following section prior to the presentation of the vortex convection rate data.

### 4.2.1 Methodology

The convection speed was determined by measuring the timing of each local peak suction for each transducer which was taken as a definite fix in vortex location. This was achieved by first visually selecting the local peak from which the closest sample number, n, was found. Adjacent Cp values in an $n - 7 \leq n \leq n + 7$ range were then examined automatically and the exact local maximum Cp value determined. These maximum Cp values were then fitted using a least squares best fit line to determine the average convection speed of the vortex on the blade. Figure 10 illustrates this for a vortex track on the upper surface of the blade and is typical of the results obtained from this method. In this case the recorded block, or revolution, was the 10th of the 16 recorded per run. Note the linear nature of this result indicated both visually and by the calculated residual sum (a value of zero signifies an exact linear fit). This signifies a relatively constant speed for the vortex as it moves over the rear ¾ of the blade.

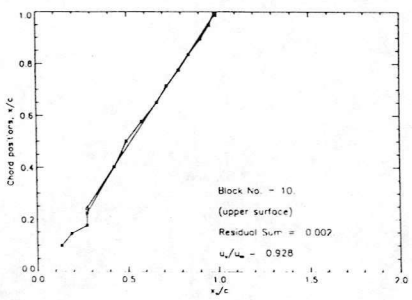


**Figure 10: Illustration of typical calculated vortex speed data. ($y_v/c = 0.1$, $z_v/c = 0$ and $\Gamma = 5.8$ $m^2/s$).**

### 4.2.2 Effect of Pitch

Figures 11 and 12 present the convection speed ratio $u_v/u_\infty$ as a function of pitch and geometric interaction height, $y_v/c$ for both the upper and lower surfaces respectively. This data was obtained for the 0.785 span station during a parallel interaction ($z_v/c=0$) with the strongest clockwise rotating vortex, $\Gamma = 5.8m^2/s$. The results are typical of those found at different vortex strengths over the same pitch range. The best results were obtained in the vortex position range $-0.4 \leq y_v/c \geq 0.4$. Outside this range, no clear vortex tracks were seen on the blade.

Figures 11 and 12, a through e show all the vortex convection speed ratios calculated for both the upper and lower surface data for each value of pitch considered. The averaged convection speed ratio trend lines have also been included in these figures.

Figures 13 and 14 have been produced using the average trend line data extracted from Figures 11 and 12. Owing to the scatter in the calculated values, it is difficult to extract any meaningful trends from these figures. However, Figure 13 suggests that the convection speed falls as pitch angle increases for $y_v/c > 0.1$. This implies that at high pitch angles the blade 'drags' the vortex along with it. It had been expected to see a greater spacing in the upper surface data as the local flow speeds on the blade increase with pitch, consequently, increasing the convection of the clockwise rotating vortex over the blade. Similarly, the apparent downward trend seen on the lower surface data is consistent with the physical interpretation of the flow by the authors. For example, consider as the vortex approaches the blade lower surface (indicated by an increasing $y_v/c$ value in Figure 14) we would expect the clockwise rotating vortex to oppose the 'natural' flow on the blade surface, hence reducing the convection rate on the blade as seen.

It is interesting to compare Figures 13 and 14 for the upper and lower surfaces respectively. Figure 14 indicates no trend with pitch angle, although Figure 13 suggests a pitch angle dependency.

Clearly, this discussion is purely speculative at present given the scatter of the results shown in Figures 11 and 12. On-going work at Glasgow is currently trying to address this problem using the local leading edge suction pressures in an attempt to better correlate the convection speed data with the true vortex height. This is an attempt to tighten up the scatter seen above, and hopefully allow more definite conclusions to be drawn from the current work.

### 4.2.3 Effect of Vortex Strength, Γ

Figures 15 and 16 present the convection speed ratio $u_v/u_\infty$ as a function of vortex strength and geometric interaction height, $y_v/c$ for both the upper and lower surfaces respectively. This data was obtained for the 0.785 span station during a parallel interaction ($z_v/c=0$) at a pitch, $\theta = 6°$. The results are typical of those found at different pitch settings over the range of vortex strengths shown. Again, the best results were obtained in the vortex position range $-0.4 \leq y_v/c \geq 0.4$.

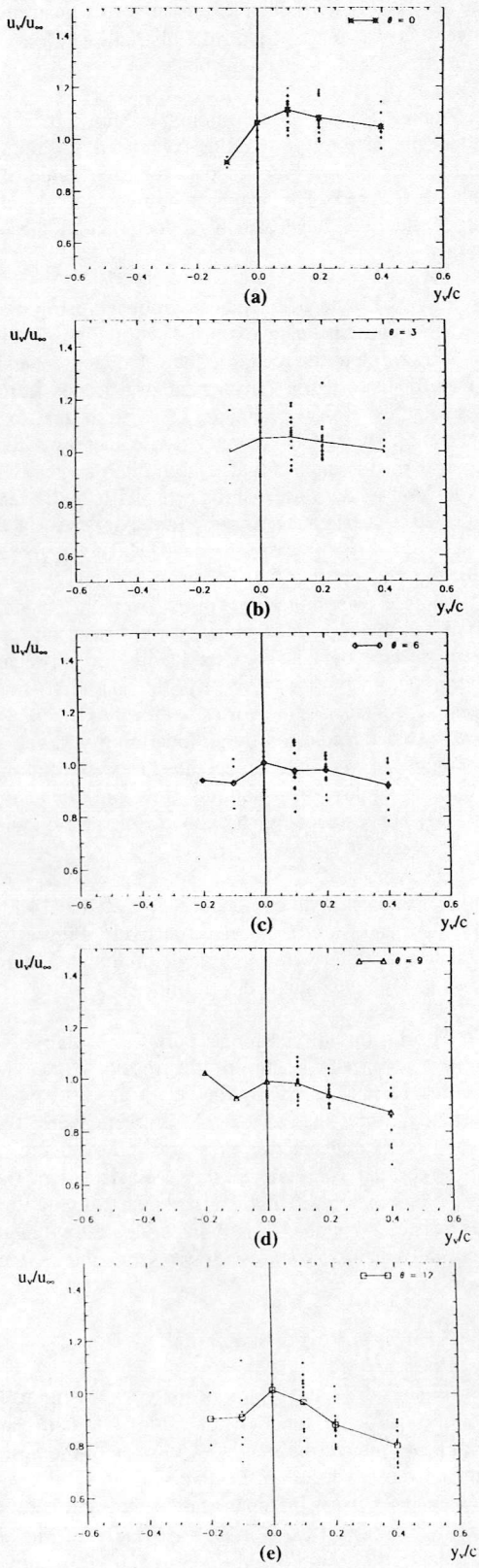


**Figure 11: Calculated upper surface convection speed ratio data, $u_v/u_\infty$, at different pitch settings. ($z_v/c = 0$ and $\Gamma = 5.8\ m^2/s$).**

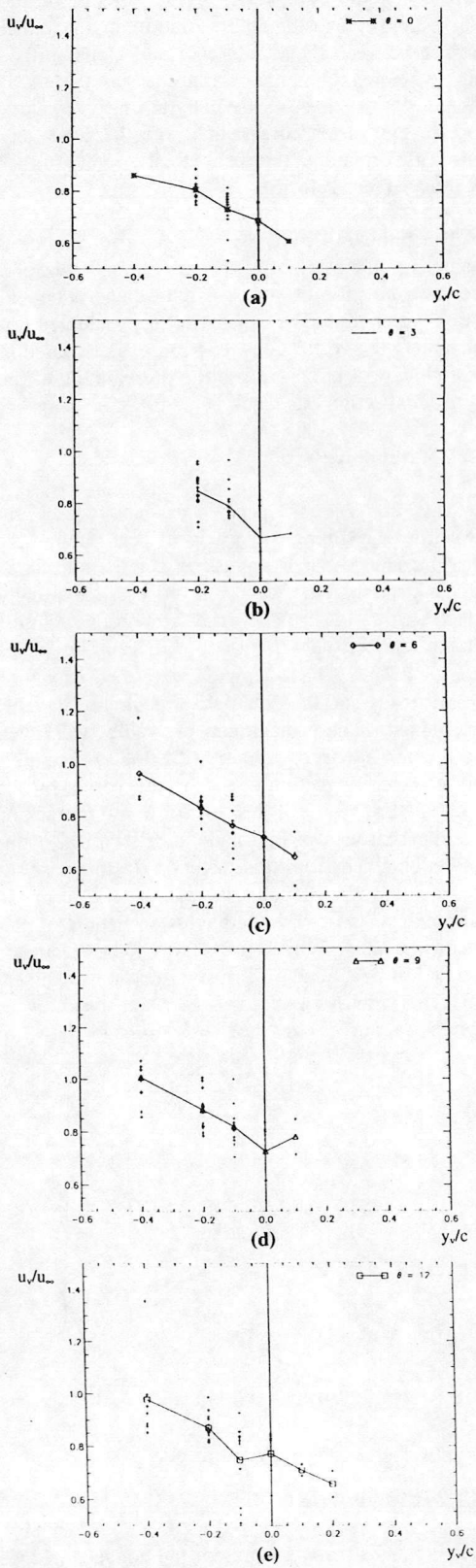


**Figure 12: Calculated lower surface convection speed ratio data, $u_v/u_\infty$, at different pitch settings. ($z_v/c = 0$ and $\Gamma = 5.8\ m^2/s$).**

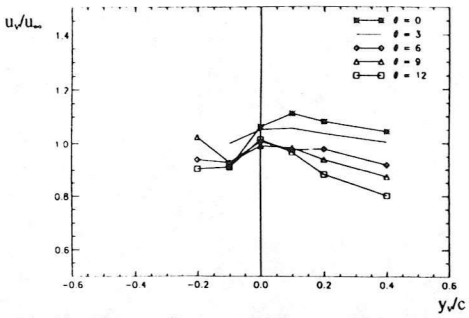


**Figure 13: Averaged upper surface convection speed ratio data, $u_v/u_\infty$, at different pitch settings. ($z_v/c = 0$ and $\Gamma = 5.8\ m^2/s$).**

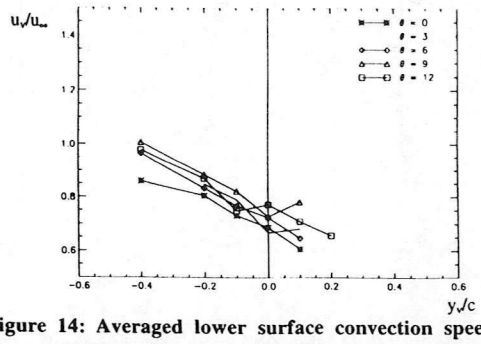


**Figure 14: Averaged lower surface convection speed ratio data, $u_v/u_\infty$, at different pitch settings. ($z_v/c = 0$ and $\Gamma = 5.8\ m^2/s$).**

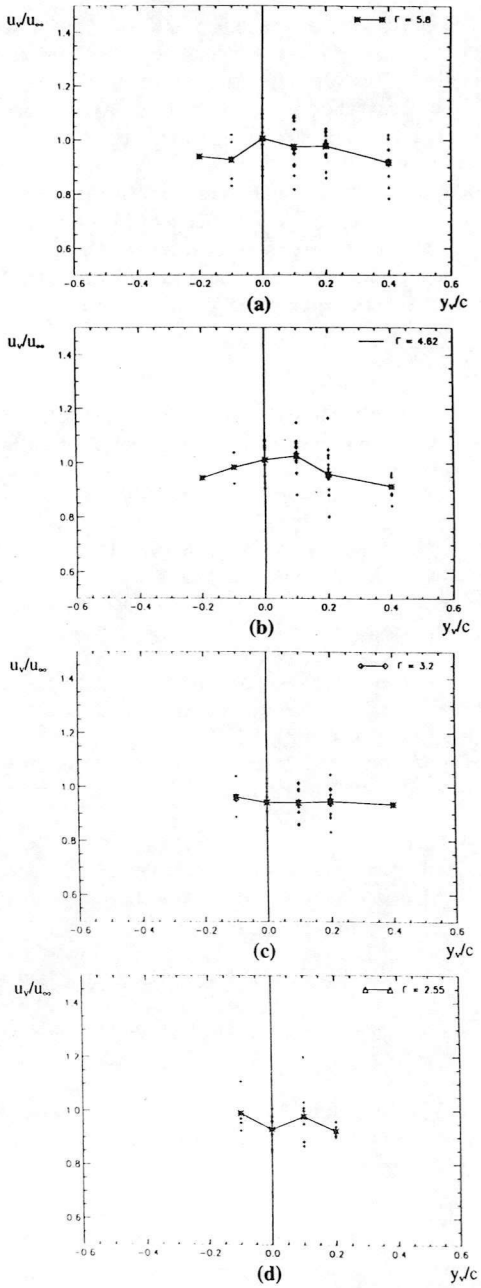


**Figure 15: Calculated upper surface convection speed ratio data, $u_v/u_\infty$, at different vortex strengths. ($z_v/c = 0$ and $\Gamma = 5.8\ m^2/s$).**

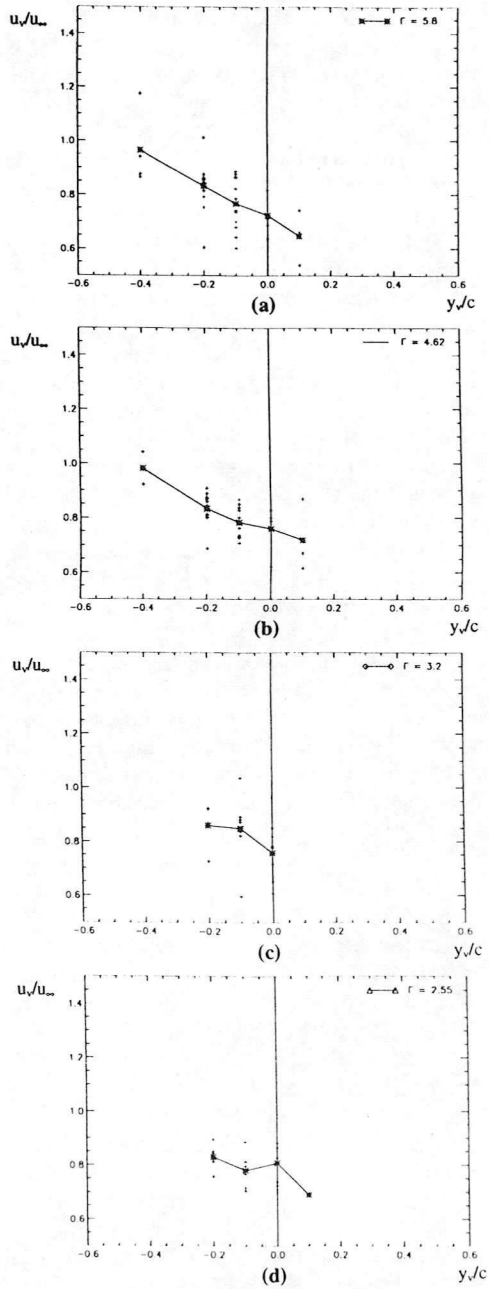


**Figure 16: Calculated lower surface convection speed ratio data, $u_v/u_\infty$, at different vortex strengths. ($z_v/c = 0$ and $\Gamma = 5.8\ m^2/s$).**

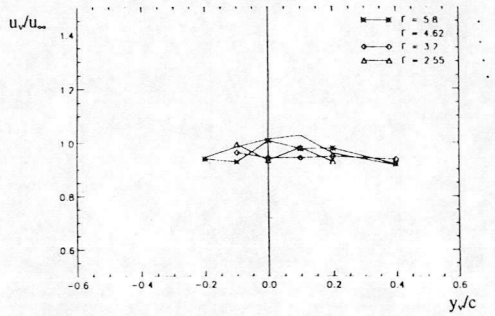


**Figure 17: Averaged upper surface convection speed ratio data, $u_v/u_\infty$, at different vortex strengths. ($z_v/c = 0$ and $\Gamma = 5.8\ m^2/s$).**

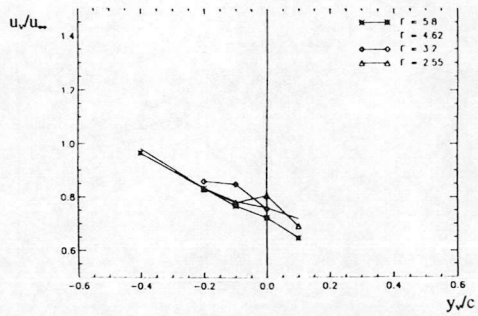


**Figure 18: Averaged upper surface convection speed ratio data, $u_v/u_\infty$, at different vortex strengths. ($z_v/c = 0$ and $\Gamma = 5.8\ m^2/s$).**

Figures 15 and 16, a through e show all the vortex convection speed ratios calculated for both the upper and lower surface data for each value of vortex strength considered, and again highlight the large scatter present in the data. The averaged convection speed ratio trend lines have also been included in these figures.

Figures 17 and 18 have been produced using the average trend line data extracted from Figures 15 and 16. Again, owing to the scatter in the measurements, it is difficult to extract any meaningful trends from these figures. Speculative conclusions concerning the relatively flat upper surface average convection ratio data (Figure 17) would suggest that possibly the convection rate of the vortex is to a first degree independent of vortex strength. Similarly, the apparent downward trend in convection rate seen on the lower surface with increasing $y_v/c$ (Figure 18) may be indicative of the small effect of the vortex strength on the convection rates seen on the lower surface.

Again, this discussion is purely speculative given the nature of the data and the present on-going work detailed in section 4.2.2 above is currently seeking to address this problem. However, Figures 17 and 18 and Figures 13 and 14 indicate different trends for the vortex convection rate with $y_v/c$ above and below the blade. This is the subject of further investigation.

## Conclusions

Details are given of a Blade Vortex Interaction (BVI) test series performed at the University of Glasgow 1.61m×2.13m low speed, closed return, 'Handley Page' wind tunnel, in which single vortex interactions with a rigid, loaded and unloaded rotor blade were investigated.

Results are presented for parallel single vortex interactions at different rotor pitch settings from which consistent vortex induced features were noted. In particular, the presence of a clearly defined vortex track, or convection ridge, on the blade was used to correlate the effects on local Cp and integrated Cn and $Cm_{1/4}$ as the vortex first approaches and then leaves the trailing edge of the blade.

This same convection ridge was taken as a definite fix on the vortex position as it traverses the blade. This allowed accurate calculations of the vortex convection speeds to be made. The effects of blade pitch and interacting vortex strength on these values were then investigated. The large scatter in convection speed data due to the influence of vortex meander precluded definite conclusions being made concerning the effects of these parameters on vortex strength, and a discussion of future work aimed at addressing this problem is given.

## References

1. Scheiman, J., Ludi, L.H., "Qualitative Evaluation of Effect of Helicopter Rotor-Blade Tip Vortex on Blade Air Loads"
*NASA Technical Note D-1637, May 1963*

2. McCormick, B.W., Surendraiah, M., " A Study of Rotor Blade/Vortex Interactions"
*The 26th Annual National Forum of the Helicopter Society, Washington DC, June 1970*

3. Horner , M.H., Galbraith, R.A.McD., "An Examination of Vortex Convection Effects During Blade-Vortex Interaction"
*The Aeronautical Journal, Vol. 96, Number 960, December 1992.*

4. Carradonna, F.X., Lautenschlager, J.L., Silva, M.J, "An Experimental Study of Rotor-Vortex Interaction"
*AIAA Paper 88-0045, AIAA 26th Aerospace Sciences Meeting, Reno, Nevada, January, 1988.*

5. Müller, R.H.G., "Special Vortices at a Helicopter Rotor Blade"
*Journal of the American Helicopter Society, October 1990.*

6. Lorber, P.F, "Blade-Vortex Interaction Data Obtained from a Pressure-Instrumented Model UH-60A Rotor at the DNW"
*Journal of the American Helicopter Society, July 1993.*

7. Gorton, S.A., Poling, D.R., Dadone, L., "Laser Velocimetry and Blade Pressure Measurements of a Blade-Vortex Interaction"
*Journal of the American Helicopter Society, April 1995.*

8. Horner, M.B., Stewart, J.N, Galbraith, R.A.McD., Grant, I., Coton, F., Smith, G.H., "Preliminary Results from a Particle Image Velocimetry Study of Blade-Vortex Interaction"
*19th European Rotorcraft Forum, Cernobbio, Italy, September 1993.*

9. Horner, M.B., Stewart, J.N, Galbraith, R.A.McD., Grant, I., Coton, F., "An Examination of Vortex Deformation during Blade-Vortex Interaction Utilising Particle Image Velocimetry"
*19th Congress of the International Council of the Aero. Sciences, Anaheim, California, September 1994.*

10. Spencer, R.N., Stermfeld Jr.,N., McCormick, B.W., "Tip Vortex Core Thickening for Application to Helicopter Rotor Noise Reduction"
*USAAVLABS Technical Report 66-1, January 1967.*

11. Tangler, J.L., "Experimental Investigation of the Subwing Tip and its Vortex Structure"
*NASA Contractor Report 3058, 1978.*

12. Copland, C.M, Coton, F.N., Galbraith, R.A.McD., "An Experimental Study on the Idealised Vortex System of a Novel Rotor Blade Tip"
*23rd, European Rotorcraft Forum, Dresden, September, 1997*

13. Coton, F.N., De La Iglesia, F., Galbraith, R.A.McD., Horner, M.B., "A Three-Dimensional Model of Low Speed Blade Vortex Interaction"
*20th European Rotorcraft Forum, Amsterdam, October, 1995.*

14. Jones, H.E., Caradonna, F.X., "Full Potential Modelling of Blade-Vortex Interactions"
*Vertica Vol. 12, No. 1/2, pp129-145, 1988.*

15. McCroskey, W.J., "Some Rotorcraft Applications of Computational Fluid Dynamics"
*NASA Technical Memorandum 100066, March 1988.*

16. Srinivasan, G.R., McCroskey, W.J. "Numerical Simulations of Unsteady Airfoil-Vortex Interactions"
*Vertica Vol. 11, No. 1/2, pp3-28, 1987.*

17. Conlisk, A.T., "Modern Helicopter Aerodynamics"
*Annual Review of Fluid Mechanics, 29: pp515-567, 1997*

18. Coton, F., Galbraith, R.A.McD., Grant, I., Hurst, D., "Analysis of Complex Flow Fields by Animation of PIV and High Resolution Unsteady Pressure Data"
*RTO/AGARD Fluid Dynamics Panel Symposium, Advanced Aerodynamic Measurement Technology, September 1997.*